Limitations and Improvement of Subcarrier Multiplexed Systems over Optical Fiber

Daniel James Tebben

Dissertation submitted to the faculty of the Virginia Polytechnic Institute and State University in partial fulfillment of the requirements for the degree of

Doctor of Philosophy
In
Electrical Engineering

Committee:
Dr. Ira Jacobs (chair)
Dr. Ahmad Safaai-Jazi
Dr. John K. Shaw
Dr. William H. Tranter
Dr. Yong Xu

April 17, 2006
Blacksburg, Virginia

Keywords: Optical Networks, Dispersion, Coherent Detection, Subcarrier Multiplexing

Limitations and Improvement of Subcarrier Multiplexed Systems over Optical Fiber

Daniel James Tebben

Abstract

Optical coherent techniques are used to eliminate the power fading found in optical subcarrier multiplexed systems. In a double-side band optical subcarrier system the signal experiences a periodic power fading that is dependent on the fiber dispersion and subcarrier frequency. This power fading is manifested during the direct detection of the subcarrier system using a square-law photodetector. Using a modified optical local oscillator to coherently detect the subcarrier channel this power fading can be eliminated.

An optical local oscillator is centered at the optical carrier in order to perform homodyne detection. However, the local oscillator is modulated by a term equal the subcarrier frequency of interest. This is then a dual-frequency optical local oscillator. By controlling the phases of the local oscillator and the local subcarrier oscillator independently in the homodyne detection scheme, both the phase error and power fading of the detected subcarrier channel can be eliminated. This technique also allows the subcarrier to be selected optically, before the optical-to-electrical conversion.

Analytical and simulation results are given to show the benefits of optical coherent detection in double-sideband subcarrier systems. By eliminating the periodic power loss found in the double-sideband subcarrier system the signal

becomes dispersion limited and not power limited. A comparison of double-sideband and single-sideband subcarrier systems is presented. Multiple subcarriers and subcarrier spacing are also investigated for both double-sideband and single-sideband subcarrier systems.

Optical phase and modulator noise are also considered in the analysis and simulation of coherent detection using a dual-frequency optical local oscillator. Since the implementation used to eliminate the power fading is a phase correction based process, the phase noise of both the source and local oscillator lasers must be considered and the technique compared to typical direct and coherent detection techniques. Also, the effects of modulator nonlinearity are simulated for multichannel subcarrier multiplexed systems and comparisons made between the performance of using the dual-frequency local oscillator and typical detection techniques. It is shown that the advantages of the dual-frequency LO are retained in the presence of both phase noise and modulator nonlinearity.

Acknowledgements

This dissertation is the product of help and sacrifices of many people. I thank Dr. Ira Jacobs for his direction, expertise and insight he lent me during my studies at Virginia Tech. It has been an honor and pleasure to work with him. I also thank the other members of my committee for their guidance.

My education at Virginia Tech was made possible by funding from two fellowships. I thank the Via/Bradley Foundation for sponsoring the Bradley Graduate Fellowship. I am also grateful to the Cunningham Fellowship through the Virginia Tech graduate school. This funding has allowed me to pursue my goal of a doctorate degree while raising three small boys.

Finally, I thank my family. First, I thank my wife, Jennifer, who has been encouraging, supportive and patient while we pursued this goal. This work could not have been accomplished without her, and I dedicate this dissertation to her. I am also very grateful to my three little super heroes. Jacob, Joshua and Isaac have been inspiring and encouraging as I studied late at night so I could spend time with them during the day. Thank you.

Table of Contents

Table of Figures

Chapter 1. Introduction

Optical communication systems have been evolving along many paths since the introduction of fiber optic networks three decades ago. Generally, these paths lead to increasing the amount of data transmitted and increasing the distance the signal propagates. Optical fibers allow for transmission of data rates measured in terabits-per-second, and distances that cross continents and oceans. In order to increase the total data transmitted on a fiber, either the bit rate per channel can be increased or the number of channels can be increased. Each of these techniques has many implications on the system architecture and performance.

For long distance telephone and internet backbone systems it makes economic sense to carry these high amounts of data on each fiber. However, when looking at networks that require less bandwidth, or cover shorter distances, the ever increasing bit-rate-per-fiber scenario may not be the most economic solution. One method to provide a solution for low bit-rate and short-distance networks is to use radio-over-fiber techniques. These networks can combine the extensive knowledgebase of radio frequency (RF) networks and the cost benefit of utilizing existing RF equipment at the network edges with the performance and reliability of optical networks. A radio-over-fiber system either directly modulates a laser or modulates an external optical modulator with an analog RF signal. This analog RF signal is generated in the electrical domain from the signal or signals that are to be propagated in the network. The RF signal itself may either be an analog signal or derived from digital signals.

One such system where the analog RF signal is derived from lower bandwidth signals is a subcarrier-multiplexed system. In a subcarrier-multiplexed (SCM) system, several information bearing signals are electrically modulated on to separate carriers. Once these separate carriers are aggregated together (frequency division multiplexed (FDM)), and used to modulate a higher frequency carrier they are considered subcarriers. This dissertation will refer to a set of electrical subcarriers used to modulate an optical carrier as optical subcarriers, or an optical-subcarrier-multiplexed (OSCM) system. The information bearing signals may be either analog or digital, and may be of various modulation formats. For the purpose of this dissertation, any type of information bearing signal could be used to modulate the subcarrier, however the examples found in the simulation section are digital signals on optical subcarriers, as that is the primary case of practical interest. Both amplitude modulation (AM) and phase modulation (PM) are considered, with the majority of examples and analysis on AM. Prior to the simulation in Chapter 4, analytical models will be considered in Chapters 2 and 3 in which single frequency information signals (i.e. sinusoidal signals on a subcarrier) are analyzed; this can be generalized to represent any signal type through a Fourier-series analysis. The purpose of the analytical models is to uncover the major phenomena and parameter ranges of importance for the subsequent simulation. The mathematical model used to represent a radio-over-fiber, or more specifically, a subcarrier-over-fiber system is explained in detail in Chapter 2.

Radio-over-fiber systems have many uses in today's communications systems. These include cable television networks (CATV); both digital and analog television can be transmitted using an OSCM network. Also, computer networks, telephone networks, radio networks and wireless infrastructure can utilize subcarrier and/or RF signals over an optical fiber network. These types of networks have a long history of RF transmission, and by using radio-over-fiber the systems can remain largely backward compatible. For instance, the tuner in today's cable ready televisions is not dependent on whether the CATV network utilizes optical or coaxial links, or both. A digital high definition television (HDTV) signal, aggregated to several channels (perhaps each consisting of multiple standard definition subchannels), is transported as an analog RF signal over the fiber-coax hybrid CATV network.

One of the benefits of using a radio-over-fiber network, specifically an OSCM network, is the ability to provide efficient aggregation and granularity. By using subcarriers to carry individual streams of information, a signal can be efficiently routed from source to destination. A set of subcarriers destined for a common region can be aggregated to one wavelength, and wavelengths of neighboring regions could be aggregated to a single fiber. An optical wavelength can support bandwidths of 100-GHz or more. This way routing can be done at both the optical and electrical levels. For instance, in an internet distribution network, such as an internet service provider (ISP) utilizing a CATV network, an individual user does not require the bandwidth provided by an optical wavelength. The ISP can use a single subcarrier to carry internet data so it can

easily be separated from the other information on the wavelength. Signals from a neighborhood or large building can be aggregated onto a wavelength using several subcarriers. Different wavelengths can then be combined onto a single fiber to aggregate a region together. This way passive optical routing can be used to distribute signals to the correct neighborhoods, and RF techniques can distribute individual subcarriers to the correct user. This hypothetical situation is used to illustrate how OSCM systems make use of increased control of aggregation and granularity.

When a SCM signal propagates through a dispersive medium, such as an optical fiber, unique degradations occur. If the SCM signal is modulated as a double-side-band (DSB) RF signal onto the optical carrier, the chromatic dispersion of the fiber causes the upper and lower sidebands to walk off from each other. This walk-off has two negative effects. First, a pulse-shape distortion occurs when the walk-off time is on the order of the bit rate. Second, a power penalty occurs during the photodetection of the signal if the walk-off time is on the order of the subcarrier period [1,2,3]. Also, in a single-side-band (SSB) subcarrier system the walk-off between the optical carrier and the subcarrier leads to a phase error during the photodetection of the signal. An optical SSB signal can be generated using either an optical filter after modulation or a Hilbert transform in the modulator circuit [4,5].

We consider a new approach using coherent detection of the OSCM system to eliminate the above phenomena [6,7]. By using optical coherent detection the power-penalty of the DSB OSCM system can be eliminated. Since

the power penalty occurs at much shorter distances than the pulse-shape distortion, the propagation distances can be dramatically increased. The phase error induced in the SSB OSCM system can be compensated using either optical or electrical coherent detection of the SCM signal. The optical coherent detection compensates for the dispersion induced penalties by independently controlling the phase of the carrier and subcarrier of the local oscillator (LO). Chapter 2 will go into detail on the structure of this unique LO.

A secondary benefit of using optical coherent detection in an OSCM system is greater optical power efficiency. In a typical OSCM system that utilizes direct detection of the signal in a photodetector a strong carrier component is required to insure linear detection. A photodetector is modeled as a square-law detector since the output current is proportional to the square of the input optical field. This creates spectral components equal not only to the frequency difference between the carrier and subcarriers, but also equal to the spacing between each subcarrier. To have the desired subcarrier terms be the dominate signal after the photodetector a high carrier-to-subcarrier power ratio is required. In other words, the optical signal needs to be modulated by the RF signal with a small modulation index. This leads to very little power in the information carrying subcarriers. By using optical coherent detection a strong carrier is not required because linear detection can be achieved with a strong LO.

When investigating the use of a dual-frequency LO, degradations besides fiber dispersion must be considered. First, since phase control is essential to the success of the new detection technique, phase noise must be considered in both

the source and LO lasers. Also, when considering OSCM systems, the nonlinearity of the modulation needs to be considered. Here, the linearity of the optical modulator and number of subcarriers affect the amount of amplitude noise of the signal before transmission.

The remainder of this dissertation will look at OSCM systems and detection both analytically and in simulation. Chapter 2 will provide an analytical model of the OSCM system, the effect of dispersion, and how various detection techniques affect the system performance. Also in Chapter 2 the performance metrics; Q-factor and bit-error-rate (BER) are explained. Chapter 3 carries out the analysis based on the models proposed in Chapter 2. Several formats of OSCM systems are analyzed and compared. Dispersion effects are examined in each case, as well as using a dual-frequency LO to overcome the dispersion induced power fading. Chapter 4 provides simulation results which closely follow the analytical models, while providing a means to visually see the system limitations and remediation. The simulations also allow modeling of realistic data waveforms instead of merely sinusoidal signals. Additionally, the simulation allows for a noisy signal and LO to be studied. BER and Q analysis of the system is performed to see how dispersion, phase noise and amplitude noise impair the system. Finally, Chapter 5 draws conclusions about OSCM systems based on the analytical and simulation results.

Chapter 2. Model and Methodology

To study the effects the optical fiber imposes on the OSCM system a model needs to be established. This model is used in both the analysis and simulation of the optical system. This chapter establishes the normalized set of parameters and the basic equations used to describe the transmitter, fiber, detector and signal. This chapter will also define the performance metrics used to assess the impact optical propagation has on the SCM signal. The component models defined here are generalized models suitable for use in the remainder of the dissertation as the building blocks for the analysis and simulation of more specific cases.

The following diagram is used to visualize the basic transmission system. Each block will be introduced in the following sections of this chapter. Chapter 3 will analyze in detail the fiber dispersion and receiver blocks, both for direct detection and coherent detection.

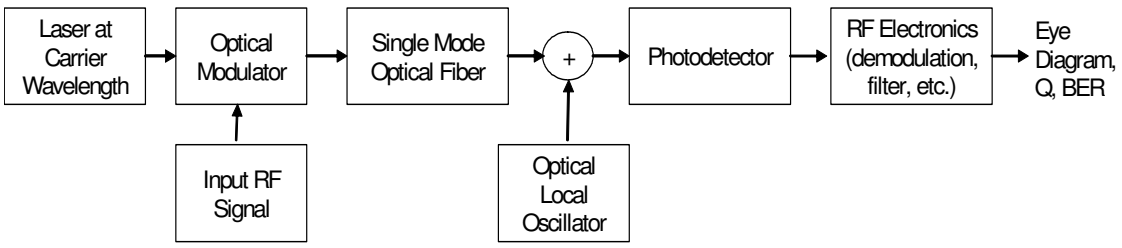

Figure 2.1: Block diagram of optical system.

The optical LO block is included when using coherent detection techniques, and is omitted when using direct detection techniques.

Section 2.1. Normalized Parameters

Optical networks are able to traverse thousands of kilometers or have bandwidths in the terahertz, but it is difficult to design a system capable of supporting both simultaneously. Dispersion causes a temporal broadening proportional to both the signal bandwidth and the distance the signal has traveled through the fiber [8]. Because of this interdependence it is useful to express frequency and distance in normalized terms. When dispersion is the main propagation effect being considered, wavelength, bandwidth (frequency), length, and fiber dispersion can all be expressed relative to each other. The following equation shows their relationship[i].

$$z = \frac{\pi L D f_s^2 \lambda^2}{c} \qquad \textbf{(2.1)}$$

Here, z is the normalized length. It will be shown later that z is also the phase shift imposed on the subcarrier by the fiber dispersion. L is the fiber length, D is the fiber dispersion parameter (delay difference per unit bandwidth per unit distance), and f_s is the subcarrier frequency. λ is the wavelength of the optical carrier and c is the speed of light.

Generally fiber dispersion is discussed in terms of the signal bandwidth, not the subcarrier frequency. However, as will be shown later, in a subcarrier

---

[i] In [8], Agrawal defines a dispersion length to indicate the distance over which dispersion plays a significant role compared to the fiber nonlinearities. This normalized dispersion length is given by

$$L_D = T_0^2 / |\beta_2| \qquad \text{[i.1]}$$

T_0 is the bit period and β_2 is the propagation constant related to the fiber dispersion. L_D is related to the normalized length (z), the physical length (L), and r using the following relationship

$$z = \frac{L}{L_D} \frac{2\pi^2}{r^2} \qquad \text{[i.1]}$$

multiplexed system the subcarrier frequency is much more important with regards to system performance. A normalization parameter is introduced to relate the subcarrier frequency to the subcarrier bit rate. The parameter, *r*, is the ratio between the bit rate (in bits/second) and subcarrier frequency (in Hertz). For a binary data format (amplitude-shift-keyed (ASK) or binary phase-shift-keyed (BPSK)) the symbol rate and data rate are the same in which case *r* is also the ratio of the symbol rate to subcarrier frequency.

$$r = \frac{R}{f_s} \tag{2.2}$$

The following example shows the use of the normalization parameters. A typical simulation might have a distance factor of $z=\pi$ and a frequency ratio of $r=0.05$. This could represent a 1-Gb/s signal on a 20-GHz subcarrier that has propagated for 18.4 km over standard single-mode-fiber (SMF) with a dispersion of 17 ps/nm/km and a 1550-nm optical carrier. The same parameters could also represent a 3-Gb/s signal on an 60-GHz subcarrier that propagated 2.0 km with the same carrier wavelength and fiber type. For lower bandwidth signals, this could represent a 500-MHz subcarrier with 2.5-Mb/s data over a distance of nearly 30,000 km. These examples vary greatly in distance, data-rate and subcarrier frequency, but each would exhibit the same dispersion induced penalties that are examined in the following chapters. The normalization factors are not required for the analytical investigation since the equations are presented in generalized terms, but they are helpful in the simulations and examples to gain an understanding of the phenomenon responsible for the degradations.

Section 2.2. Analytical Model

The analytical model is introduced here and will be used in both the analysis (Chapter 3) and the simulation (Chapter 4). The basic model for each block of Figure 2.1 is described in this section. The analysis section will use this model to explore the effects that the modulation format, fiber dispersion and other distortions have on the optical signal. The model consists of equations for the optical carrier with RF subcarrier modulation, fiber dispersion, modulator nonlinearity, phase noise, receiver and performance metrics.

Section 2.2.1. Subcarrier Modulation

The first item that needs to be defined is a noise-free continuous-wave source. This will represent the optical source and subcarriers. Later modulation, noise and nonlinearity will be added to this model. The ideal laser source is modeled simply as a sinusoid wave.

$$S = 2K\cos(2\pi f_\lambda t + \phi_\lambda) = 2K\cos(\omega_\lambda t + \phi_\lambda) \quad \textbf{(2.3)}$$

The optical carrier frequency is represented by f_λ in Hertz and ω_λ in radians/sec. The λ subscript is use to indicate the frequency refers to the optical carrier. The carrier phase is used as the reference phase to which all phases are referenced, therefore $\phi_\lambda = 0$ and is dropped from any future equations. K is half the amplitude of the signal, and the factor of 2 is used simply to avoid using a factor of ½ when representing (2.3) in exponential form. K is related to the optical power and electric field as

$$2K \propto \sqrt{P_\lambda} \propto |E_\lambda| \quad \textbf{(2.4)}$$

Since the assumption is made that optical power levels are kept low enough that distortion due to the fiber nonlinearity is negligible, the system is normalized to the optical power, where $K = 1$, and thus K can be excluded from the equations. (When considering the effects of noise, the noise power is scaled relative to the optical signal power.) It is useful to express (2.3) and the following subcarrier expressions in exponential form in order to clearly see the upper and lower sidebands.

$$S = e^{j2\pi f_\lambda t} + e^{-j2\pi f_\lambda t} \tag{2.5}$$

The above equations refer to the optical frequency which is typically in the 200-THz range. Optical systems are frequently referred to in terms of the optical wavelength, λ, which is related to the frequency by the speed of light, c. The wavelengths of typical communication systems are in the 1310-nm or 1550-nm range.

$$f = c / \lambda \tag{2.6}$$

The laser is amplitude modulated by the RF signal. The RF signal is the information source and can be in the form of a baseband digital signal, analog signal or a FDM signal. The modulation of the subcarrier can be amplitude modulation (AM), frequency modulation (FM) or phase modulation (PM). The analysis leaves the modulation format arbitrary; however, AM is used throughout the examples and simulation, with a few PM examples given for comparison. The RF signal is $A(t)$, so the amplitude modulated carrier becomes

$$S = A(t)\left(e^{j2\pi f_\lambda t} + e^{-j2\pi f_\lambda t}\right) \tag{2.7}$$

which gives a double-sideband suppressed carrier (DSB-SC) signal. For a non-suppressed optical carrier, the equation becomes

$$S = (1 + \mu A(t))\left(e^{j2\pi f_\lambda t} + e^{-j2\pi f_\lambda t}\right) \quad \textbf{(2.8)}$$

where μ is the optical modulation index. For incoherent square-law detection, the modulation index needs to be kept low in order to ensure linear detection. For coherent detection the local oscillator power needs to be sufficiently high to ensure linear detection.

As stated above, the SCM system is either a set of digital or analog channels. This work focuses on digital SCM systems. Therefore, the carrier needs to be modulated by the subcarrier system. Each subcarrier is in turn modulated by the information bearing signal (usually ASK). The subcarrier is modulated either single sideband or double sideband. A double-sideband subcarrier (without data) is represented as

$$A(t) = 2\cos\left(2\pi f_s t + \phi_s\right) = e^{j(2\pi f_s t + \phi_s)} + e^{-j(2\pi f_s t + \phi_s)} \quad \textbf{(2.9)}$$

where f_s is the subcarrier frequency and ϕ_s is the phase of the subcarrier. By substituting (2.9) into (2.7) or (2.8), the subcarrier is represented at the optical frequency. When the optical carrier is suppressed, filtered out, or ignored, a single channel of the OSCM systems is given by

$$S = e^{j(2\pi(f_\lambda + f_s)t + \phi_s)} + e^{j(2\pi(f_\lambda - f_s)t - \phi_s)} + e^{-j(2\pi(f_\lambda + f_s)t + \phi_s)} + e^{-j(2\pi(f_\lambda - f_s)t - \phi_s)} \quad \textbf{(2.10)}$$

When N subcarriers are present, the signal is represented as the summation of subcarriers with frequency of f_s where s=1 to N. This can be seen in the following equation, where the optical carrier has not been suppressed.

$$S = \cos\left(2\pi f_\lambda t\right) + \mu \sum_{s=1}^{N} \left(\cos\left(2\pi\left(f_\lambda + f_s\right)t + \phi_s\right) + \cos\left(2\pi\left(f_\lambda - f_s\right)t - \phi_s\right)\right) \quad \textbf{(2.11)}$$

μ is the modulation index and is assumed to be the same for each subcarrier. Equation (2.11) is concise and convenient for double-sideband modulation of the optical carrier, however in the analysis it is often necessary to see the upper and lower sidebands individually. This is because dispersion causes a different phase shift for the upper and lower sidebands. In this case, (2.11) can be rewritten as

$$S = e^{j2\pi f_\lambda t} + e^{-j2\pi f_\lambda t} + \mu \sum_{s=1}^{N} \left(e^{j(2\pi(f_\lambda + f_s)t + \phi_s)} + e^{j(2\pi(f_\lambda - f_s)t - \phi_s)} + e^{-j(2\pi(f_\lambda + f_s)t + \phi_s)} + e^{-j(2\pi(f_\lambda - f_s)t - \phi_s)}\right) \quad \textbf{(2.12)}$$

The base-band representation of equation (2.10) is the complex envelope, and is simply *A(t)* shown in (2.9) for a suppressed carrier signal.

There are four variations of this basic signal that will be specifically addressed in the analysis. OSCM systems have different benefits and draw backs depending on whether the carrier and subcarrier are modulated with a single-sideband or double-sideband format. Each of the four formats will be evaluated in Chapter 3 and simulated in Chapter 4. It is easy to identify the upper and lower sidebands of the signal in equation (2.10) by noticing which frequencies are added and which are subtracted. In the analysis and simulation single-sideband signals are generated using a Hilbert-transform technique and compared to the results found in literature of a single-sideband optical modulator [5].

Section 2.2.2. Dispersion Model

Optical fiber propagation imposes three adverse effects on the information bearing signal. These effects are dispersion, nonlinearity and attenuation. At power levels and distances of interest, an optical fiber is a linear medium, exhibiting attenuation and a frequency dependent phase shift. At higher power levels, fiber nonlinearity distorts the signal and is not investigated here since network operators typically operate the system to avoid nonlinearity. Attenuation is the power loss the signal experiences during propagation due largely to scattering in the fiber, and is constant over the bandwidth of the signal, so it can be neglected for this dissertation. However, loss is not neglected in general. A bulk system loss is used in the simulation and is discussed below. The frequency dependent phase shift is evident as chromatic dispersion. Chromatic dispersion is a phenomenon of optical transmission that is due to the dependence of the propagation velocity on the wavelength of the light. Different wavelengths (or frequencies) of light propagate at different velocities in an optical fiber. In the absence of nonlinearities, dispersion can be modeled as a lump sum phase value based on the fiber dispersion parameter, fiber length and spectrum of the signal. Relating this back to the normalized parameters presented above, the phase shift at the subcarrier is equal to the normalized length.

Lump-sum, or bulk, dispersion can be modeled as a frequency dependent phase shift in the frequency domain representation of the optical signal. The bulk dispersion is defined as [8]

$$D_S(f) = \frac{L\pi D\lambda^2 f^2}{c} \qquad \textbf{(2.13)}$$

f in (2.13) is the RF frequency of the signal. Note that $D_S(f)$ is a frequency dependent phase shift and is dimensionless. Further more, when $f = f_s$, $D_s(f_s) = z$.

To find the output signal from a dispersive fiber, the bulk dispersion is applied to the input signal. In this way a transfer function can be defined for the fiber. First the Fourier Transform, $\mathcal{F}$, of the time domain signal is defined below. S_0 denotes the optical signal before transmission.

$$\tilde{S}_0 = \mathcal{F}\{S_0\} = \int_{-\infty}^{\infty} S_0 e^{-j2\pi ft} dt \qquad \textbf{(2.14)}$$

Dispersion is included as a frequency dependent phase term in the frequency domain, $e^{jD_S(f)}$, such that the signal at the output of the fiber is [8].

$$\tilde{S}_F = \tilde{S}_0 \cdot e^{jD_S(f)} \qquad \textbf{(2.15)}$$

$$S_F = \mathcal{F}^{-1}\left\{\mathcal{F}\{S_0\} e^{jD_S(f)}\right\} \qquad \textbf{(2.16)}$$

The subscript F indicates the signal is at the end of fiber length L.

The signal shown in equation (2.10) is not useful in a communication system because it doesn't carry any information. The signal is simply constructed of delta-bandwidth sinusoidal signals. For the purpose of defining the dispersion model, it is sufficient to assert the assumption that the data's bandwidth is much smaller than the subcarrier frequency. When solving equation (2.16) for a simple sinusoidal signal, a solution can be found analytically. However, when the transmitted signal includes random data a

numerical method is required to evaluate the time domain signal at the fiber end. For the analysis of dispersion in radio-over-fiber systems, signals with either a few discrete, delta spectral components, or one in which the bandwidth of the signal is narrow enough to be assumed a delta, will be examined. Chapter 4 will simulate broad spectrum signals in order to validate that the analysis of Chapter 3.

Section 2.2.3. Nonlinear Modulator

The modulator presented in Section 2.2.1 is a strictly linear modulator. No signal dependent distortion occurs. Today's optical modulators are not strictly linear, and present a distortion to the modulated signal [9]. Also, external modulators (such as a Mach-Zehnder) have a steady state transfer function that is sinusoidal in nature [1,10,11]. The Mach-Zehnder transfer function as given in [1] is

$$E_{out}(t) = \frac{E_{in}}{\sqrt{2}}\left(\cos\left(\beta_m(t)L_{\text{mod}}\right)\right) \qquad \textbf{(2.17)}$$

where E_{out} and E_{in} are the output and input optical fields, respectively. $\beta_m(t)$ is the phase delay in each arm of the Mach-Zehnder and is proportional to $A(t)$. L_{mod} is the length of each branch of the Mach-Zehnder. Equation (2.17) is specifically for the case where each branch of the Mach Zehnder is driven with equal, but inverted, modulating voltages. V_π is the voltage required to generate a π phase shift in one arm of the Mach-Zehnder and is related to $\beta_m(t)L_{\text{mod}}$, the

modulation voltage, $u(t)$, and the phase constant of the arm without a voltage applied, β_0, by [1]

$$\beta_m(t) = \beta_0 - \frac{\pi}{L_{\text{mod}}} \frac{u(t)}{V_\pi} \tag{2.18}$$

The figure below depicts this transfer function over $2V_\pi$.

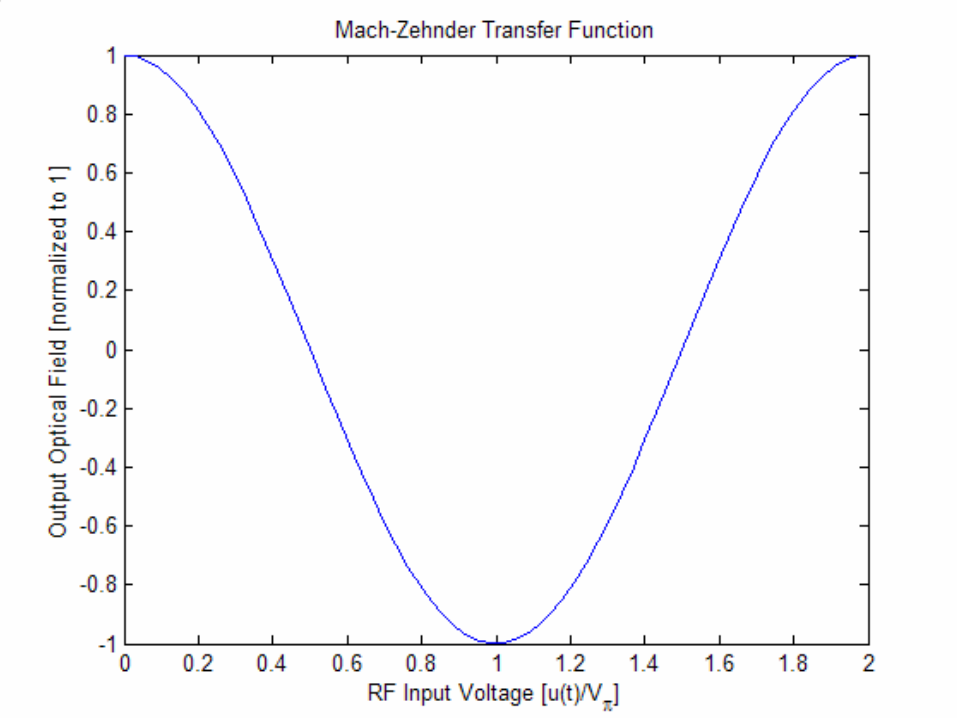

Figure 2.2: Mach-Zehnder modulator transfer function. Optical power is normalized to the input optical power.

When scaling and biasing the input RF signal it is necessary to keep the signal within the linear region of the transfer function and where $u(t)/V_\pi > 1$. If the input RF signal is biased below 1 the output will be inverted, which may be acceptable to the network operator. Clearly, the transfer function is most linear between about $1.3V_\pi$ and $1.7V_\pi$. However, when the number of subcarriers is altered, or a higher extinction ratio is desired, the signal will not remain in the

linear region of the transfer function. The simulation of the nonlinear modulator allows the bias and the amplitude of the RF input to be varied. By increasing the number of subcarriers, and adjusting both the RF bias and amplitude, the effects of the nonlinear modulator can be studied.

Section 2.2.4. Data and Pseudo-Random Bit Sequence

The information signal needs to be added to the subcarrier before the optical modulator. The data, or bit-sequence, *B(t)* is first used to modulate the RF subcarrier and then the complete RF signal is used to modulate the optical carrier. As stated earlier, the modulation format of *B(t)* is left arbitrary in analysis, and is either ASK or PSK in the simulation. For an ASK system, *A(t)* becomes

$$A(t) = \left(1 + \eta B(t)\right)\left(e^{j2\pi f_s t} + e^{-j2\pi f_s t}\right) \qquad \textbf{(2.19)}$$

where η is the RF modulation index. The analysis and simulation employ several RF detection schemes (as outlined below), many of which can detect a suppressed RF subcarrier. *A(t)* with a suppressed RF carrier is

$$A(t) = B(t)\left(e^{j2\pi f_s t} + e^{-j2\pi f_s t}\right) \qquad \textbf{(2.20)}$$

B(t) consists of a pseudo-random bit sequence (PRBS) that is extrapolated to the required samples per bit and filtered with a third-order Butterworth filter at 0.67 times the bit rate. The filter shape and bandwidth was chosen to be comparable to the SONET standard [29].

The PRBS is determined by the number of bits desired in the simulation. The method for generating the PRBS is using a modulo-2 shift register, summing the previous *n* bits according to the primitive polynomial, to generate a sequence

2^n-1 bits long [12, 13]. The length of the PRBS in the simulations is 511 bits long. 511 bit long sequence is chosen as a compromise that includes a sufficient number of transitions without overtaxing the computer resources. Increasing the number of samples to 1023 greatly increases the simulation run time without producing noticeable changes in the results. The sequence is then up-sampled to generate a waveform that is used to modulate the subcarrier. The number of samples-per-bit (SPB) dictates the simulation spectrum [12] and is determined using the following relation

$$SPB=2^{\lceil \ln(4/r) \rceil} \qquad \textbf{(2.21)}$$

where the $\lceil \ \rceil$ brackets denote the ceiling function. This ensures that the simulation bandwidth is larger then the highest subcarrier frequency. In most cases, the SPB is set equal to 64 when modeling a single subcarrier, and 128 for multiple subcarriers.

The filtering that is imposed by the RF electronics and the optical modulator is executed by filtering the data signal (*B(t)*) prior to modulating the subcarrier. Again, the data waveform is used in the simulation and the analysis leaves the data format arbitrary.

The analysis uses a Fourier series to express *B(t)*, realizing that any real data stream can be represented as the sum of sinusoidal functions [14]. In this form, *B(t)* is given by

$$B(t) = b_0 + 2\sum_{k=1}^{\infty} b_k \cos(2\pi k F_0 t + \phi_k) \qquad \textbf{(2.22)}$$

where b_o is the DC component of the data. In the analysis the phase shift of each frequency component is dependent on the frequency, and it is necessary to compensate for each frequency component of the data. Because each frequency component is treated equally and arbitrarily in the analysis, it is necessary to perform the analysis for only one frequency component of the data. Therefore, the data is represented as a single frequency component such that $f_r = kF_0$ and $\phi_r = \phi_k$. The phase term determines the degradation of the signal and therefore it is convenient to normalize the data to a magnitude such that $b_r = 1$. Therefore, in the analysis, double-sideband data prior to transmission through the dispersive medium is given by

$$B(t) = 2\cos(2\pi f_r t + \phi_r) = e^{j(2\pi f_r t + \phi_r)} + e^{-j(2\pi f_r t + \phi_r)} \quad \textbf{(2.23)}$$

It will be shown by comparing the analysis (Section 3.5) to the simulations (Section 4.2.1) that this is equivalent to performing the dispersion analysis for the complete signal shown in (2.22).

Section 2.2.5. Optical Phase Noise

Optical lasers do not have a perfect delta spectrum. Phase noise in the laser causes a spectral linewidth. Furthermore, coherent detection is used in this study to reduce the effect of the dispersion induced phase shift, and in homodyne coherent detection the phase of the local oscillator must be matched to the phase of the received optical signal. So clearly the phase of both the optical signal and local oscillator play an important role in coherent optical systems. For this reason phase noise must be included.

Phase noise of the optical signal is due to spontaneous emissions within the laser [10]. This process may be modeled as a Gaussian random walk. That is, the phase shift, $\Delta\phi_t$, over a period of time is Gaussian [15].

$$\Delta\phi_t = \phi(t+\tau) - \phi(t) \qquad \textbf{(2.24)}$$

In (2.24), $\phi(t+\tau)$ is the phase after a period of time, τ.

In coherent detection, the phase of the local oscillator is locked to the phase of the incoming optical signal [16,17]. When this occurs, the phase of the local oscillator tracks the phase of the optical signal with some offset. In this situation, the 'walk' portion of the process can be eliminated and the phase noise of signal and local oscillator can be modeled as a Gaussian random variable. Since the phase of the optical carrier is always taken as the reference, it is modeled as a zero-mean Gaussian random variable. The phase noise of the local oscillator is modeled as non-zero mean Gaussian random variable. The mean of the LO phase noise represents the average phase offset between the local oscillator and received signal, and is dependent on the feedback of the optical phase-lock loop [16,18,19].

Section 2.2.6. Received Power

Optical systems are susceptible to power loss in many forms. First, fiber attenuation due to scattering within the fiber causes loss. Also, optical splitters and combiners have an inherent loss due to the fact that they divide the light into multiple paths. Furthermore, other components introduce loss both internally and from the connections to the fiber. These are only a few of the sources of loss in

an optical system, but they show that loss is not strictly distance dependent. For this reason, along with the fact that we have made the assumption power is kept low enough to avoid nonlinear effects of the fiber, the power is normalized to the input signal power. An optical network has gain elements and loss elements, and these are not the focus of this study; however the receiver design is dependent on received power. At the receiver, a bulk loss is introduced for the purpose of evaluating the effect received power has on the signal quality for a given receiver design and modulation format. When there is no power penalty due to dispersion or modulator nonlinearity, and no bulk loss is included, the received signal eye-opening (see Section 2.3) is unity. This also implies an optical one to zero difference of unity.

Section 2.2.7. Receiver Design

The optical receiver is used to convert the optical power into an electrical current. The main component of the receiver is the photodetector. Prior to the photodetector are optical components such as a preamplifier, optical filters and the injection of an optical LO. After the photodetector is the electrical decision circuit. The decision circuit usually determines whether the bit is a one or a zero. However, in this work, the signal quality is more informative; therefore, the RF portion of the receiver is used to generate a Q measurement, bit-error rate (BER) estimate, or an eye diagram. Q, a measurement of the signal-to-noise ratio (SNR), is defined below and under certain assumptions the BER can be estimated from the Q. The simulation section uses all three quality metrics, while the analysis uses Q (or SNR).

The right hand side of Figure 2.1 shows a block diagram of the receiver. The receiver designs can be separated into two categories, direct detection and coherent detection. In a direct detection receiver, the optical LO shown in Figure 2.1 is omitted.

Section 2.2.7.1. Square Law Detector

The photodetector is a squaring device [10,11,15]. The output electrical current is proportional to the square of the input optical field. In general, the equation that relates the output photocurrent to the input optical signal is [15]

$$I_p = \Re M P_{in} \tag{2.25}$$

$$P_{in} = K\left|\mathbf{E}_{in}\right|^2 \tag{2.26}$$

where I_p is the output current of the photodetector, $\Re$ and M are the responsivity and gain of the photodetector, respectively. I_p is often referred to as the photocurrent. P_{in} is the power of the optical signal at the input of the detector, and $\mathbf{E}_{in}$ is the electric field vector of the optical signal and K is a constant. As will be shown shortly, it is important to remember that $\mathbf{E}_{in}$ is a vector that includes the polarization of the optical field. For simplicity, and since in this analysis the powers, gains and responsivities are arbitrary, the equation to describe the photodetection process can be written as

$$I_P = \left|\mathbf{E}_{in}\right|^2 = \mathbf{E}_{in}\mathbf{E}_{in}^* \tag{2.27}$$

where the asterisk (*) denotes the complex conjugate operator. Equation (2.27) is used throughout the paper when discussing an ideal photodetector.

For a direct detection system, (2.27) describes the current that is the input to the RF circuit described below. For a coherent detection system, the optical LO must be added to the input optical signal before the photodetector.

Section 2.2.7.2. Coherent Detection

In a coherent detection receiver, the electrical field, $\mathbf{E}_{in}$, is defined as the sum of the optical LO electrical field and received signal field. Here, $\mathbf{E}_{in}$, is given by

$$\mathbf{E}_{in} = \mathbf{E}_{sig} + \mathbf{E}_{LO} \tag{2.28}$$

where the subscripts '*sig'* and '*LO'* denote the electric field of the incoming optical signal and the optical local oscillator, respectively. In practice, care must be taken to ensure that the polarizations of $\mathbf{E}_{sig}$ and $\mathbf{E}_{LO}$ are aligned to ensure there is no power penalty [11]. This dissertation will assume that some method has been taken to align the polarizations, and therefore equation (2.28) can be rewritten as either (2.29) or (2.30).

$$\sqrt{P_{in}} = \sqrt{P_{sig}} + \sqrt{P_{LO}} \tag{2.29}$$

$$\left|\mathrm{E}_{\mathrm{in}}\right| = \left|\mathrm{E}_{sig}\right| + \left|\mathrm{E}_{LO}\right| \tag{2.30}$$

Other coherent receiver designs have been proposed in [11,20,21,22] that do not require the polarizations of the LO and signal to be aligned at the receiver input, such as a polarization diverse receiver.

When talking about the absolute value of the optical field, it is useful to describe the signal in terms of the field magnitude. When the polarization of the

field can be ignored this can greatly simplify the equations used. For this purpose we define

$$S = \sqrt{P} \propto |\mathbf{E}| \tag{2.31}$$

S is the instantaneous magnitude of the optical signal and is time-varying according to the optical frequency and modulation of the optical carrier. For a subcarrier multiplexed optical signal, S, has been described in equations (2.7) through (2.10).

By combining equations (2.27), (2.28) and (2.31) an equation to be used throughout the analysis for coherent detection is defined as

$$I_P = \left(S_{sig} + S_{LO}\right)\left(S_{sig}^* + S_{LO}^*\right) \tag{2.32}$$

Within the category of coherent receivers, the system can utilize either homodyne or heterodyne detection. In a homodyne detection scheme, the optical frequency of the LO (f_{LO}) and the carrier (f_λ) are matched and the resulting photocurrent is at baseband. In a heterodyne receiver, f_{LO} is not equal to f_λ and the resulting photocurrent is at some intermediate RF frequency. A homodyne receiver has a 3-dB advantage over a heterodyne receiver, but has increased complexity because the optical phase of the signal and LO must be locked [11]. The analysis in Chapter 3 and simulation in Chapter 4 model both optical homodyne and heterodyne detection schemes.

Section 2.2.7.3. RF Demodulation

After the optical signal is converted to a photocurrent in the detector the current needs to be processed to yield a Q, BER or eye-diagram. In a real

system the processing would be a decision circuit that determines if the bit is a one or zero. Much of the RF circuitry for finding the Q or eye-diagram is the same as that for making a bit decision.

In either homodyne or heterodyne detection of an OSCM system, the resulting photocurrent is a RF signal with modulated carriers. Each carrier has data modulated by some RF frequency. The purpose of the RF circuitry is to isolate and demodulate a single RF signal. Several techniques are used within the simulation to accomplish this RF detection. The analysis assumes either ideal envelope or ideal homodyne detection of the desired RF channel.

In the simulation, non-ideal filtering and detection is considered. The first method for detecting a single RF channel is envelope detection. This technique is beneficial in that it works for each of the modulation formats explored and for both direct and coherent optical detection. However, it requires that the modulation index on the subcarrier is less than 1. The process involves the use of two RF filters. The first filter is a 3^{rd} order Butterworth passband filter around the desired RF channel. The bandwidth of the filter is the equal to the bit rate of the signal. The second filter is a 3^{rd} order Butterworth baseband filter, matched to the transmitter filter, with a bandwidth of 0.67 times the bit rate. This pair of filters reduces the entire spectrum of the photodetector's output to that of just the baseband data waveform. The waveform looks like a train of ones and zeros, but no decision circuit has been used to retrieve the binary data from the waveform.

The second category of RF demodulation is to utilize a coherent detector. As in the optical coherent detection, this can be either homodyne or heterodyne detection. In a homodyne scenario, the photocurrent is mixed with a RF LO at the frequency of the desired channel. The resulting signal is then filtered with the same baseband filter described above.

In heterodyne detection, the photocurrent is first filtered with a broadband RF filter that selects a group of channels. This is required to avoid any cross-channel interference due to having multiple channels at the intermediate frequency (IF). Next, a LO with a frequency of $f_{LO} = f_s - f_{if}$ is mixed with the filtered RF signal, where f_{if} is the intermediate frequency. A bandpass filter centered at f_{if} with a 3-dB bandwidth equal to the bit rate is used to isolate the channel. Then envelope detection is done to remove the IF.

A special case needs to be addressed for RF homodyne detection where the optical carrier is double sideband and the FDM signal is closely spaced and modulated single sideband. When the RF spacing of the subcarriers is less then two times the signal bandwidth, then standard homodyne detection of the channel will suffer from adjacent channel crosstalk. That is, the upper sideband of one adjacent channel will overlap the spectrum of the lower sideband of the desired channel, and accordingly, the lower sideband of the other adjacent channel will overlap the upper sideband of the desired channel. There are two ways to avoid this problem. The first is to use a form of envelope detection, either at the IF or the subcarrier frequency. The other method is to use a

homodyne detection scheme that utilizes a Hilbert transform that effectively nulls the adjacent channels. This technique is described in detail in Appendix A.

When using the proposed dual-frequency LO [6,7], the sinusoidal modulation of the optical LO can be tuned to the desired subcarrier frequency. In this way the channel is selected with the optical LO instead of the RF LO. The resulting photocurrent is at either an IF or baseband and is either coherently detected or envelope detected as above. Since the dual-frequency LO is used to counteract the effects of dispersion on a specific modulation technique, the details of this receiver design are covered in the analysis section.

Section 2.2.7.4. Mode-Locked Laser Coherent Detection

An alternative coherent detection design is one that uses a mode-locked laser (MLL) as the optical LO. A MLL is a laser that has a comb-spectrum, consisting of equally spaced spectral peaks [23,24,25]. A mode-locked laser can be generated in many ways [26,27,28], but is commonly done in a laser diode by modulating the input current with a sinusoid. The output of the laser is then a pulse train with a spectrum of evenly spaced peaks. The spectrum is defined by [24,25]

$$S_{MLL} = \sum_{n=1}^{N} x\cos(2\pi f_n t + \phi_0) \qquad \textbf{(2.33)}$$

where $f_n = f_0 + f_{\Delta L}$ and $f_{\Delta L}$ is the frequency spacing of the peaks and is equal to the frequency of the driving sinusoid. Since the MLL produces a pulse train, when used as a LO, the resulting photocurrent will be a sampled form of the data. As long as the sampling rate is higher than the bit rate the data can be

recovered. Using a MLL as the optical LO the spacing between the subcarriers in the optical domain can be changed when converting to the RF domain. For example, the channels can be more closely spaced in the RF domain where detection technologies are more mature than they are in the optical domain. This can be useful when trying to fit a large number of channels into the limited bandwidth of the RF circuitry.

A detailed explanation of the process and limitations of using a MLL as an optical LO is given in Appendix B. The resulting RF spectrum can be viewed as a set of channels at several different IF, with a frequency spacing different from that of the optical subcarriers or the MLL. The respacing of the subcarriers when that occurs in the photodetection process is given by

$$f_{IF,n} = \left| nf_{os} - f_{\delta} \right| = \left| f_{\delta} - nf_{os} \right| \qquad \textbf{(2.34)}$$

$f_{IF,n}$ is the intermediate frequency for the nth channel. f_{os} is the offset frequency and determines the RF domain frequency spacing. f_{os} is defined by $f_{os} = f_{\Delta L} - f_{\Delta}$, where f_{Δ} is the optical subcarrier spacing. The difference between the MLL central frequency and the optical carrier is given by f_{δ}.

Use of a MLL LO is limited by the number of subcarriers that can be supported. Since a peak of the MLL can be considered the LO for each optical subcarrier, the maximum number of detectable channels is determined by the optical frequency spacing and the offset frequency.

$$N < \frac{f_{\Delta}}{2f_{os}} \qquad \textbf{(2.35)}$$

Appendix B details variations of the MLL that can allow for a greater number of subcarriers to be detected. This is done by using each MLL peak to detect more than one channel and tuning the MLL center frequency such that a fixed IF can be used.

Section 2.3. System Metrics (Q, BER, Eye-Diagram)

The exact determination of the performance of a communication system is the bit-error rate (BER). This is defined as the ratio of the number of errant bits received to the total number of bits received. Optical systems are inherently very low noise systems and therefore have extremely low BER. Typical systems have a BER on the order for 10^{-9} to 10^{-13} [29]. In order to accurately measure a BER when the errors occur due to Gaussian noise one needs to find at least 50-100 errors, and more errors must be detected if the impairments are not dominated by Gaussian noise [29]. In order to collect 50 errors for a system where the BER is 10^{-9}, the system would need to run for an average of 500 billion ($500*10^9$) bits. This is a prohibitive amount of bits for a simulation to produce in order to make an actual BER measurement, and this is only the minimum system quality of a single channel.

Since a direct BER measurement is not feasible for even a basic optical system, much less so for a multichannel, low noise, optical SCM system, an estimate of the BER must be performed, based on the SNR. A common method to access the SNR of an optical system using the output photocurrent of the receiver is the so called Q measurement [30,31,32]. Q is defined as

$$Q \equiv \frac{|\mu_1 - \mu_0|}{\sigma_1 + \sigma_0} \tag{2.36}$$

In (2.36), μ_1 and μ_0 are the means of the ones and zeros, respectively, while σ_1 and σ_0 are the standard deviations.

From the Q measurement, a BER estimate can be made [30]. This estimate is based on the assumption that the noise of in the photocurrent has a Gaussian distribution. This noise can be assumed Gaussian under the presence of optical amplifier noise, small amounts phase noise, or for large numbers of channels contributing crosstalk. The BER estimate is found from the following relationship.

$$BER = \frac{1}{2}\text{erfc}\left(\frac{Q}{\sqrt{2}}\right) \tag{2.37}$$

efrc(·) is the complementary error function[i]. This is the estimate of the minimum possible BER based on Q since it assumes that the decision level is set at the optimum point in the receiver [15,33]. Since this work is focused on signal degradations and power penalties due to fiber dispersion, phase noise and modulator non-linearity, the receiver model used in the simulation also assumes that the decision circuit is optimally set to minimize the probability of errors.

Besides the Q measurement and the BER estimate, a third system performance tool is utilized. In many cases it is informative to visualize the signal

---

[i] The error function and complementary error function are defined differently in different sources. Here the complementary error function is $1 - \text{erf}(x) = \text{erfc}(x) = \frac{2}{\sqrt{\pi}}\int_x^\infty e^{\left(-t^2\right)}dt$, as defined in MATLAB®.

impairments. For this an eye diagram is used [29]. An eye diagram is generated by superimposing the waveform of several bits, making sure that the bits are aligned correctly to the clock. The resulting diagram, for an arbitrary PRBS and noise level, is shown below.

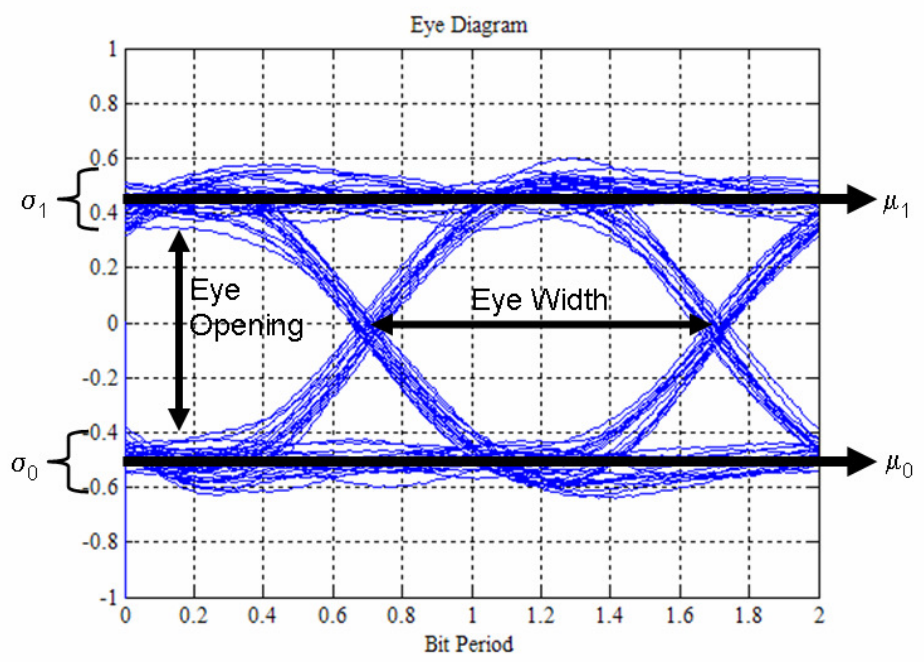

Figure 2.3: Sample Eye Diagram, used to help visualize the Q parameter.

The heavy arrows pointing to the right show where the one and zero means are measured. The brackets pointing to the left indicate where the standard deviations are measured. The other important signal qualities that can be seen in an eye diagram are the eye opening and the eye width. The eye opening is a qualitative view of Q, since it incorporates both the amount of noise seen and the magnitude of the signal. An eye that is closed will have a low Q parameter and correspondingly a high BER. The eye width is the distance between the one and zero crossings. This indicates any pulse broadening or distortion due to system impairments. As can be seen in Figure 2.3, the x-axis is

normalized to the bit period. This is consistent with the normalization parameters presented above.

The method for generating the eye-diagram in the simulation first involves removing the DC component of the waveform, so the eye is centered around 0, as shown in the figure above. Also, prior to calling the eye-diagram plotting routine, the signal is normalized such that if the signal were ideal (i.e. at the source, noise free and linearly modulated) the amplitude of the eye is unity. This is done so that any deviation from an eye-opening of one readily shows signal degradation.

The rational for determining the PRBS length was stated earlier and indicated that a sufficient number of transitions are needed. The PRBS length is further determined by the method which the eye-diagrams are generated. When dispersion causes a signal to temporally extend beyond the simulation window the waveform becomes distorted. This distortion is an artifact of the simulation and not representative of the system being modeled. With small amounts of dispersion (short fiber, low dispersion fiber, small signal bandwidth) the distortion appears at the edges of the window (the first and last bits). As the total dispersion increases the distortion moves to the center bits as well. A simple way to avoid distortion due to the simulation window size is to ignore the first and last bits of the PRBS. The eye generating routine here discards the first fourth and last fourth of the bits before the eye-diagram is plotted. In order to ensure sufficient variation in the bits used to generate the eye-diagram the PRBS is 511 bits long. The eye-diagrams therefore show the middle 255 bits (i.e. bits 128

through 383). The same argument holds true for the calculation of Q. The Q measurement is found using the same center bits as the corresponding eye diagram.

The MATLAB® routine for generating the eye-diagram is given in Appendix F.1.

Section 2.4. Chapter 2 Summary

In this chapter the basic building blocks required to analyze, simulate, and quantify an optical SCM system have been presented. First, normalized parameters are used through out the report so the trends can be seen that apply to all bit rates, subcarrier frequencies, distances and fiber parameters. Next analytical models for the transmitted signal, fiber dispersion and receiver have been given. These models will be the starting point when investigating the different SCM formats and detection techniques in the next two chapters. Finally, two quantitative and one qualitative metric are introduced for the purpose of evaluating the system performance.

Chapter 3. Analysis of SCM Optical Systems

The purpose of this chapter is to identify the phenomena caused by transmitting OSCM signals over a dispersive optical fiber and the ranges of parameters that require simulation. This chapter also introduces a new method to eliminate some system impairments that are identified for OSCM systems. This method is based on individually compensating for the dispersion induced phase shift of the upper and lower sidebands of the optical carrier [6,7].

This dissertation considers four types of optical subcarrier systems, differentiated by the sidebands of the signal. The optical carrier can be either single sideband (SSB or DSB), and likewise for the subcarrier. The following figure depicts these four modulation techniques.

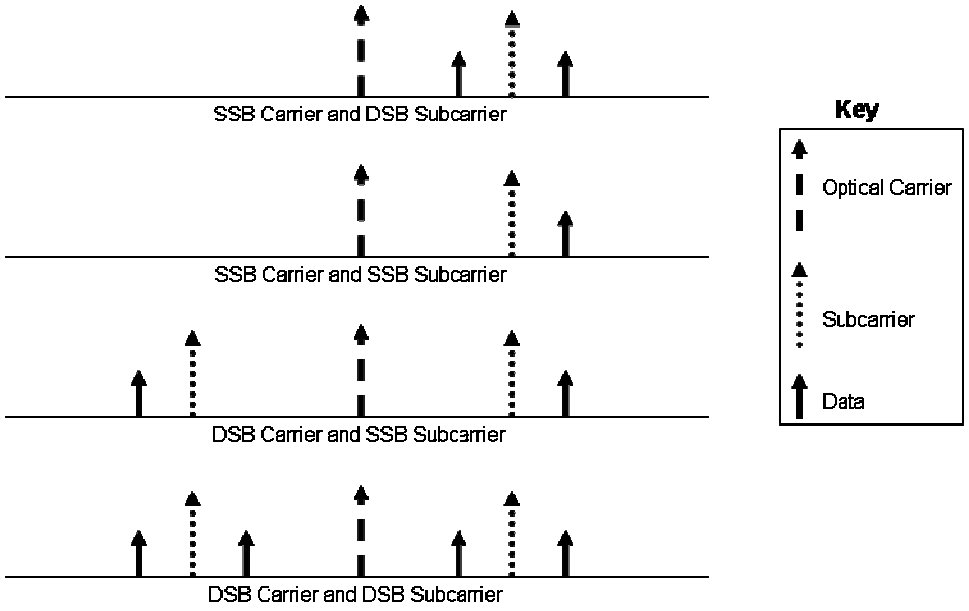

Figure 3.1: Four types of OSCM systems considered. Only positive frequencies are shown and these are not drawn to scale.

In Figure 3.1 the data is shown as a delta for simplicity and to coincide with the majority of the analysis. In practice and in the simulation, data has a non-zero bandwidth. The carrier and subcarrier are both represented with dashed lines to indicate that they may be suppressed depending on the receiver design. Also, only the upper sideband (USB) case is shown for the SSB signals. The following analysis can be easily modified for lower-sideband (LSB) signals with the same results.

In terms of performance, the greatest differences are between SSB and DSB carriers, not between SSB and DSB subcarriers. This is because the frequency separation is greater between the upper and lower sidebands of the carrier than between the sidebands of the subcarrier. Each of these cases has a different set of dispersion induced penalties and solutions for addressing the penalty.

Section 3.1. Optical Single-Sideband Modulation

As stated in the discussion of the signal model it is useful to write the equations representing the signal in exponential form so the upper and lower sidebands can easily be seen. In a physical system, an USB signal is not derived simply by ignoring the LSB, the LSB must be removed either with a filter or a Hilbert-transform modulator [4,5,34,35]. To generate an USB signal using a Hilbert-transform modulator a dual-input Mach-Zehnder is required. The transfer function of the optical electric field is [5]

$$E_{out} = \frac{E_{in}}{2} e^{j\pi \frac{d_1}{V_\pi}} + \frac{E_{in}}{2} e^{j\pi \frac{d_2}{V_\pi}} \qquad \textbf{(3.1)}$$

where d_1 and d_2 are the inputs to each Mach-Zehnder terminal and are defined as

$$d_1(t) = xV_\pi\left(B(t) + \hat{B}(t)\right) - \frac{V_\pi}{4} \quad \textbf{(3.2)}$$

$$d_2(t) = xV_\pi\left(-B(t) + \hat{B}(t)\right) + \frac{V_\pi}{4} \quad \textbf{(3.3)}$$

V_π is the input to the modulator that results in a π phase shift. In simulation V_π is arbitrary and will actually be eliminated from the equations when combining (3.2) and (3.3) into (3.1). $B(t)$ is the AC-coupled binary data stream, filtered accordingly for the modulator bandwidth. $\hat{B}(t)$ is the Hilbert transform of the binary signal. (The Hilbert transform is explained in Appendix C.) x is scaled such that $x\pi$ is equal to the modulation index. This model needs to be compared to the method that will be used in the simulation and analysis. In the simulation, a SSB signal is found by taking the Hilbert transform of the data or FDM signal and modulating it with either the subcarrier or optical carrier, respectively.

To verify the simulation model and methodology the following results were compared to results found in literature [5]. The figures below show the eye-diagrams of a USB signal after 0, 75 and 150 km of fiber. The simulation parameters used are a 10-Gb/s (PRBS), standard single mode fiber ($D = 17\frac{ps}{nm\,km}$), with an ideal receiver. Both the modulator and receiver assume a third-order Butterworth filter with a 3-dB cutoff frequency of 6.5 GHz.

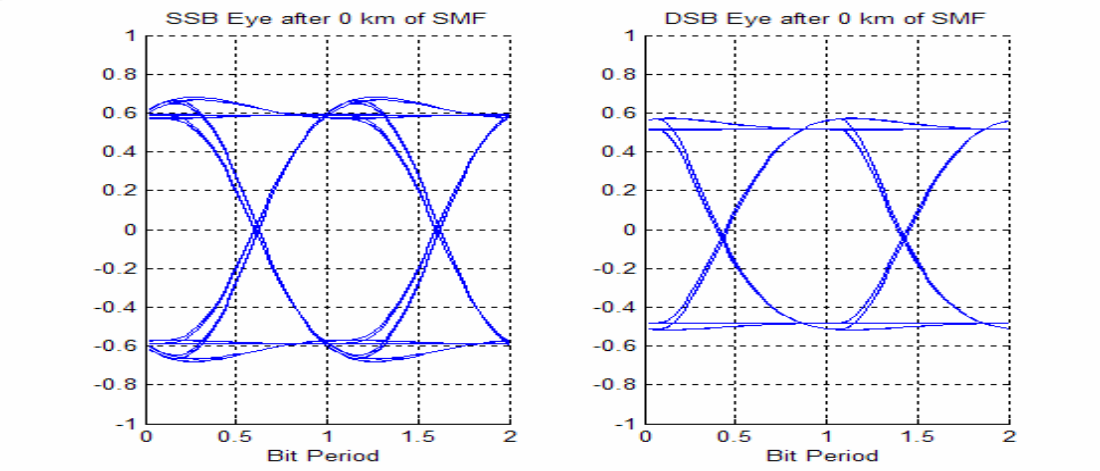

Figure 3.2: Eye-diagram for SSB and DSB signal after 0-km fiber, normalized to the bit rate and arbitrary power.

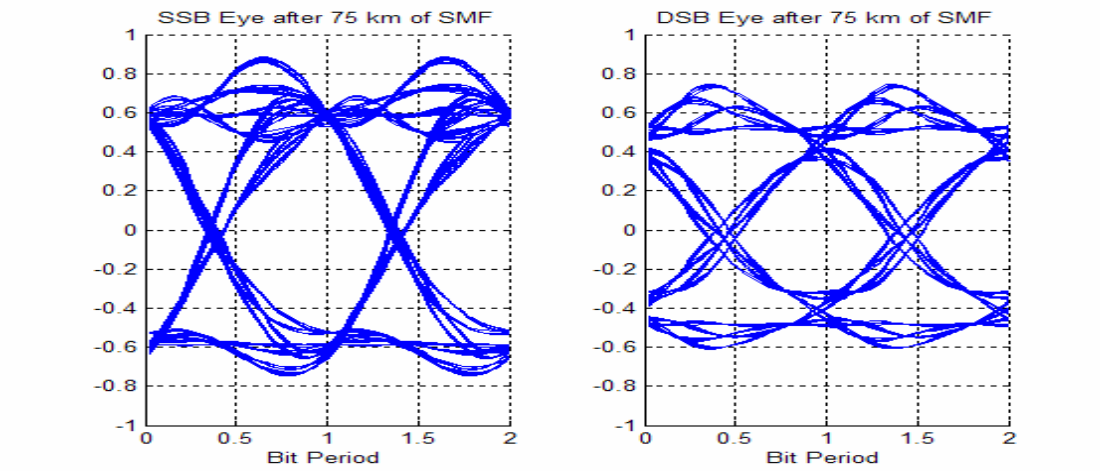

Figure 3.3: Eye-diagram for SSB and DSB signal after 75-km fiber, normalized to the bit rate and arbitrary power.

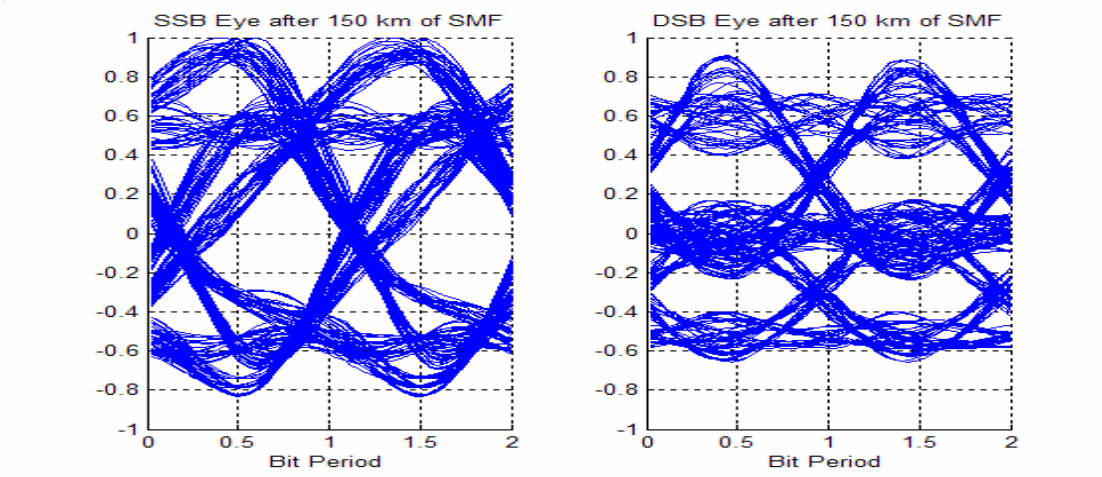

Figure 3.4: Eye-diagram for SSB and DSB signal after 150-km fiber, normalized to the bit rate and arbitrary power.

These figures are in very good agreement with the results given in [5], and confirm several factors about the simulation technique used. First, it shows that the dispersion model accurately predicts both SSB and DSB propagation. Second, the SSB modulator model used is consistent with models in literature that have been experimentally verified. Finally, it shows that the receiver design described Section 2.2.7 is a good approximation of a physical optical receiver.

Since to first order approximation, equation (3.1) can be simplified as an ideal SSB signal, the following equation is used to model a baseband USB signal through out the analysis and simulations. Equation (3.4) was used for the modulation and dispersion was included as a lump-sum as described in Section 2.2.2 to generate the figures above.

$$S_{USB} = 1 + \mu\left(B(t) + j\hat{B}(t)\right) \qquad \textbf{(3.4)}$$

Section 3.2. SSB Optical Carrier with DSB Subcarriers

In terms of the analysis of an OSCM system, equation (3.4) can be simplified further based on the properties of the Hilbert transform. In the analysis, equation (2.9) is used to represent the subcarrier (without data included) and applying this to equation (3.4) the USB SSB subcarrier is

$$S_{USB} = 1 + \mu e^{j(2\pi f_s t + \phi_s)} \tag{3.5}$$

The derivation of equation (3.5) is found in Appendix C. The same approach is used to find the SSB representation of the data on the subcarrier. In the analysis the data is included as a sinusoid at the data rate, while in the simulation the data is included as PRBS filtered at 0.67 the data rate. The simulation does not use the method shown in Appendix C to find a SSB carrier or subcarrier since a PRBS is used for the data rather than a sinusoid and MATLAB® can calculate the Hilbert transform of an arbitrary real waveform. In this way, the simulation is used to validate the methods used in the analysis and the analysis validates the simulation technique.

By applying a sinusoidal signal to (3.5) to represent the data as explained in Section 2.2.4, the signal at the input to the fiber (z=0) becomes $S_{0,SD}$. The subscripts S and D denote SSB carrier and DSB subcarrier, and similar notation will be used for all four scenarios depicted in Figure 3.1.

$$S_{0,SD} = 1 + \mu\left(e^{j(2\pi(f_s+f_r)t)} + e^{j(2\pi(f_s-f_r)t)}\right) \tag{3.6}$$

Since this is the input to the optical fiber, the phase of the subcarrier is considered the initial phase and is defined as zero, that is $\phi_S = 0$. Unlike the

optical carrier phase, which is assumed the reference phase of the system at any point along the fiber, the subcarrier phase will change with respect to the reference along the fiber. The subcarrier is suppressed in equation (3.6) because the information bearing, and therefore interesting, part of the signal is in the sideband of the subcarrier. This also simplifies the equations making the derivation easier to follow. For a complete analysis without suppressed carriers or subcarriers see Appendix D.

The dispersion due to the fiber is applied to this signal. The phase shift for the upper and lower sideband can be found in the time domain since each is a single frequency. After a fiber propagation of distance *z* the dispersion is found using equation (2.13). The frequency domain signal at the end of the fiber is $\tilde{S}_{F,SD}$.

$$\tilde{S}_{F,SD} = 1 + \mu\left(2\pi\Delta\left(f + f_s + f_r\right) + 2\pi\Delta\left(f + f_s - f_r\right)\right)e^{jD_s(f)} \quad \textbf{(3.7)}$$

Here it is important to note that the delta (Δ) function means that the inverse Fourier transform only needs to be evaluated at $f_s \pm f_r$. Therefore, the dispersion term, in a discrete frequency model, also needs to only be evaluated at these frequencies. The dispersion causes a frequency dependent phase shift; this shift is given as

$$\phi_{D,U} = \frac{L\pi D\lambda^2\left(f_s + f_r\right)^2}{c} = D_s(f = f_s + f_r) \quad \textbf{(3.8)}$$

and

$$\phi_{D,L} = \frac{L\pi D\lambda^2\left(f_s - f_r\right)^2}{c} == D_s(f = f_s - f_r) \quad \textbf{(3.9)}$$

Assuming that f_r is at the bit rate such that $(f_s + f_r) = f_s(1+r)$ and $(f_s - f_r) = f_s(1-r)$, ϕ_D can be rewritten in normalized terms as

$$\phi_{D,U} = z + \left(r^2 + \frac{2r}{f_s} \right) z \tag{3.10}$$

$$\phi_{D,L} = z + \left(r^2 - \frac{2r}{f_s} \right) z \tag{3.11}$$

Next the inverse Fourier transform of (3.7) is to be taken. In a linear system, such as described above, equations (3.8) and (3.9) can be written directly for a sinusoidal signal. However, the work here can be expanded to a non-sinusoidal signal (such as a digital data stream) so the steps above were outlined. This also makes the analysis consistent with the simulation, which is for a digital signal not a sinusoidal signal.

$$S_{F,SD} = 1 + \mu \left(e^{j(2\pi(f_s+f_r)t+\phi_{D,U})} + e^{j(2\pi(f_s-f_r)t+\phi_{D,L})} \right) \tag{3.12}$$

When performing the direct detection it is necessary that the modulation index, μ, is small such that $\mu^2 \ll 1$ and therefore any μ^2 terms can be neglected. In a coherent detection receiver, the same result can be accomplished by ensuring the local oscillator is sufficiently large, even if the optical carrier is suppressed. The output of the photodetector, before any RF demodulation is

$$I_{SD} = 1 + \mu \left(e^{j(2\pi(f_s+f_r)t+\phi_{D,U})} + e^{-j(2\pi(f_s+f_r)t+\phi_{D,U})} + e^{j(2\pi(f_s-f_r)t+\phi_{D,L})} + e^{-j(2\pi(f_s-f_r)t+\phi_{D,L})} \right) \tag{3.13}$$

By applying homodyne detection and baseband filtering, the data signal can be recovered from (3.13). A RF LO at the subcarrier frequency is mixed with I_{SD} to

find I_{EH}. The *EH* subscript indicates this is the electrical homodyne current. By applying a gain of $1/\mu$ to remove the modulation index, the output of the RF homodyne receiver is

$$I_{EH} = e^{j(2\pi f_r t+\phi_{D,U})} + e^{-j(2\pi f_r t+\phi_{D,U})} + e^{j(2\pi(-f_r)t+\phi_{D,L})} + e^{-j(2\pi(-f_r)t+\phi_{D,L})} \quad \textbf{(3.14)}$$

By expressing this equation in terms of cosines, the degradation becomes clear.

$$I_{EH} = 2\cos(2\pi f_r t + \phi_{D,U}) + 2\cos(2\pi f_r t - \phi_{D,L}) \quad \textbf{(3.15)}$$

With the assumption that *r*<<1 equations (3.11) and (3.12) show that that $\phi_{D,U} \approx \phi_{D,L}$, which is simply ϕ_D in the following equations. This means that we have two cosine terms with equal, but opposite, phase shifts. Using the product of cosines trigonometric identity, and this approximation, we can rewrite (3.15) as

$$I_{EH} = 4\cos(2\pi f_s t)\cos(\phi_D) \quad \textbf{(3.16)}$$

(3.16) shows that if the phase of the RF LO was locked to the optical carrier phase (note that the LO phase is not included in the equations above, implying that it is the same as the reference phase) there is a power loss equal to the cosine of the dispersion induced phase, or the normalized length, $z = \phi_D$. This clearly is not how the RF homodyne detection would be done in practice, and furthermore RF envelope detection avoids the use of a RF LO and therefore there is not an RF LO phase to lock. In a physical RF homodyne receiver the phase of the LO would be locked to ϕ_D and no power loss would occur. That is, the RF LO phase, ϕ_{RLO} would be included and the resulting current is

$$I_{EH} = 4\cos(2\pi f_s t)\cos(\phi_D - \phi_{RLO}) \quad \textbf{(3.17)}$$

In (3.17), the power penalty is due only to the inaccuracy of the phase-lock loop.

The inclusion of equation (3.16) is not to suggest that one would ever try to use homodyne detection without a phase-lock loop to maximize the received signal. Equation (3.16) is included because it will be used as comparison to the double-sideband optical carrier scenario that has a similar power loss due to the dispersion induced phase shift between the optical sidebands. The power penalty seen for the DSB optical carrier system needs to be corrected for in the optical domain, while here the phase error can be corrected for in the RF domain. This is a key difference that will be explained in greater detail later in this chapter.

Section 3.3. SSB Optical Carrier with SSB Subcarriers

Following a similar derivation the SSB SC case can be examined. This section applies to the system shown on the second axis of Figure 3.1. In many ways the analysis is more straightforward in the SSB case because there is only one spectral component to consider per channel. As above, the derivation will show only one channel of the OSCM system and either a strong LO or small modulation index is assumed to ensure that interchannel crosstalk does not occur during the photodetection process. To begin, the SSB signal at the fiber input is defined. Both the data and subcarrier are USB in this example and the subcarrier is suppressed.

$$S_{0,SS} = 1 + \mu e^{j(2\pi(f_s+f_r)t)} \quad \textbf{(3.18)}$$

After fiber propagation, the signal has a dispersion term, $\phi_{D,U}$, and is written as

$$S_{F,SS} = 1 + \mu e^{j\left(2\pi(f_s+f_r)t+\phi_{D,U}\right)} \quad \textbf{(3.19)}$$

Using the same technique and assumptions about the photodetector as in the DSB SC case, the photodetector output is

$$I_P = e^{j(2\pi(f_s+f_r)t+\phi_{D,U})} + e^{-j(2\pi(f_s+f_r)t+\phi_{D,U})} \quad \textbf{(3.20)}$$

Next the subcarrier must be removed from the RF signal. The subcarrier signal is mixed with a LO at the subcarrier frequency and homodyne detected.

$$I_{EH} = \left(e^{j(2\pi(f_s+f_r)t+\phi_{D,U})} + e^{-j(2\pi(f_s+f_r)t+\phi_{D,U})}\right)\left(e^{j2\pi f_s t} + e^{-j2\pi f_s t}\right) \quad \textbf{(3.21)}$$

$$I_{EH} = e^{j((4\pi f_s+2\pi f_r)t+\phi_{D,U})} + e^{-j((4\pi f_s+2\pi f_r)t+\phi_{D,U})} + e^{j(2\pi f_r t+\phi_{D,U})} + e^{j(2\pi f_r t+\phi_{D,U})} \quad \textbf{(3.22)}$$

Assuming a perfect filtering of the baseband signal, with no double frequency terms present, one finds

$$I_{EH} = e^{j(2\pi f_r t+\phi_{D,U})} + e^{-j(2\pi f_r t+\phi_{D,U})} = 2\cos(2\pi f_r t + \phi_{D,U}) \quad \textbf{(3.23)}$$

which is the original data waveform with a frequency dependent phase error. This phase error causes distortion to the eye-diagram if not compensated, as is shown in the figures of Chapter 4. As above in the DSB-SC case, in practice one would not lock the RF phase to the optical carrier, but since $\phi_{D,U}$ is a frequency dependent term, each spectral component of the data has a different phase shift that needs to be compensated. To better understand the frequency dependent phase error, the dispersion phase term, $D_s(f) = \phi_D$, needs to be expanded.

Section 3.3.1. Expansion of the Dispersion Induced Phase Term

The analysis for SSB and DSB SC with sinusoidally represented data above can be expanded to represent any data structure through Fourier analysis. When analyzing the compensation of the power penalty or phase error care must

be taken concerning the assumptions of the data bandwidth and subcarrier frequency. The care comes into play when calculating ϕ_D. ϕ_D is a frequency dependent term, which includes both the subcarrier and data frequency. By defining ϕ_D to include a term relevant to the subcarrier and a term relevant to the data frequency component, the effect of each component can be individually defined. In this way a non-sinusoidal signal can be analyzed. This expansion was alluded to when stating $\phi_{D,U} \approx \phi_{D,L} \approx \phi_D$ above, but a more complete look is required here.

$$\phi_D = D_{SC} + \Delta D_r \qquad \textbf{(3.24)}$$

where D_{SC} is the phase shift due to the dispersion resulting from the subcarrier frequency, and ΔD_r is the deviation from the subcarrier dispersion due to the specific frequency component of the data. Since the dispersion profile is not linear, ΔD_r cannot be determined without knowledge of the subcarrier frequency.

A numerical example based on typical fiber and OSCM parameters is useful to explain the expansion of ϕ_D. The figure below illustrates the dispersion profile of a 15-GHz subcarrier channel after 10 km of standard single mode fiber ($D = 17 \frac{ps}{nm\,km}$). Here we are assuming a relatively low bandwidth data channel (R=1 GHz which means r=1/15).

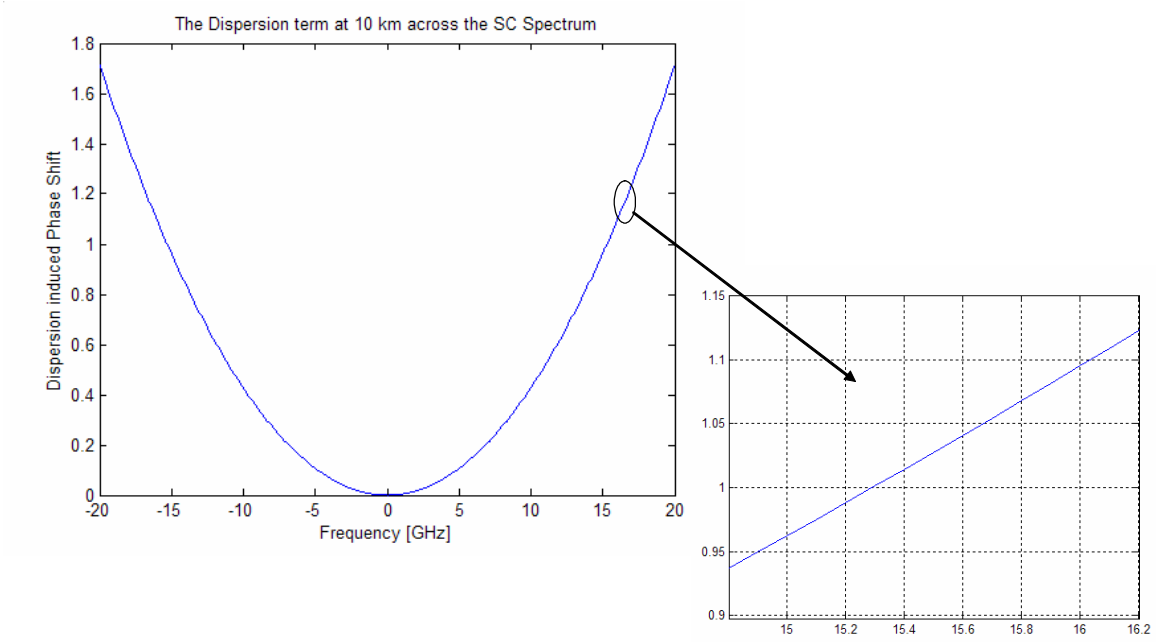

Figure 3.5: Dispersion induced phase shift at 10 km. The insert shows the area around the 15-GHz channel.

As can be seen in the insert of Figure 3.5 , the dispersion term is not constant across the bandwidth of the data channel. The differential phase shift across the bandwidth of the data accounts for a broadening of the data pulse. However, the average phase shift due to the subcarrier frequency is what causes the signal degradation in the received SSB carrier signal seen in Chapter 4. The same phase shift is also what causes the power penalty in the DSB carrier case. The following equations and figures will illustrate that the differential phase term (ΔD_r) only causes a small distortion for small data bandwidths. When the data bandwidth becomes large, or the fiber length becomes sufficiently long, the differential phase terms increases and leads to pulse broadening. In other words, each frequency component arrives at the receiver with a different time delay that cannot be removed with a simple phase term in the homodyne detector.

To clearly see how the phase error leads to an eye distortion in the SSB case equation (3.23) can to be rewritten in terms of a time delay instead of a phase shift.

$$S_{EH} = 2\cos(2\pi f_r t + \phi_D) = 2\cos\left(2\pi f_r \left(t + \tfrac{\phi_D}{2\pi f_r}\right)\right) \quad \textbf{(3.25)}$$

From this a time delay term, Δt, can be defined.

$$\Delta t = \frac{\phi_D}{2\pi f_r} \quad \textbf{(3.26)}$$

This time delay is the ratio of the subcarrier proportional phase term and the data frequency component. Lower frequency components of the data experience greater time delays in the received signal. This distortion will be seen clearly in the simulations; however, by examining a specific case the nature of the penalty can be clarified.

Using the numbers from the above example, one can find the amount of distortion different frequency components of the data experience. Assume a 10-km link of standard-single-mode fiber ($D = 17 \frac{ps}{nm\,km}$), a center wavelength of 1550 nm, a 15-GHz subcarrier and signal bandwidth of 1 GHz. By isolating two frequency components of the signal, the difference in delay can be calculated and a distortion metric can be found. Over the 1-GHz signal, ϕ_D has the range of 0.9623 to 1.095. Using equation (3.26) a frequency dependent time delay can be found for each spectral component of the signal.

Choosing to evaluate the time delay for a term at the bit-rate and one at ¼ the bit rate, the source of the eye degradation can be found. The relative time delay found for the frequency component at the bit rate is 174 ps. The delay for

the component at ¼ the bit rate is 158 ps. When one considers that the bit period for a 1.0-GHz signal is 1.0 ns, it is clear that the dispersion induced differential time delay is significant. This is illustrated in the two figures below. The first shows the two frequency components plotted as cosines with no time delay, as would be the vase before any dispersion. Figure 3.7 shows the two cosines after 10 km of fiber.

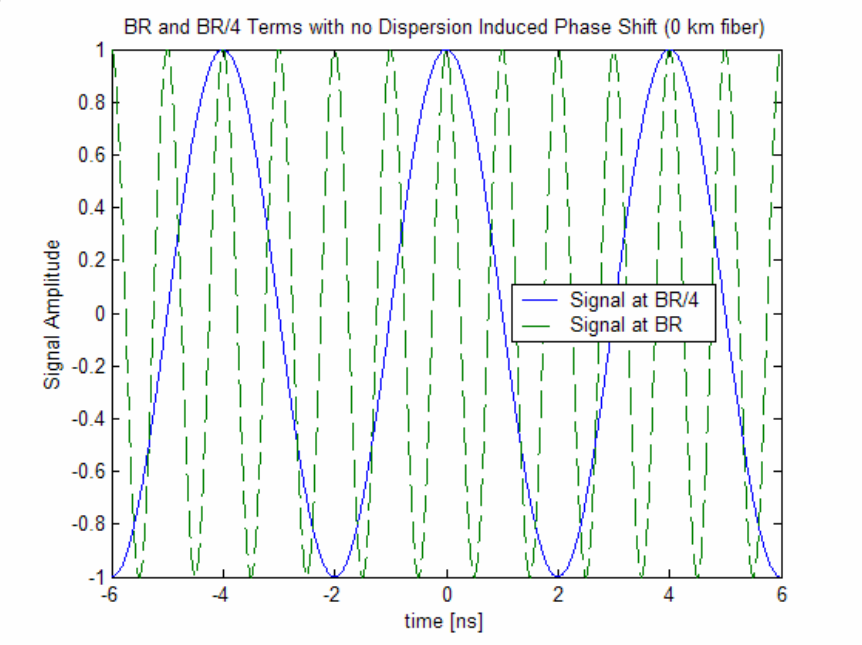

Figure 3.6: Two frequency components plotted with no dispersion induced time delay.

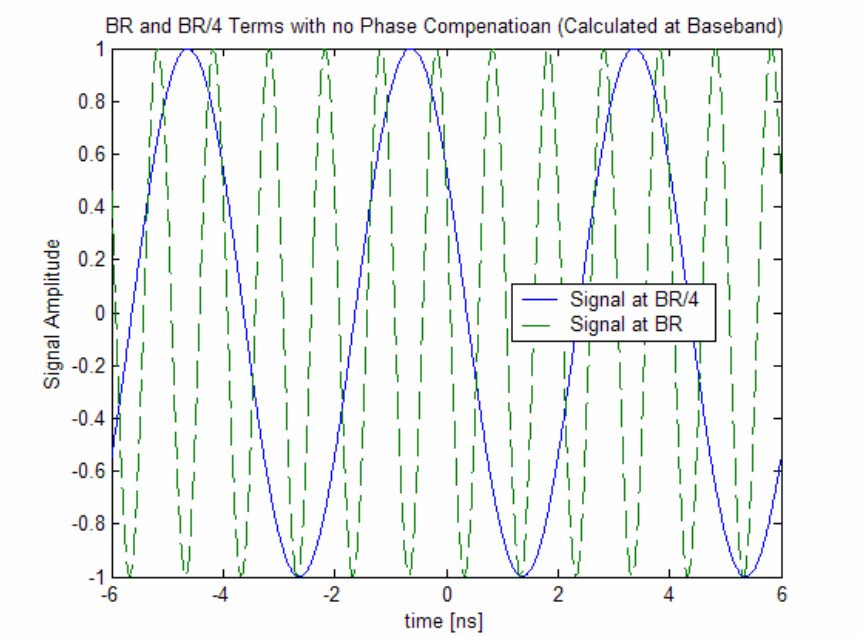

Figure 3.7: Two frequency components plotted after 10 km of SMF fiber.

In Figure 3.6 the peaks of the low frequency waveform line up with every fourth peak of the higher frequency waveform. This alignment can be used as the reference point for no relative time delay between the two signals. If the peaks align then the one-zero and zero-one transitions in an eye diagram will align. In Figure 3.7 the peaks clearly do not align after the dispersion is included.

By realizing that D_{SC} is much greater than ΔD_r in cases where the subcarrier frequency is much greater than the data bandwidth, we can make the assumption that $\phi_D \approx D_{SC}$. When compensating for the phase error, in both SSB and DSB SC signals, this assumption becomes very important. Using the example above, $D_{SC} = 0.9623$ and $\Delta D_r = 0.1327$. By setting $\phi_D = D_{SC}$, one only needs to adjust for the phase shift of the subcarrier to compensate for the penalty due to the fiber dispersion. If in addition one could compensate for ΔD_r, the pulse broadening due to chromatic dispersion would be eliminated.

In a method that will be analogous to the method used to detect a DSB optical carrier signal using phase locking, it will be shown here that phase locking to the subcarrier will produce a signal with a greatly reduced distortion. Examining equations (3.21) and (3.24), one finds that locking the phase of the RF LO to the SC, the received signal has a phase error of ΔD_r, thereby eliminating the larger effect due to D_{SC}. The following equations quickly step through the detection process using a phase-locked RF-LO. The LO phase is locked to D_{SC}.

$$S_{EH} = \left(e^{j(2\pi(f_s+f_r)t+\phi_D)} + e^{-j(2\pi(f_s+f_r)t+\phi_D)}\right)\left(e^{j(2\pi f_s t+D_{SC})} + e^{-j(2\pi f_s t+D_{SC})}\right) \quad \textbf{(3.27)}$$

$$S_{EH} = e^{j((4\pi f_s+2\pi f_r)t+\phi_D+D_{SC})} + e^{-j((4\pi f_s+2\pi f_r)t+\phi_D+D_{SC})} + e^{j(2\pi f_r t+\phi_D-D_{SC})} + e^{j(2\pi f_r t+\phi_D-D_{SC})} \quad \textbf{(3.28)}$$

After filtering to remove the double frequency terms, and using the equality set in (3.24), the received signal using a phase-locked RF LO is

$$S_{EH} = e^{j(2\pi f_r t+\Delta D_r)} + e^{j(2\pi f_r t+\Delta D_r)} = \cos\left(2\pi f_r t + \Delta D_r\right) \quad \textbf{(3.29)}$$

As indicated above, the frequency dependent time delay due to ΔD_r is negligible compared to the time delay due to D_{SC}. This is clearly illustrated using the same data example as above. In the phase compensated case the signal written in terms of time delay is

$$S_{SH} = \cos\left(2\pi f_r t + \Delta D_r\right) = \cos\left(2\pi f\left(t + \tfrac{\Delta D_r}{2\pi f_r}\right)\right) \quad \textbf{(3.30)}$$

Here the time delay is dependent on the differential phase shift due to the data frequency; it is not directly dependent on the frequency of the subcarrier. Using the same example as above, the time delay for the data rate and ¼ data rate

components are 21 ps and 5 ps, respectively. Clearly this is an improvement over the uncompensated case, where the phase is locked to the optical carrier. Figure 3.8 shows the phase compensated waveforms.

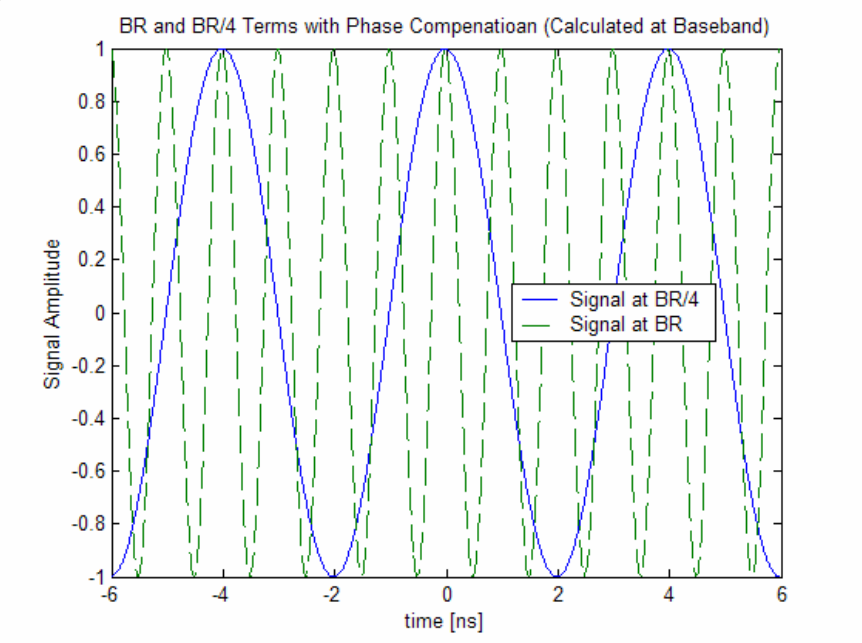

Figure 3.8: The phase shift due to the SC frequency is eliminated. Only the differential phase shift due to the data frequency is left.

In Figure 3.8 the peaks of the two waveforms align in the same way as they do with no dispersion. This shows that by phase compensating the subcarrier, one can compensate the majority of the time-delay differences in the data frequency terms. Figure 3.6 through Figure 3.8 show waveforms calculated at baseband. The calculations have also been done at the subcarrier frequency with the same results. While the above compensation of the distorted signal is done in the RF domain, it could have been done in the optical domain. This is the important distinction between detecting SSB and DSB optical subcarrier systems. When the optical carrier is DSB, the compensation necessarily has to

take place before the photocurrent is found. It takes place in the optical domain, or more specifically, within the nonlinear (squaring) portion of the photodetector.

Section 3.4. DSB Optical Carrier with SSB Subcarriers

In this section, one of the key obstacles for OSCM systems is explored. If one of the sidebands of the system is removed as in Section 3.2 and Section 3.3 then the transmitter complexity is increased and half of the signal power is removed for a given optical carrier power and modulation index. If an amplifier with a fixed output is used then the power loss does not occur, but the added transmitter complexity remains. In many situations this added complexity or power loss is acceptable to the network operator. However, it is not always desirable to add complexity or signal loss at the transmitter side of the system and a DSB carrier is desired. As will be seen later, this will move the complexity to the receiver end of the network. This would be a desirable situation if the transmitter cost and complexity needs to be kept low because they are at the customer's premises while the more costly and complex receiver can be located at the operator's site.

Presented first is the simpler of the two cases to analyze, the DSB carrier with SSB subcarrier, seen in the third axis in Figure 3.1. In order understand the effect that dispersion has on a DSB subcarrier multiplexed signal one can look at the single subcarrier case. Again, a sinusoidal modulation will be used to represent the information (digital or analog) that is on the subcarrier.

By applying a SSB modulation to represent the data on to the SCM signal of equation (2.10) one finds equation (3.31). This is the input signal to the fiber,

and therefore all phase terms are dropped. It is assumed that initially the phase of the signal is zero, and as the signal propagates any phase will be measured as its shift relative to the carrier's phase.

$$S_{0,DS} = e^{j(2\pi(f_\lambda+f_s+f_r)t)} + e^{j(2\pi(f_\lambda-f_s-f_r)t)} + e^{-j(2\pi(f_\lambda+f_s+f_r)t)} + e^{-j(2\pi(f_\lambda-f_s-f_r)t)} \quad \textbf{(3.31)}$$

This equation represents a suppressed carrier, suppressed subcarrier signal. Fundamental concern is with the information bearing component of the signal, so this representation is adequate for the analysis. Just as in the SSB carrier systems, the carrier and subcarrier, along with a modulation index for the subcarrier, and the optical LO power and phase need to be considered during photodetection in a practical system.

A baseband model can be used for the calculations required, so to simplify matters a baseband DSB carrier, USB subcarrier signal will be defined here. Note that this analysis can be (and has been) carried out with the full optical representation. When looking at solutions to overcome the dispersion induced penalties special care of the phase term needs to be taken when solving the equations at baseband. The baseband representation of the signal at the fiber input is

$$S_{0,DS} = e^{j(2\pi(f_s+f_r)t)} + e^{-j(2\pi(f_s+f_r)t)} \quad \textbf{(3.32)}$$

Similar to finding the dispersion term in equation (3.7), the dispersion term for the DSB-carrier signal is found with

$$\tilde{S}_{F,DS} = \left(2\pi\Delta\left(f+f_s+f_r\right) + 2\pi\Delta\left(-f+f_s+f_r\right)\right)e^{jD(f)} \quad \textbf{(3.33)}$$

Since $\tilde{S}_{F,DS}$ is only evaluated at $\pm(f_s + f_r)$ the dispersion causes the frequency dependent phase shift of

$$\phi_D = \frac{L\pi D\lambda^2 \left(f_s + f_r\right)^2}{c} = \frac{L\pi D\lambda^2 \left(-f_s - f_r\right)^2}{c} \tag{3.34}$$

$\phi_D = D(f_s + f_r) = D(-f_s - f_r)$ and can be substituted into equation (3.33). By transforming equation (3.33) back to the time domain the signal at the end of the fiber, $S_{F,DS}$, is found.

$$S_{F,DS} = e^{j\left(2\pi(f_s+f_r)t+\phi_D\right)} + e^{-j\left(2\pi(f_s+f_r)t-\phi_D\right)} \tag{3.35}$$

It is clear that the upper and lower sidebands experience a phase shift of opposite sign and equal magnitude. As the signal propagates through the fiber, the phase shift becomes larger and will cause a power fading. This power degradation is due to the upper and lower sidebands adding together out of phase when detected in the photodetector. Since this phase shift is converted to a power fading during the photodetection process it cannot be removed once the signal is in the RF domain. This is a key difference from the power fading seen in the SSB carrier with DSB subcarriers case analyzed in Section 3.2.

Although not included in the equations here, a strong carrier with a low subcarrier modulation index is required for linear photodetection. Alternatively, a strong local oscillator could be used when receiving the signal to ensure linearity. After removing double frequency terms and the DC bias, the output of the photodetector is

$$I_P = e^{j(2\pi(f_s+f_r)t)}\left(e^{j\phi_D} + e^{-j\phi_D}\right) + e^{-j\left(2\pi(f_s+f_r)t\right)}\left(e^{j\phi_D} + e^{-j\phi_D}\right) \tag{3.36}$$

After the signal is photodetected, the data must be recovered from the subcarrier. This can be accomplished using electrical homodyne detection and a low-pass filter or envelope detection (if a small subcarrier modulation index is used), both lead to the same result. Using a RF LO with a frequency equal to f_s, and a lowpass filter with a bandwidth appropriate to remove the double frequency terms (and other subcarriers if present) the received signal is

$$I_{EH} = (e^{j\phi_D} + e^{-j\phi_D})(e^{j2\pi f_r t} + e^{-j2\pi f_r t}) \quad \textbf{(3.37)}$$

This can be rewritten in sinusoidal form using trigonometric identities. In this form it is clear that a power penalty due to the fiber dispersion is present in a direct detection, DSB SC optical system. By observing equation (3.36) it is evident that this power penalty is present at the output of the photodetector and cannot be avoided using electrical compensation.

$$I_{EH} = 4\cos(\phi_D)\cos(2\pi f_r t) \quad \textbf{(3.38)}$$

The power fading is given by $\cos(\phi_D)$ just as in the SSB carrier with DSB subcarriers case when the penalty arose during RF homodyne detection with a mismatched phase of the RF LO. Since the phase error here occurs due to a mismatched phase of the optical LO with the optical carrier one needs to ensure that the optical phases are locked. The unique problem for the DSB optical carrier is that the USB and LSB terms have phase shifts with opposite signs. Since the phase shift of the upper sideband is not equal to the phase shift of the lower sideband a single optical LO cannot be phase locked to the signal. A unique solution to this problem is presented below.

Section 3.5. DSB Optical Carrier with DSB Subcarriers

The derivation of the system represented by the fourth axis of Figure 3.1 is fundamentally the same as that of Section 3.4 so the mathematics will be stepped through quickly. The DSB data signal in equation (2.23) is modulated by the subcarrier in equation (2.10) to obtain the signal at the input to the fiber. Once again, the initial phase of the entire system is assumed to be zero.

$$S_{0,DD} = e^{j(2\pi(f_\lambda+f_s+f_r)t)} + e^{-j(2\pi(f_\lambda+f_s+f_r)t)} + e^{j(2\pi(f_\lambda+f_s-f_r)t)} + e^{-j(2\pi(f_\lambda+f_s-f_r)t)} + e^{j(2\pi(f_\lambda-f_s+f_r)t)} + e^{-j(2\pi(f_\lambda-f_s+f_r)t)} + e^{j(2\pi(f_\lambda-f_s-f_r)t)} + e^{-j(2\pi(f_\lambda-f_s-f_r)t)} \quad \textbf{(3.39)}$$

Since both the carrier and subcarrier are DSB, this is indeed the simplest of the four modulation techniques described to implement. As in the previous section, the carrier terms have been dropped so the equations will clearly express the components that are vital to the system performance.

$$S_{0,DD} = \cos\left(2\pi\left(f_\lambda + f_s + f_r\right)t\right) + \cos\left(2\pi\left(f_\lambda + f_s - f_r\right)t\right) + \cos\left(2\pi\left(f_\lambda - f_s + f_r\right)t\right) + \cos\left(2\pi\left(f_\lambda - f_s - f_r\right)t\right) \quad \textbf{(3.40)}$$

$$S_{0,DD} = \cos\left(2\pi f_\lambda t\right)\cos\left(2\pi f_s t\right)\cos\left(2\pi f_r t\right) \quad \textbf{(3.41)}$$

The baseband representation of (3.39) is used for the derivation of the dispersion induced power penalty.

$$S_{0,DD} = e^{j(2\pi(f_s+f_r)t)} + e^{-j(2\pi(f_s+f_r)t)} + e^{j(2\pi(f_s-f_r)t)} + e^{-j(2\pi(f_s-f_r)t)} \quad \textbf{(3.42)}$$

The dispersion term is found using equation (2.13) for each frequency component in (3.42). Reading the terms from left to right in (3.42) the associated phase shift terms are $\phi_{D,UU}$, $\phi_{D,LU}$, $\phi_{D,UL}$, and $\phi_{D,LL}$, where the L and U subscripts indicate the lower and upper sidebands of the carrier and subcarrier, respectively.

$$D_S(f_s + f_r) = D_S(-f_s - f_r) = \phi_{D,UU} = \phi_{D,LU} = \phi_{DU} \quad \textbf{(3.43)}$$

$$D_S(f_s - f_r) = D_S(-f_s + f_r) = \phi_{D,UL} = \phi_{D,LL} = \phi_{DL} \quad \textbf{(3.44)}$$

Equations (3.43) and (3.44) show that the dispersion induced phase shift is the same for the upper and lower sidebands of the optical carrier and are only differentiated by the subcarrier sideband frequency. The signal at the end of the fiber is

$$S_{F,DD} = e^{j(2\pi(f_s+f_r)t+\phi_{DU})} + e^{-j(2\pi(f_s+f_r)t-\phi_{DU})} + e^{j(2\pi(f_s-f_r)t+\phi_{DL})} + e^{-j(2\pi(f_s-f_r)t-\phi_{DL})} \quad \textbf{(3.45)}$$

After adding a strong LO with the same frequency as the optical carrier, photodetection, and removing the DC and double frequency terms, the received signal is

$$\begin{aligned} I_P = {} & e^{j(2\pi(f_s+f_r)t+\phi_{DU})} + e^{-j(2\pi(f_s+f_r)t-\phi_{DU})} + e^{j(2\pi(f_s-f_r)t+\phi_{DL})} + e^{-j(2\pi(f_s-f_r)t-\phi_{DL})} + \\ & e^{-j(2\pi(f_s+f_r)t+\phi_{DU})} + e^{j(2\pi(f_s+f_r)t-\phi_{DU})} + e^{-j(2\pi(f_s-f_r)t+\phi_{DL})} + e^{j(2\pi(f_s-f_r)t-\phi_{DL})} \end{aligned} \quad \textbf{(3.46)}$$

$$\begin{aligned} I_P = {} & e^{j2\pi(f_s+f_r)t}\left(e^{j\phi_{DU}} + e^{-j\phi_{DU}}\right) + e^{-j2\pi(f_s+f_r)t}\left(e^{j\phi_{DU}} + e^{-j\phi_{DU}}\right) + \\ & e^{j2\pi(f_s-f_r)t}\left(e^{j\phi_{DU}} + e^{-j\phi_{DL}}\right) + e^{-j2\pi(f_s-f_r)t}\left(e^{j\phi_{DU}} + e^{-j\phi_{DL}}\right) \end{aligned} \quad \textbf{(3.47)}$$

$$\begin{aligned} I_P = {} & \left(e^{j2\pi(f_s+f_r)t} + e^{-j2\pi(f_s+f_r)t}\right)\left(e^{j\phi_{DU}} + e^{-j\phi_{DU}}\right) + \\ & \left(e^{j2\pi(f_s-f_r)t} + e^{-j2\pi(f_s-f_r)t}\right)\left(e^{j\phi_{DL}} + e^{-j\phi_{DL}}\right) \end{aligned} \quad \textbf{(3.48)}$$

In equation (3.48), it is once again clear that both the LSB and USB experience a power penalty during the photodetection process that cannot be removed in the RF domain. Using the approximation established in Section 3.3.1 because $r \ll 1$, (3.48) can be simplified using $\phi_D \approx \phi_{DU} \approx \phi_{DL}$.

$$I_P = \left(e^{j2\pi(f_s+f_r)t} + e^{-j2\pi(f_s+f_r)t} + e^{j2\pi(f_s-f_r)t} + e^{-j2\pi(f_s-f_r)t}\right)\left(e^{j\phi_D} + e^{-j\phi_D}\right) \quad \textbf{(3.49)}$$

$$I_P = 2\left(e^{j2\pi(f_s+f_r)t} + e^{-j2\pi(f_s+f_r)t} + e^{j2\pi(f_s-f_r)t} + e^{-j2\pi(f_s-f_r)t}\right)\cos(\phi_D) \qquad \textbf{(3.50)}$$

The power penalty is again the cosine of the dispersion induced phase shift of the subcarrier. This power penalty occurs during the photodetection process and the RF demodulation technique, whether it is envelope, homodyne or heterodyne detection, will not be able to remove the penalty. After RF demodulation the received data waveform is

$$I_{EH} = 8\cos(\phi_D)\cos(2\pi f_r t) \qquad \textbf{(3.51)}$$

The factor of two between (3.51) and the SSB subcarrier result seen in equation (3.38) is because both initial signals were normalized so each frequency component of the data has an amplitude of one, and the DSB subcarrier case has twice as many frequency components. If the total input magnitude of the data signal is normalized to one (as in the simulations) then all four cases above ((3.16), (3.23), (3.38) and (3.51)) have the same scaling factors.

Section 3.6. Power Fading and Pulse Broadening

The power fading shown in the DSB carrier and subcarrier cases above are directly related to the pulse broadening seen in systems subject to chromatic dispersion. Pulse broadening imposes distance-bandwidth limits on the system that can be extended through the use of dispersion compensating techniques and has been very well documented in the literature [25]. This limit is, however, based on the bandwidth of the data signal which is much smaller than the subcarrier frequency. The distance that power fading occurs is related to the

subcarrier frequency and therefore occurs at much shorter distances than the pulse-broadening limit.

The power fading is a cyclic phenomenon in which the distance to the first null (100% power penalty) can be found by solving equation (2.13) for length and setting a phase shift of $D_S(f_s) = \pi/2$ since $\cos(\pi/2) = 0$. Also, the normalized length is equal to the phase shift.

$$L_{null} = \frac{c}{2Df_S^2\lambda^2} \tag{3.52}$$

$$z_{null} = \frac{\pi}{2} \tag{3.53}$$

This equation finds the null for the subcarrier, but since the signal bandwidth is assumed to be small compared to the subcarrier frequency, the entire signal will experience a null at the same distance. This is in contrast to a radio-over-fiber signal that is not a SCM system, where dispersion will cause the spectral power to have nulls at certain frequencies for a given distance. The phenomenon occurs for any DSB SCM optical system, and as the SC frequency increases, the distance to the first null decreases. For instance, a signal using a 60-GHz subcarrier will have its first null at 1 km, while a 15-GHz subcarrier has it's first null at 16.3 km, both for 1550-nm wavelength carriers on standard single-mode fiber.

The power fading is most detrimental where simply designing the RF demodulator correctly cannot mediate the problem. This is the case for both of the DSB optical carrier scenarios. By looking at equations (3.35) and (3.45) one sees that each sideband has the full strength of the electric field, and that the

power penalty does not occur until the photodetection process. The photodetection process causes each sideband to add together using superposition. However, since each sideband has a different phase shift (opposite sign phase shift) the two sidebands are out of phase. When this phase offset is $\pi/2$, a null occurs; when the phase shift causes a time delay on the order of the bit period a pulse distortion occurs.

If the power fading can be eliminated from the system then pulse broadening will become the limiting factor. A common rule of thumb measurement is that dispersion will cause intersymbol interference (ISI) when the chromatic dispersion causes the bits to spread beyond 25% of the bit period [8]. Other authors use different metrics to define the bandwidth-distance limit of a system [11,25] but the 25% rule is comparable to the discussion above. This dispersion limit is a length that depends on the dispersion parameter of the fiber, the bandwidth of the data signal and the bit period, it does not depend on the subcarrier frequency. Allowing up to a 25% pulse spreading leads to a pulse spreading limited length of L_{ISI} [8].

$$L_{ISI} = \frac{0.3927c}{DR^2\lambda^2} \qquad \textbf{(3.54)}$$

Equation (3.54) is for a SSB subcarrier signal and R is the frequency component at the bit rate. Next it is important to see the relation of the power fading limit to the pulse spreading limit. Specifically, it is interesting to know how much further a signal could travel if the power fading impairments were removed. γ is defined as the ratio of the power fading limit to the pulse spreading limit. This is useful when defining the fiber lengths used in the simulation.

$$\gamma = \frac{L_{ISI}}{L_{null}} \tag{3.55}$$

Substituting equations (3.52) and (3.55), γ is

$$\gamma = \frac{0.8 f_s^2}{R^2} \tag{3.56}$$

and using the definition of r from equation (2.2)

$$\gamma = \frac{4}{5r^2} \tag{3.57}$$

When the data is modulated with a SSB format, then the pulses will spread $1/\sqrt{2}$ half as fast since they have half the bandwidth. For a SSB subcarrier signal γ is found to be

$$\gamma = \frac{4\sqrt{2}}{5r^2} = \frac{1.13}{r^2} \tag{3.58}$$

So for a typical DSB subcarrier signal ($r = 0.05$), the first power null occurs $z = \pi/2$, but if that is eliminated then ISI becomes a problem at $z = 160\pi$, or a full 320 times as far. For a SSB subcarrier system ISI becomes a problem at $z = 226\pi$, 452 times further than the first null would have occurred. The γ factors above are for a SSB optical carrier. When the optical carrier is DSB the distance is much shorter since the upper and lower sidebands still have differential phase shifts with opposite signs. Clearly an optical subcarrier system is limited not by pulse broadening but by power fading and a solution to eliminate or reduce the power fading needs to be implemented.

Section 3.7. Dual-Frequency Optical Local Oscillator

In order to avoid the power fading that is caused by the superposition of out of phase upper and lower sidebands, the phase of each sideband needs to be adjusted to match each other. Several approaches have been proposed in the literature that negate the power fading. This is done by a variety of methods that include transmitting an optically SSB signal [2,4,5,34,36], using coherent detection in a manner that eliminates one of the sidebands [3,37] or other optical phase correction techniques [38]. Use of a dual frequency LO with independent control of the phase of each frequency to eliminate the power fading is introduced in this dissertation and in [6,7]. The technique avoids the 3-dB power loss experienced when one sideband is removed as most of the previous methods use to avoid the power fading, and it also avoids needing to place compensation within the optical link.

In order to compensate the bulk phase shift, optical coherent detection will be used. Since the upper and lower sidebands have different phase shifts the local oscillator will need to address each sideband independently. An optical source that is modulated with a sinusoidal RF input at the subcarrier frequency will create a dual-frequency LO. If the phase of the optical source and the RF sinusoid are independently controlled then the USB and LSB of the LO can have opposite phase shift signs. This is exactly the LO needed to compensate for the dispersion induced phase error of a DSB SC. A diagram illustrating the structure of the LO and receiver is given in Figure 3.9

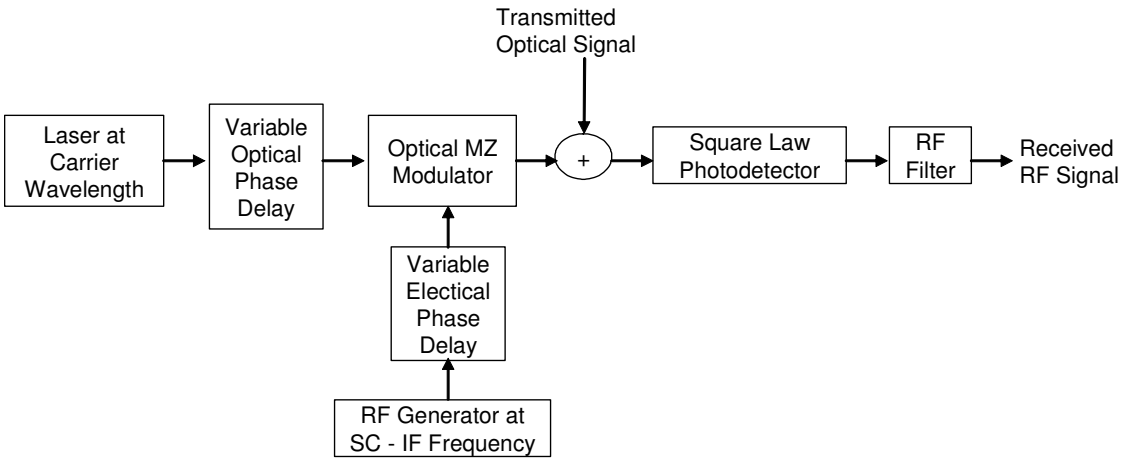

Figure 3.9: Optical LO with Sinusoidal Modulation in Coherent Receiver

Initial defining of the local oscillator should be done at the optical frequency, not baseband, in order to fully understand the mathematics involved. The optical LO is defined as

$$S_{LO} = \left(e^{j(2\pi f_\lambda t+\phi_{LO})} + e^{-j(2\pi f_\lambda t+\phi_{LO})}\right)\left(e^{j(2\pi f_s t+\phi_s)} + e^{-j(2\pi f_s t+\phi_s)}\right) \quad \textbf{(3.59)}$$

ϕ_{LO} is the phase of the optical source and ϕ_s is the phase of the RF sinusoid at the SC frequency. Manipulation of equation (3.59) leads to

$$S_{LO} = e^{j(2\pi(f_\lambda+f_s)t+\phi_{LO}+\phi_s)} + e^{j(2\pi(f_\lambda-f_s)t+\phi_{LO}-\phi_s)} + e^{-j(2\pi(f_\lambda+f_s)t+\phi_{LO}+\phi_s)} + e^{-j(2\pi(f_\lambda-f_s)t+\phi_{LO}-\phi_s)} \quad \textbf{(3.60)}$$

In cosine notation this is

$$S_{LO} = 2\cos(2\pi(f_\lambda + f_s)t + \phi_{LO} + \phi_s) + 2\cos(2\pi(f_\lambda - f_s)t + \phi_{LO} - \phi_s) \quad \textbf{(3.61)}$$

It is clear that both frequency components of the optical LO have different phase shifts that can be independently controlled. By being able to lock these independent phase shifts appropriately to the incoming optical signal, the power penalty is avoided. Referring back to equation (3.60) , we can write the LO in baseband representation. This is done merely to simplify the equations below. For the derivation at the optical frequency see Appendix E.

$$S_{LO} = e^{j(2\pi f_s t + \phi_{LO} + \phi_s)} + e^{-j(2\pi f_s t + \phi_{LO} - \phi_s)} \quad \textbf{(3.62)}$$

Optical coherent detection was described above and defined in equation (2.32), which is repeated here for convenience.

$$I_P = \left(S_{sig} + S_{LO}\right)\left(S_{sig}^* + S_{LO}^*\right) \quad \textbf{(3.63)}$$

Using equation (3.35) as S_{sig} and equation (3.62) as the LO, the output of the photodetector, before any simplification is

$$\begin{aligned} I_P = &\left(e^{j(2\pi(f_s+f_r)t+\phi_D)} + e^{-j(2\pi(f_s+f_r)t-\phi_D)} + e^{j(2\pi f_s t+\phi_{LO}+\phi_s)} + e^{-j(2\pi f_s t+\phi_{LO}-\phi_s)}\right)\bullet \\ &\left(e^{-j(2\pi(f_s+f_r)t+\phi_D)} + e^{j(2\pi(f_s+f_r)t-\phi_D)} + e^{-j(2\pi f_s t+\phi_{LO}+\phi_s)} + e^{j(2\pi f_s t+\phi_{LO}-\phi_s)}\right) \end{aligned} \quad \textbf{(3.64)}$$

Since simplifying this equation is the key element of compensating the power loss experienced in DSB SC optical system, the steps will be briefly summarized below. First, the multiplication needs to be carried out. Since only terms at the data rate are relevant, and higher order terms, such as double subcarrier frequency terms, will be filtered out by either the photodetector itself or a low pass electrical filter, only the terms at $\pm 2\pi f_r$ need to be carried along. This leaves 4 terms in the photocurrent equation.

$$I_P = e^{-j(2\pi f_r t+\phi_D-\phi_{LO}-\phi_s)} + e^{j(2\pi f_r t+\phi_D-\phi_{LO}-\phi_s)} + e^{-j(2\pi f_r t-\phi_D+\phi_{LO}+\phi_s)} + e^{j(2\pi f_r t-\phi_D+\phi_{LO}+\phi_s)} \quad \textbf{(3.65)}$$

Each exponential above contains the term $2\pi f_r t - \phi_s$, so that can be factored out and the equation can be rewritten as

$$\begin{aligned} I_P = &e^{-j(2\pi f_r t-\phi_s)}e^{j(\phi_{LO}-\phi_D)} + e^{j(2\pi f_r t-\phi_s)}e^{-j(\phi_{LO}-\phi_D)} + \\ &e^{-j(2\pi f_r t-\phi_s)}e^{-j(\phi_{LO}-\phi_D)} + e^{j(2\pi f_r t-\phi_s)}e^{j(\phi_{LO}-\phi_D)} \end{aligned} \quad \textbf{(3.66)}$$

By recognizing the trigonometric identity $e^{-j(x)} + e^{j(x)} = 2\cos(x)$ it is useful to regroup equation (3.66) as

$$I_P = e^{-j(2\pi f_r t-\phi_s)}\left(e^{j(\phi_{LO}-\phi_D)} + e^{-j(\phi_{LO}-\phi_D)}\right) + e^{j(2\pi f_r t-\phi_s)}\left(e^{j(\phi_{LO}-\phi_D)} + e^{-j(\phi_{LO}-\phi_D)}\right) \quad \textbf{(3.67)}$$

$$I_P = \left(e^{-j(2\pi f_r t-\phi_s)} + e^{j(2\pi f_r t-\phi_s)}\right)\left(e^{j(\phi_{LO}-\phi_D)} + e^{-j(\phi_{LO}-\phi_D)}\right) \quad \textbf{(3.68)}$$

By applying the trigonometric identity stated above, the photocurrent simplifies to

$$I_P = 4\cos(2\pi f_r t - \phi_s)\cos(\phi_{LO} - \phi_D) \quad \textbf{(3.69)}$$

Equation (3.69) clearly shows that by independently controlling the phase of the optical source and RF subcarrier of the LO, the dispersion induced power penalty can be avoided. The local oscillator phase, ϕ_{LO}, is used to compensate for the dispersion induced phase, ϕ_D, and the subcarrier phase, ϕ_s, should be locked to the signal phase. Remember that the signal phase is assumed to be zero, meaning it is the reference phase, so ϕ_s should be set to this reference.

The above analysis was carried out at baseband assuming that the optical carrier and RF subcarriers are suppressed. In the numerical study using MATLAB® in Chapter 4 these assumptions are relaxed and non-suppressed carriers with modulation indexes less than 100% are used. Since filtering is used to remove the carriers and gain is used to compensate for less than unity modulation index, the above results are equivalent to the results found in the numerical model.

The very same steps used to perform the optical homodyne detection with the dual frequency LO above are used to analyze optical heterodyne detection. In this case the sinusoid on the LO is not modulated at the same frequency as the subcarrier, but at some offset equal to the intermediate frequency.

$$f_{IF} = f_s - f_{slo} \quad \textbf{(3.70)}$$

where f_{slo} is the frequency of the RF sinusoid used to modulate the optical LO. The resulting photocurrent in the heterodyne case becomes

$$I_P = 8\cos(2\pi f_{IF} t + 2\pi f_r t - \phi_s)\cos(\phi_{LO} - \phi_D) \quad \textbf{(3.71)}$$

Again the power penalty is controlled by phase locking the LO to the dispersion induced phase, however the information bearing signal needs to be electrically demodulated from the intermediate frequency. This can be done either with RF coherent or envelope detection if the subcarrier has not been suppressed. Both methods are demonstrated numerically in Chapter 4.

Of the methods found in literature used to avoid the power fading due to dispersion, the dual-frequency LO with phase control most closely resembles that used by Kuri et al in [3,37]. That technique uses a dual frequency optical LO where the frequency spacing is equal to the subcarrier frequency and is used to simultaneously detect the carrier and one subcarrier (the USB in the articles). It does not correct for the phase difference between the subcarriers but rather eliminates one subcarrier and thus effectively detects a single sideband system. Such a technique will have a 3-dB power loss compared to the technique described in this section where both the USB and LSB are detected and included in the final photocurrent. In [37] the authors propose that their technique is immune to phase noise of the LO and source so a network operator would have to consider the trade-offs between noise and power loss. The RF portion of the receiver design is also more complex than that required for the dual-frequency LO proposed here so that would also need to be considered when constructing a network.

Another similar technique found in the literature [1,39,40] is remote heterodyne detection. This technique uses the same source for the signal and the LO and both are transmitted together and mixed in the remote photodetector to perform the heterodyning. In this way, a 'remote LO' can be created that has the required relative phase shift between the upper and lower sidebands. It does require, however, that the distance is limited such that the signal and the remote LO do not walk-off from each other due to the dispersion. A large time delay between the LO and signal causes a great increase in the phase noise of the heterodyned signal. It also moves the complexity to the transmitter, which may not be desired by the network.

Section 3.8. Phase Noise Implications

In any detection technique phase noise is a concern since it translates to intensity noise during photodetection. A low noise LO needs to be used, and the design of a low-noise dual-frequency laser has been considered possible in the literature [41]. The use of a dual-frequency local oscillator where the phase is carefully controlled to eliminate the phase shift effects of dispersion shown above does not include any phase noise on the source laser or the optical LO. In reality both the source and LO lasers will have some non-zero linewidth due to the phase noise as described in Section 2.2.5. The impact of the phase noise on the final received signal can be examined analytically by assuming a Gaussian random variable to represent the phase of the source laser and LO. This phase noise will lead to an amplitude noise during the photodetection process and therefore a finite SNR of the photocurrent.

A Gaussian random term is included in both the equation for the source laser (2.5) and the local oscillator laser (3.59). The analysis for the dispersion and photodetection is then repeated including the random phase terms Q_s and Q_{LO} for the source and LO, respectively. For this analysis a DSB carrier with SSB subcarrier that is optically homodyne detected is evaluated. The same analysis can be carried out for DSB subcarriers and also for optical heterodyne detection with the same conclusions.

The USB-subcarrier signal at the input of the fiber is

$$S_0 = \left(e^{j(2\pi f_\lambda t + Q_s)} + e^{-j(2\pi f_\lambda t + Q_s)}\right)\left(e^{j(2\pi(f_s+f_r)t)} + e^{-j(2\pi(f_s+f_r)t)}\right) \quad \textbf{(3.72)}$$

After the dispersion (ϕ_D) is included, the signal at the end of the fiber is

$$\begin{aligned} S_F = {} & e^{j(2\pi(f_\lambda+f_s+f_r)t+Q_s+\phi_D)} + e^{j(2\pi(f_\lambda-f_s-f_r)t+Q_s+\phi_D)} + \\ & e^{-j(2\pi(f_\lambda-f_s-f_r)t+Q_s+\phi_D)} + e^{-j(2\pi(f_\lambda+f_s+f_r)t+Q_s-\phi_D)} \end{aligned} \quad \textbf{(3.73)}$$

The dual frequency LO with phase noise is given by

$$S_{LO} = \left(e^{j(2\pi f_\lambda t + Q_{LO}+\phi_{LO})} + e^{-j(2\pi f_\lambda t + Q_{LO}+\phi_{LO})}\right)\left(e^{j(2\pi f_s t+\phi_s)} + e^{-j(2\pi f_s t+\phi_s)}\right) \quad \textbf{(3.74)}$$

$$\begin{aligned} S_{LO} = {} & e^{j(2\pi(f_\lambda+f_s)t+Q_{LO}+\phi_{LO}+\phi_s)} + e^{j(2\pi(f_\lambda-f_s)t+Q_{LO}+\phi_{LO}-\phi_s)} + \\ & e^{-j(2\pi(f_\lambda-f_s)t+Q_{LO}+\phi_{LO}-\phi_s)} + e^{-j(2\pi(f_\lambda+f_s)t+Q_{LO}+\phi_{LO}+\phi_s)} \end{aligned} \quad \textbf{(3.75)}$$

Once the signal and LO are correctly written with the phase noise term included, a baseband representation can be extracted and used for the remainder of the analysis. The baseband representations for the signal and the LO are

$$S_F = e^{j(2\pi(f_s+f_r)t+Q_s+\phi_D)} + e^{-j(2\pi(f_s+f_r)t-Q_s-\phi_D)} \quad \textbf{(3.76)}$$

$$S_{LO} = e^{j(2\pi f_s t+Q_{LO}+\phi_{LO}+\phi_s)} + e^{-j(2\pi f_s t-Q_{LO}-\phi_{LO}+\phi_s)} \quad \textbf{(3.77)}$$

Equations (3.76) and (3.77) are substituted into (3.63) to perform the coherent detection and find the resulting photocurrent. Keeping only the terms related to the data (removing the DC and double frequency components) the received signal is

$$I_P = e^{j(2\pi f_r t + Q_s - Q_{LO} + \phi_D - \phi_{LO} - \phi_s)} + e^{-j(2\pi f_r t - Q_s + Q_{LO} - \phi_D + \phi_{LO} - \phi_s)} + e^{-j(2\pi f_r t + Q_s - Q_{LO} + \phi_D - \phi_{LO} - \phi_s)} + e^{j(2\pi f_r t - Q_s + Q_{LO} - \phi_D + \phi_{LO} - \phi_s)} \quad \textbf{(3.78)}$$

By factoring out the $(\phi_{LO} - \phi_D)$ and the $(Q_{LO} - Q_s)$ terms and carrying out some simple algebraic manipulations the photocurrent can be rewritten as

$$I_P = \left(e^{j(2\pi f_r t - \phi_s)} + e^{-j(2\pi f_r t - \phi_s)}\right)\left(e^{j(Q_{LO} - Q_s + \phi_{LO} - \phi_D)} + e^{j(Q_{LO} - Q_s + \phi_{LO} - \phi_D)}\right) \quad \textbf{(3.79)}$$

$$I_P = 4\cos(2\pi f_r t - \phi_s)\cos(Q_{LO} - Q_s + \phi_{LO} - \phi_D) \quad \textbf{(3.80)}$$

By applying the same control to the phases of the dual-frequency LO as used above this can be simplified further. The phase of the sinusoid (ϕ_s) is locked to that of the optical carrier, which is the reference phase for all analysis and simulations, so $\phi_s = 0$. Likewise, the phase of the LO is controlled in order to eliminate the power fading due to the dispersion, $\phi_{LO} = \phi_D$. When this is done, the optimized photocurrent is

$$I_P = 4\cos(2\pi f_r t)\cos(Q_{LO} - Q_s) \quad \textbf{(3.81)}$$

It is clear that the phase noises of the source and the LO lead to an amplitude noise after photodetection. The amplitude fluctuation is the cosine of the sum of two Gaussians, which it itself Gaussian. Since the phase-lock loop is used to maximize the power by locking the phase of the LO to that of the signal,

the mean of Q_{LO} will track the mean of Q_s and therefore both Q_{LO} and Q_s can be modeled as zero-mean Gaussian random variables. A new term can be introduced, Q_T, that represents the total noise present in the photocurrent. Assuming a perfect PLL, the mean and standard deviation of Q_T, μ_T and σ_T, are

$$\mu_T = \mu_{LO} - \mu_s = 0 \tag{3.82}$$

$$\sigma_T = \sqrt{\sigma_{LO}^2 + \sigma_s^2} \tag{3.83}$$

If the PLL is not ideal then $\mu_T \neq 0$ and this offset will introduce a power loss that reduces the signal and the noise. When finding the SNR due to the phase noise, the factor of four can be eliminated from equation (3.81) since it scales both the noise and the signal equally. The received power is proportional to the square of the photocurrent, so neglecting any proportionality constants,

$$P_R = I_P^2 = \cos^2(2\pi f_r t)\cos^2(Q_T) \tag{3.84}$$

$$P_R = \cos^2(2\pi f_r t)\left(1 - \sin^2(Q_T)\right) = \cos^2(2\pi f_r t) - \cos^2(2\pi f_r t)\sin^2(Q_T) \tag{3.85}$$

Here the signal is the term before the minus sign and the noise is the term after the minus sign, therefore the SNR is written as

$$SNR = \frac{\left\langle \cos^2(2\pi f_r t)\right\rangle}{\left\langle \cos^2(2\pi f_r t)\right\rangle\left\langle \sin^2(Q_T)\right\rangle} = \frac{1}{\left\langle \sin^2(Q_T)\right\rangle} \tag{3.86}$$

Since we know that Q_T is zero mean, and we assume that the lasers have low noise, we can use the small angle approximation, $\sin(Q_T) \approx Q_T$, to further simplify (3.86). Also realizing that the noise power is the variance of the signal,

$$SNR \approx \frac{1}{\left(\sigma_T^2\right)} \tag{3.87}$$

This is the electrical SNR ratio while σ_T^2 is the variance of the optical phase noise. It is very important to realize that the variance here needs to be found only over the bandwidth of the receiver. This relation can be useful when doing a simulation and the optical phase noise is known and knowledge of the electrical SNR is desired. It could also be used to find the optical phase noise from the detected SNR assuming that all other noise sources are known. The electrical SNR is related to the Q measurement defined in Section 2.3 by [31]

$$Q = \sqrt{SNR} \tag{3.88}$$

Since the work presented in this dissertation is concerned with the phase effects of dispersion on OSCM the phase noise is important to the analysis. However in real systems many other sources of noise are present in the photocurrent and the SNR defined above is not the total SNR [10,11,15]. Since those noise sources have been well documented in the literature for many years, and since they do not impact the simulations or analysis they are not included here.

In order to determine if the phase noise of the dual-frequency LO is more detrimental to the system than a direct detection or conventional coherent detection system the SNR needs to be calculated for each of these systems as well. Since we are considering OSCM systems and it has been established that DSB carrier OSCM systems experience dispersion induced power fading, the meaningful comparison will be to compare the SNR in equation (3.87) to the SNR of a SSB optical carrier system that also avoids dispersion induced power fading. First, the coherent detection system will be analyzed. As above, the carrier can

be suppressed in this technique, and the LO should be locked to the optical carrier frequency for homodyne detection. The signal at the input to the fiber is

$$S_0 = e^{j(2\pi(f_\lambda+f_s+f_r)t+Q_s)} + e^{-j(2\pi(f_\lambda+f_s+f_r)t+Q_s)} + e^{j(2\pi(f_\lambda+f_s-f_r)t+Q_s)} + e^{-j(2\pi(f_\lambda+f_s-f_r)t+Q_s)} \quad \textbf{(3.89)}$$

and the baseband representation is

$$S_0 = e^{j(2\pi(f_s+f_r)t+Q_s)} + e^{j(2\pi(f_s-f_r)t+Q_s)} \quad \textbf{(3.90)}$$

At the end of the fiber, the dispersion term (ϕ_D) is included and the result is S_F.

$$S_F = e^{j(2\pi(f_s+f_r)t+Q_s+\phi_D)} + e^{j(2\pi(f_s-f_r)t+Q_s+\phi_D)} \quad \textbf{(3.91)}$$

This is then mixed with a single frequency LO at the optical wavelength. The baseband representation of this with the phase noise included is simply

$$S_{LO} = e^{jQ_{LO}} \quad \textbf{(3.92)}$$

Keeping only the terms at the subcarrier frequency by removing the DC and double frequency components, the photocurrent is

$$I_P = e^{j(2\pi(f_s+f_r)t+\phi_D+Q_s-Q_{LO})} + e^{-j(2\pi(f_s+f_r)t+\phi_D+Q_s-Q_{LO})} + e^{j(2\pi(f_s-f_r)t+\phi_D+Q_s-Q_{LO})} + e^{-j(2\pi(f_s-f_r)t+\phi_D+Q_s-Q_{LO})} \quad \textbf{(3.93)}$$

After electrical homodyne detection of this signal, with appropriate RF LO phase control to eliminate the distortion caused by the dispersion term as described above, the data signal at baseband is

$$I_P = e^{j(2\pi f_r t+Q_s-Q_{LO})} + e^{-j(2\pi f_r t+Q_s-Q_{LO})} + e^{j(2\pi f_r t-Q_s+Q_{LO})} + e^{-j(2\pi f_r t-Q_s+Q_{LO})} \quad \textbf{(3.94)}$$

As in the case above, the $(Q_{LO}-Q_s)$ term can be factored out and the photocurrent can be rewritten in cosine notation.

$$I_P = 4\cos(2\pi f_r t)\cos(Q_{LO}-Q_s) \quad \textbf{(3.95)}$$

So in conventional coherent detection of a SSB optical carrier using a single frequency LO, the final photocurrent is the same as that for the dual-frequency LO homodyne detection of a DSB carrier, with the same SNR penalty due to the phase noise. It should be noted that the same results are found when a DSB carrier signal is coherently detected at distances where no power loss is found (i.e. when z is a multiple of π).

Direct detection of a SSB optical carrier is evaluated in a similar fashion. In this case the carrier cannot be suppressed. It is important here to realize that the subcarrier is time-delayed from the carrier according to equation (2.27), where the delay is inversely proportional to the subcarrier frequency rather than the frequency component of the data. For this a phase noise term (Q_s^τ) is introduced that has the same mean and variance as the source phase noise (Q_s), but is time delayed according to the bulk dispersion. The signal at the end of the fiber is (after a DC block and $1/\mu$ gain)

$$S_F = e^{jQ_s} + \mu e^{jQ_s^\tau}\left(e^{j(2\pi(f_s+f_r)t+\phi_D)} + e^{j(2\pi(f_s-f_r)t+\phi_D)}\right) \qquad \textbf{(3.96)}$$

This is then squared within the photodetector according to equation (2.27) and the resulting current is

$$\begin{aligned} I_P = {} & e^{j\left(2\pi(f_s+f_r)t+\phi_D+Q_s-Q_s^\tau\right)} + e^{-j\left(2\pi(f_s+f_r)t+\phi_D+Q_s-Q_s^\tau\right)} + \\ & e^{j\left(2\pi(f_s-f_r)t+\phi_D+Q_s-Q_s^\tau\right)} + e^{-j\left(2\pi(f_s-f_r)t+\phi_D+Q_s-Q_s^\tau\right)} \end{aligned} \qquad \textbf{(3.97)}$$

Using RF homodyne detection with the appropriate phase and gain, and simplifying in the same manor as above, the baseband data signal is

$$I_P = 4\cos(2\pi f_r t)\cos(Q_s^\tau - Q_s) \qquad \textbf{(3.98)}$$

Q_s and Q_s^τ are not independent random processes since one is just the delayed version of the other. Since both Q_s and Q_s^τ are random walk variables their mean drifts over time so we are assuming that any drift is slow and therefore $\mu_s - \mu_s^\tau \approx 0$, and therefore no power loss is experienced due to the overall drift of the source phase. Also, any difference between the means of phase of the carrier and subcarrier produces a slow varying phase shift that can be tracked with the PLL of the RF LO. The noise power is due to the phase variance over a bit period and the total variance is given by

$$\sigma_T = \sqrt{\left(\sigma_s^\tau\right)^2 + \left(\sigma_s\right)^2} = \sqrt{\sigma_s^2 + \sigma_s^2} = \sigma_s\sqrt{2} \qquad \textbf{(3.99)}$$

This assumes that enough dispersion has accumulated to make Q_s and Q_s^τ uncorrelated. So, if the phase variance of the source and the optical LO above are the same, the direct detection and coherent detection have the same SNR penalty due to phase noise. In all cases above, expect for the direct detection, the optical carrier has been suppressed. If phase noise is a concern then this is necessary since the inclusion of the carrier introduces a third noise term at DC after photodetection that greatly reduces the SNR [1]. This is especially true when a low modulation index is used and the optical carrier is therefore very strong.

Section 3.9. Chapter 3 Summary

In this chapter four variations of optical subcarrier multiplexed systems have been analyzed with respect to the adverse effects of dispersion. Dispersion

causes a phase shift of the subcarrier relative to the optical carrier in each of the four cases. If this phase shift is not corrected then each type of system will experience performance degradation.

Three of the four cases (DSB carrier with DSB or SSB subcarriers and SSB carrier with DSB subcarriers) result in a power penalty equal to the cosine of the phase shift, or normalized length. In the SSB carrier with DSB subcarrier system the power fading can be avoided by controlling the phase of the RF LO during demodulation of the RF signal. For both DSB carrier scenarios the dispersion induced phase shift must be corrected during the photodetection process in order to avoid power fading. The fourth system type, SSB carrier with SSB subcarrier, does not experience power fading but does experience signal distortion if the phase shift between the carrier and subcarrier is not corrected. Again, this phase shift can be corrected during the RF demodulation.

A new compensation technique that uses a dual-frequency optical LO with independent control of the phase of each frequency is presented in this chapter. This technique is used to compensate the different phase shifts of the USB and LSB sidebands in a DSB carrier system. The dual-frequency LO is constructed by simply sinusoidally modulating a laser and having feedback to control the phase of both the RF sinusoid and laser.

The impact that phase noise of the source and LO laser has on the system is analyzed and compared to the impact phase noise has on conventional direct and coherent detection systems. Phase noise is the most important noise source to consider for the dual-frequency LO receiver since control of the phase

is expressly what makes the technique work. Other noise sources are equivalent for this technique and conventional techniques, so they are not repeated here.

Chapter 4. Simulation and Modeling in MATLAB®

The previous chapter analyzed the impairments due to fiber dispersion in four different types of OSCM systems. Each system has distance limitations when the subcarrier dispersion is either compensated or uncompensated. The first limit is proportional to the subcarrier frequency and causes a cyclic power fading for DSB carrier or subcarrier systems. If the system is SSB carrier with SSB subcarrier, then uncompensated dispersion of the subcarrier can cause a signal distortion. It was seen in the previous chapter that these degradations occur over distances on the order of $z_{null} = \pi/2$. From Section 2.1, z is the normalized length corresponding to the distance at which the dispersion induced phase shift of the subcarrier frequency is z. It was also seen that the penalties are cyclic in nature with a fading cycle occurring every distance of $z = \pi$. The second dispersion limit is due to the bandwidth of the data signal, and since it is assumed that the bandwidth of the data is much less than the subcarrier frequency (their ratio, $r \ll 1$) the pulse broadening distance limit is on the order of $0.8/r^2$ to $1.13/r^2$ times greater than the power fading limit, depending on the modulation format. The sideband walk-off limit of a DSB carrier system is between these lengths and will be illustrated later in Section 4.5.

This chapter shows the results of numerical simulations performed in MATLAB® for the four OSCM systems presented in Chapter 3. The simulations use the normalized parameters defined in Section 2.1 so generalized trends can be observed. Occasionally a system will be simulated with typical system

parameters in order to illustrate a point and to put the results into perspective. Generally the distances simulated will be the shorter of the two limits; however, in cases where the dispersion due to the subcarrier frequency is compensated the second dispersion limit will be shown. Eye diagrams will be shown to visualize the system degradation due to dispersion. Q measurement curves will be plotted to show the performance trends related to distance, received power, phase variance and number of subcarriers. Since the phase noise and modulator nonlinearity are both signal dependant noises changing the received power will not affect the Q, and for this reason a small thermal noise will be added to the receiver. The thermal noise is modeled as an additive white Gaussian noise (AWGN) to the received photocurrent [15] such that at large received power the system is dominated by phase or modulator noise, but for low received power then thermal noise causes a Q penalty. Choosing a receiver noise variance of 0.01 ensures that the signal is phase noise dominated when the power loss is small. The phase and thermal noises are modeled as Gaussian random variables. Since the simulations do not count actual bit errors, but use Q (a measure of means and variances), these simulations are semi-analytic performance estimators [12].

Section 4.1. Simulation of Dispersion and Photodetection

Section 2.2.2 discusses the bulk dispersion model used for the analysis and the simulation. As stated above, in the analysis where discrete frequency components are evaluated the dispersion can be treated as a phase shift that can be calculated and applied in the time domain. In the simulation the signals

are not restricted to sinusoids but are PRBS data extrapolated to several samples-per-bit. These waveforms have a non-delta spectral content and therefore the dispersion needs to be addressed in the frequency domain as described in Section 2.2.2 [8]. The following block diagram illustrates the procedure used.

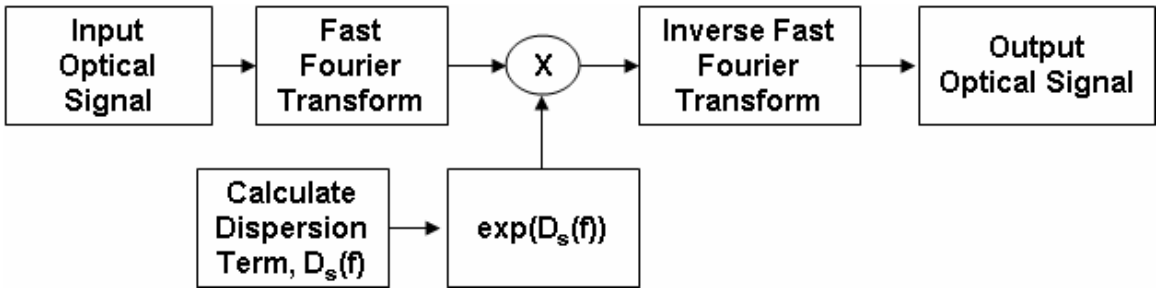

Figure 4.1: Fiber Dispersion Model

The dispersion term is a function of the frequency in a baseband model. Accordingly, $D_S(f=0)=0$, and the upper and lower sidebands of the carrier are symmetric, see Figure 3.5 for an example. This corresponds with the analysis where phase is measured relative to the optical carrier phase delay throughout propagation. The fast Fourier transform (FFT) and inverse FFT (IFFT) are MATLAB® commands that translate the signal from the time to the frequency domain and back.

As in the analysis, the photodetector is modeled as an ideal square-law device. In the simulation, however, the DC and high-order frequency terms are not dropped as they are in the analysis, but are filtered or removed by the RF demodulation techniques described in Section 2.2.7. The resulting photocurrent is a baseband PRBS waveform that is used to generate either an eye-diagram or

a Q measurement. Since the filters are not ideal, interchannel interference occurs that was not seen in the analysis.

When the Q measurement is performed in the simulation a few more aspects need to be addressed beyond the definition of Q given in Section 2.3. As was mentioned earlier, the Q measurement is based on the same bits that are included in the eye diagram in order to avoid the windowing effects of the simulation. Also, a true Q measurement needs to be taken at the same timing window within a bit that a one-zero decision is made. In practice a clock-recovery circuit is used to determine the optimal point to sample the bit to make a decision. In the simulation a routine is used to find the 15% of the eye that is the most open. Taking the samples from the 15% of the eye that is the most open, rather than a single sample at the very widest part, allows the simulation to model a timing jitter between the clock and data and also takes into account that the received signal is not a square wave, but a filtered waveform. This increases the variance measured in the waveform from that of a square wave so that for very low noise signals the measured Q will be lower than the ideal Q. This will be seen in the section on phase noise measurements. This is consistent with actual system measurements since timing jitter and filtering effects are present.

Section 4.2. Comparison of Four OSCM Systems

The simulation results shown in this section will compare how dispersion distorts of the four scenarios shown in Figure 2.1. In each case the signal is transmitted over a length of $z = \pi$, with plots shown for lengths of 0, π/4, π/2 and π. By transmitting over a length of π the cyclic nature of the signal can be seen.

When the power fading is eliminated the signal will also be shown for a distance where the ISI becomes an issue. In normalized form, the only parameters that need to be considered are the length, *z*, and the subcarrier to data ratio, *r*. *r* is 0.05 in the following eye-diagrams. For example, this could correspond to a 1-Gb/s signal on a 20-GHz subcarrier.

The equations used to represent the input signals are shown in (4.1) through (4.4). Each signal is demodulated using direct-detection and dual-frequency LO coherent detection followed by RF demodulation to achieve the baseband binary signal. Amplitude modulation is used in each case, with a modulation index of 0.1 for the optical carrier, and 0.33 for the subcarrier. The subcarrier modulation index is adjusted to represent the typical definition because the data, *m(t)* is defined as (0,1), rather than as (-1,1). Appropriate gains are applied in the receiver to ensure that the eye-opening is always unity at the fiber input.

While the equations used to model the four cases were discussed somewhat in Chapter 3 for sinusoidal signals a summary is given here. The first character of the subscript of the signal (S) denotes a DSB or SSB carrier ('D' or 'S') and the second character denotes a DSB or SSB subcarrier. Again, $m(t)$ denotes the PRBS data after filtering (not a sinusoid), and μ_s is the modulation index of the subcarrier signal onto the optical carrier. This section compares the dispersion effects on these four systems without phase noise and modulator nonlinearity which are covered in a later section. Multichannel OSCM systems are also covered in a following section.

$$S_{DD} = 1 + \mu_s \left(\left(1 + m(t) \right) \cos\left(2\pi f_s t \right) \right) \quad \textbf{(4.1)}$$

$$S_{DS} = 1 + \mu_s \left(1 + m(t) \cos\left(2\pi f_s t \right) - \hat{m}(t) \sin\left(2\pi f_s t \right) \right) \quad \textbf{(4.2)}$$

$$S_{SD} = 1 + \mu_s \left(1 + m(t) \right) e^{j2\pi f_s t} \quad \textbf{(4.3)}$$

$$S_{SS} = 1 + \mu_s \left(1 + m(t) + j\hat{m}(t) \right) e^{j2\pi f_s t} \quad \textbf{(4.4)}$$

Section 4.2.1. DSB Carrier with DSB Subcarrier

The first system modeled is the DSB carrier with DSB subcarrier. According to the analysis of Chapter 3 this system should have the poorest uncompensated performance since the DSB carrier will cause power fading and the DSB subcarrier will cause more pulse broadening than SSB subcarriers. The spectrum of this signal is shown in the following figure. The abscissa (1/r) is the ratio of the subcarrier frequency to the data rate.

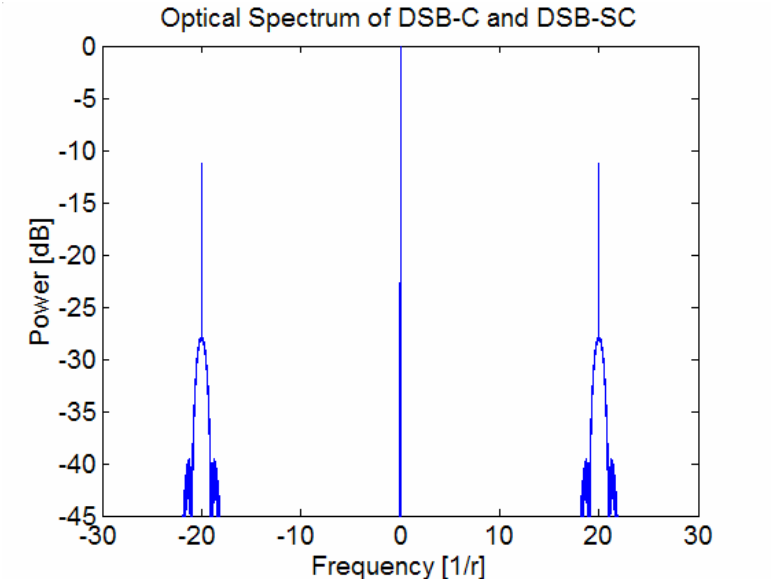

Figure 4.2: Input spectrum of signal with DSB-Carrier with SSB Subcarrier

The eye-diagrams for the direct detection signal are shown in Figure 2.1. As can be clearly seen there is an amplitude null at a length of $\pi/2$. Furthermore, the cyclic nature of the fading can be seen since the eye opening at a length of π is unity, the same as the input signal. The pulse does not experience any visible pulse broadening over this length. The signal as received with a dual-frequency LO is shown in Figure 4.4. No power fading is experienced when the phase of the LO laser is matched to the phase shift induced by the fiber dispersion.

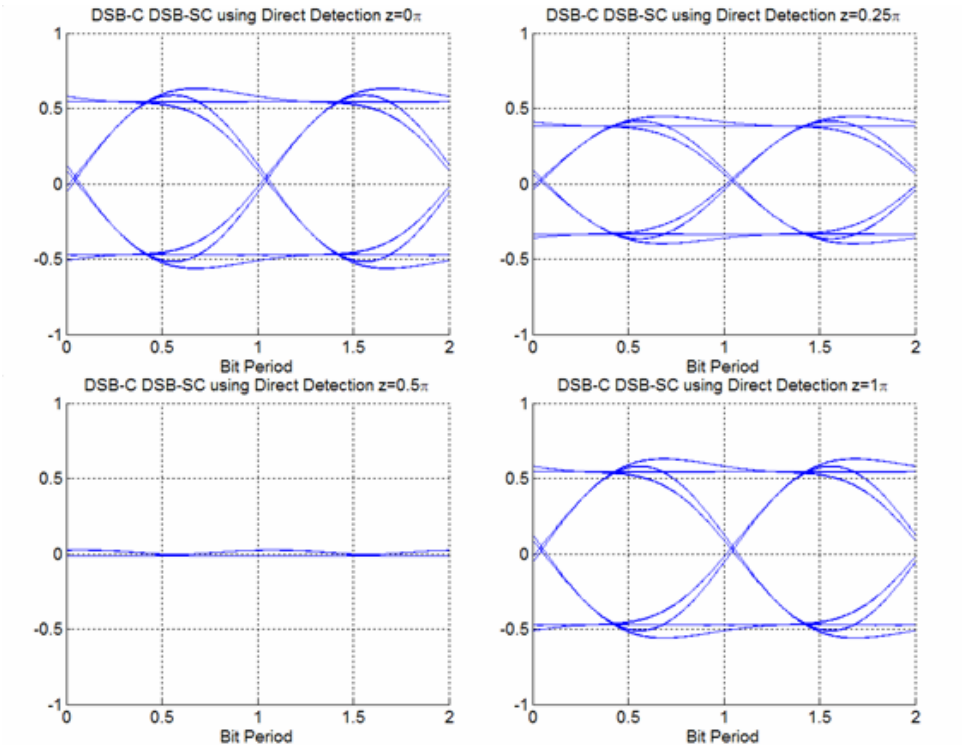

Figure 4.3: Eye-diagram for DSB-C with DSB-SC over a distance of π.

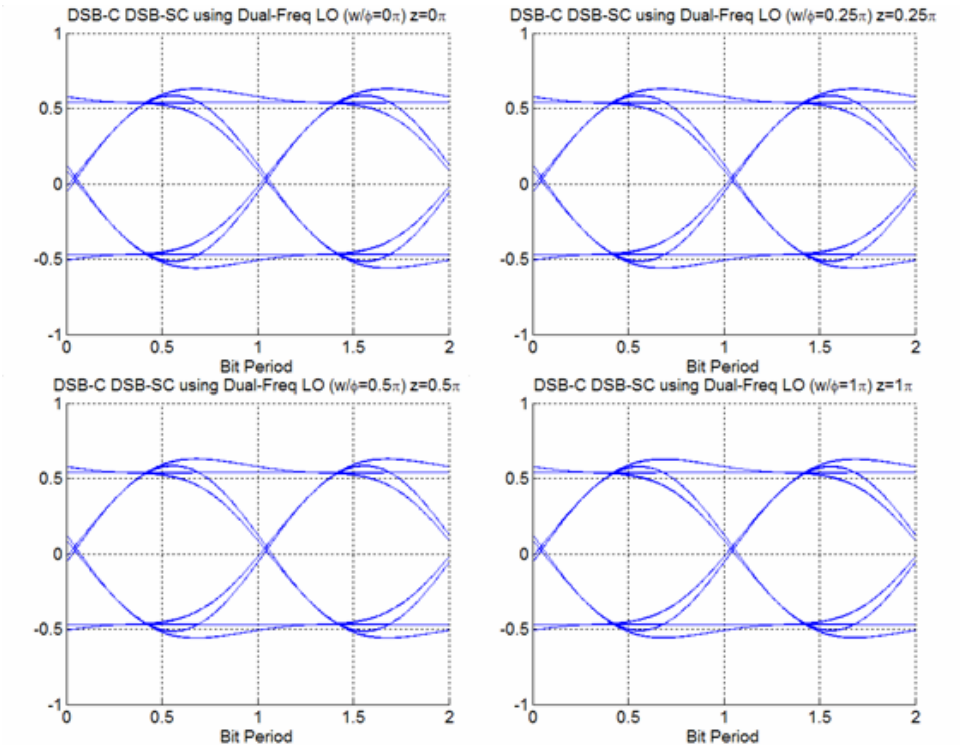

Figure 4.4: Compensated Eye-diagram for DSB-C with DSB-SC. The phase of the LO is given in the parenthesis of each heading.

The power loss occurs during the photodetection process as shown in the analysis. The spectrum of the signal immediately following the photodetector shows this loss before any further RF demodulation is done. This verifies that the signal cannot be recovered using strictly RF techniques. The figure below shows the spectrum immediately following the photodetector. A dotted line has been annotated to each plot to indicate the subcarrier and modulation peaks for the input signal. Also seen is the fact that the carrier does not fade along with the subcarriers; this is because the carrier is a single frequency (or very small linewidth if phase noise is included) and does not add constructively or destructively with another term.

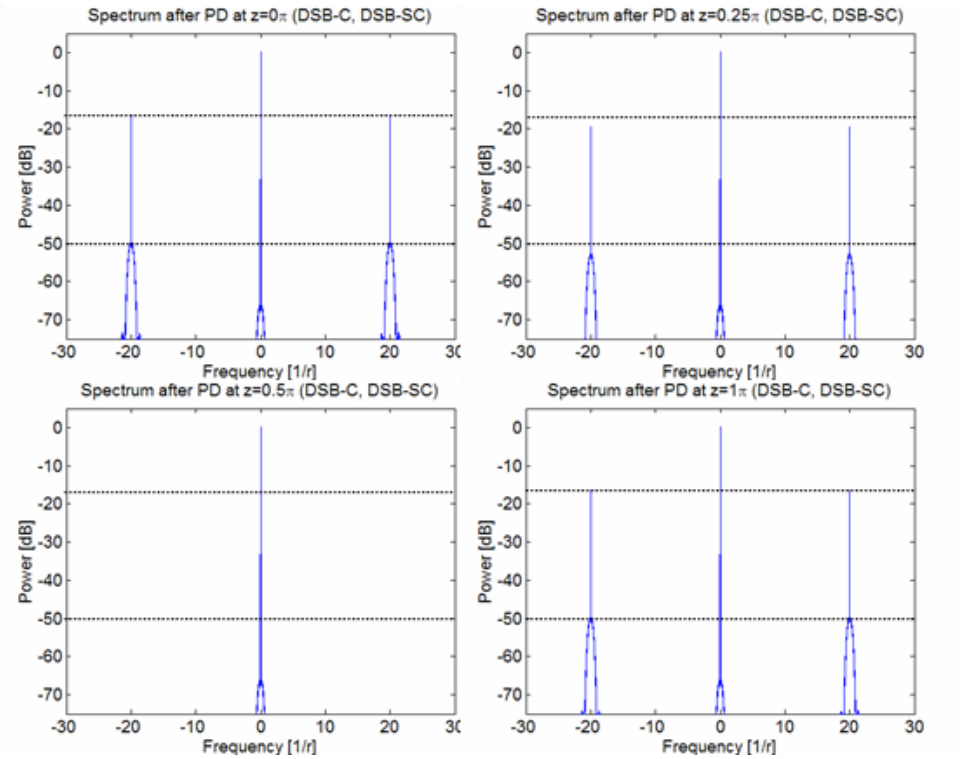

Figure 4.5: DSB-carrier spectrum immediately after the photodetector, before any RF demodulation.

Section 4.2.2. DSB Carrier with SSB Subcarrier

This case will have similar performance since the optical sidebands are spectrally spaced the same distance apart as above. In this case, either a small subcarrier modulation index is required for electrical envelope detection, or electrical homodyne detection can be used for RF demodulation. Another approach is to select the desired optical subcarrier by tuning the sinusoid that modulates the optical LO to the subcarrier frequency and therefore perform optical homodyne detection which then only requires electrical baseband filtering. This is the approach used here and the following figures use electrical baseband filtering to demodulate the signal. The previous section used optical heterodyne detection followed by electrical envelope detection, showing both approaches

work in the simulation. The first figure shows the spectrum of the signal at the input of the fiber as defined in (4.2).

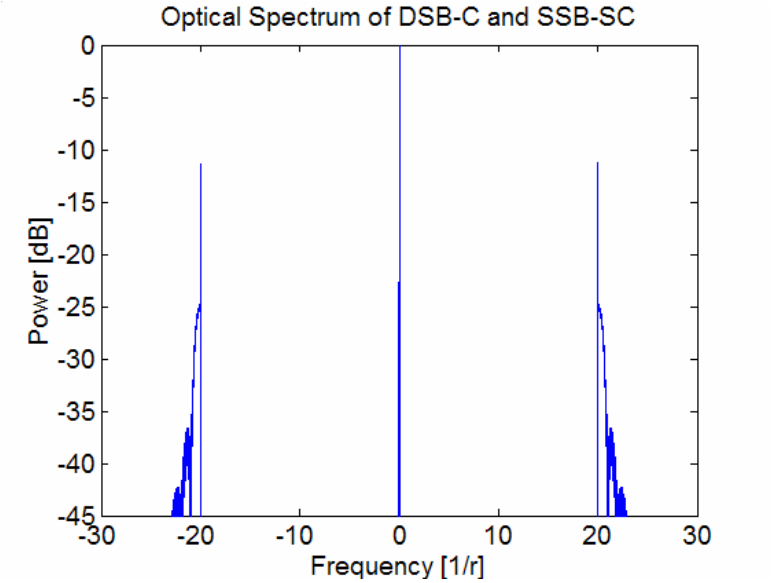

Figure 4.6 Input spectrum of signal with DSB-Carrier with SSB-Subcarrier

Figure 4.7 shows the uncompensated signal at the four locations along the fiber. Figure 4.8 shows the signal using a dual-frequency LO in an optical homodyne detector. Clearly the power fading is eliminated in this case as well when using the phase controlled dual-frequency LO.

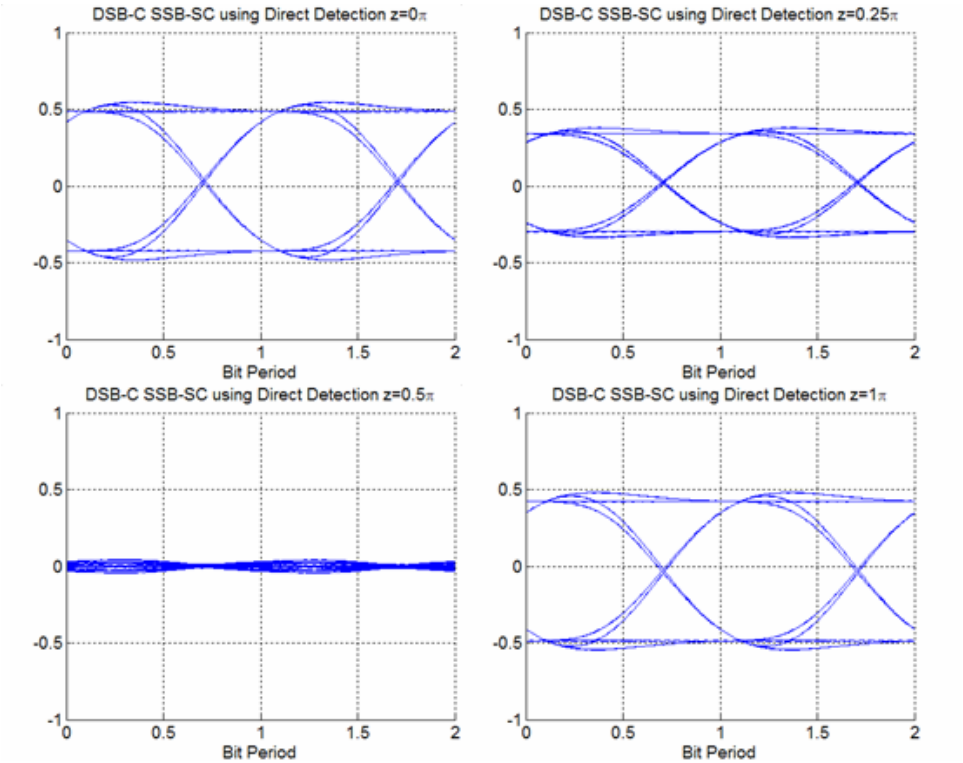

Figure 4.7: Eye-diagram for DSB-C with DSB-SC over a distance of π.

It is interesting to note that upon close observation of the signal at $z = \pi$ the polarity of the direct detection signal with RF homodyne detection case is reversed after the $\pi/2$ point. This can either be left alone and the polarity reversed back in the logic circuit or the phase of the RF local oscillator can be adjusted to correct the polarity. Since in the dual-frequency LO case below the dispersion induced phase shift is tracked by the LO phase no inversion is seen. However, if the PLL is designed simply to maximize the eye-opening then either the original data sequence is recovered or the inverted one is recovered.

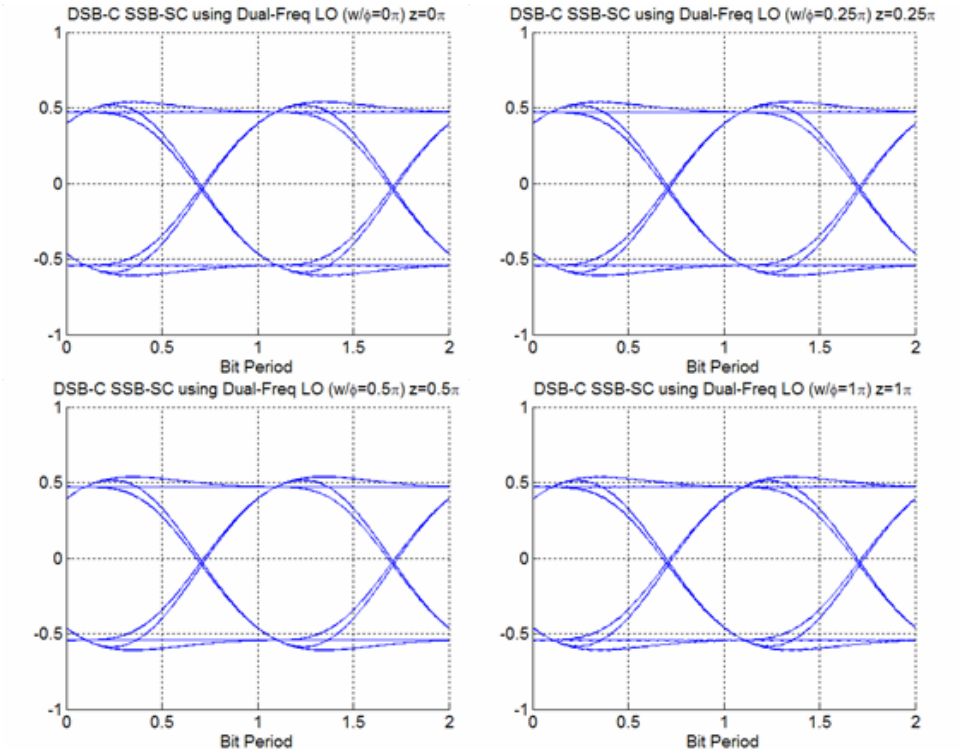

Figure 4.8: Compensated Eye-diagram for DSB-C with SSB-SC

Section 4.2.3. SSB Carrier with DSB Subcarrier

In the SSB carrier with DSB subcarrier situation the power fading does not occur in the photodetector but in the RF demodulation step. The phase shift is translated to the upper and lower sidebands signal during the photodetection process, however the sidebands are not superimposed until they are brought to baseband. For this reason, the phase shift discrepancy can be corrected in either the RF or optical domains. The following figures and discussion will illustrate both techniques, as well as the fading that occurs if all phases are matched to the optical carrier (the worst choice in this situation). The first two figures show the spectrum of the signal, the optical input spectrum and the spectrum immediately after the photodetector, respectively. By comparing Figure

4.10 to Figure 4.5 is clear that for a SSB carrier the power fading does not occur during the photodetection.

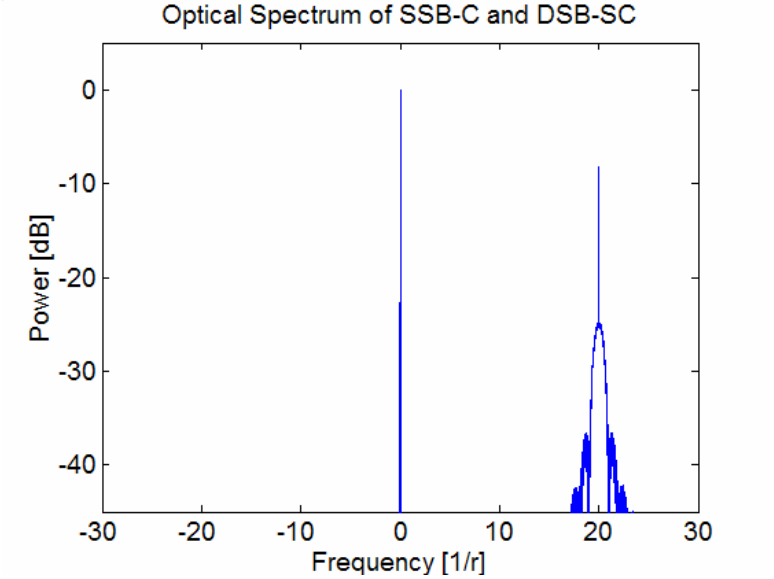

Figure 4.9: SSB carrier with DSB subcarrier at the input of the fiber.

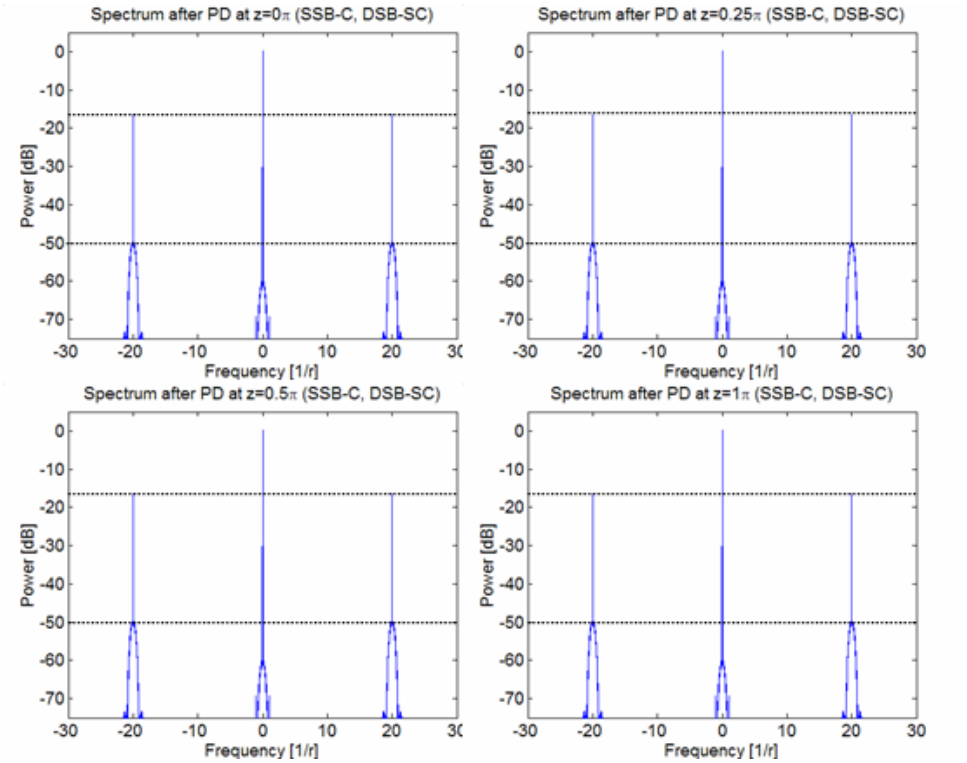

Figure 4.10: SSB carrier with DSB subcarrier spectrum immediately after the photodetector, before any RF demodulation.

The next figure implements optical direct detection followed by RF homodyne detection. In this iteration, the phase is not compensated and the signal experiences a power loss. The next two figures use RF envelope detection and dual-frequency LO optical homodyne detection to illustrate that the phase correction can utilize either optics or electronics.

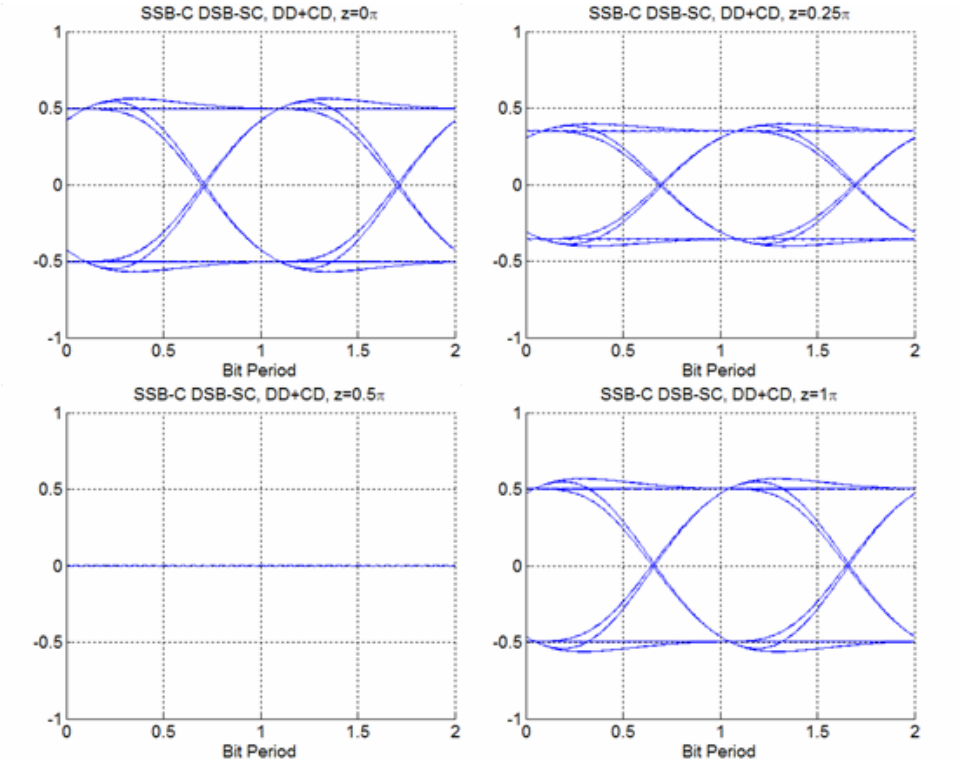

Figure 4.11: SSC carrier with DSB subcarrier using direct detection followed by RF homodyne detection. RF LO phase is locked to the reference phase.

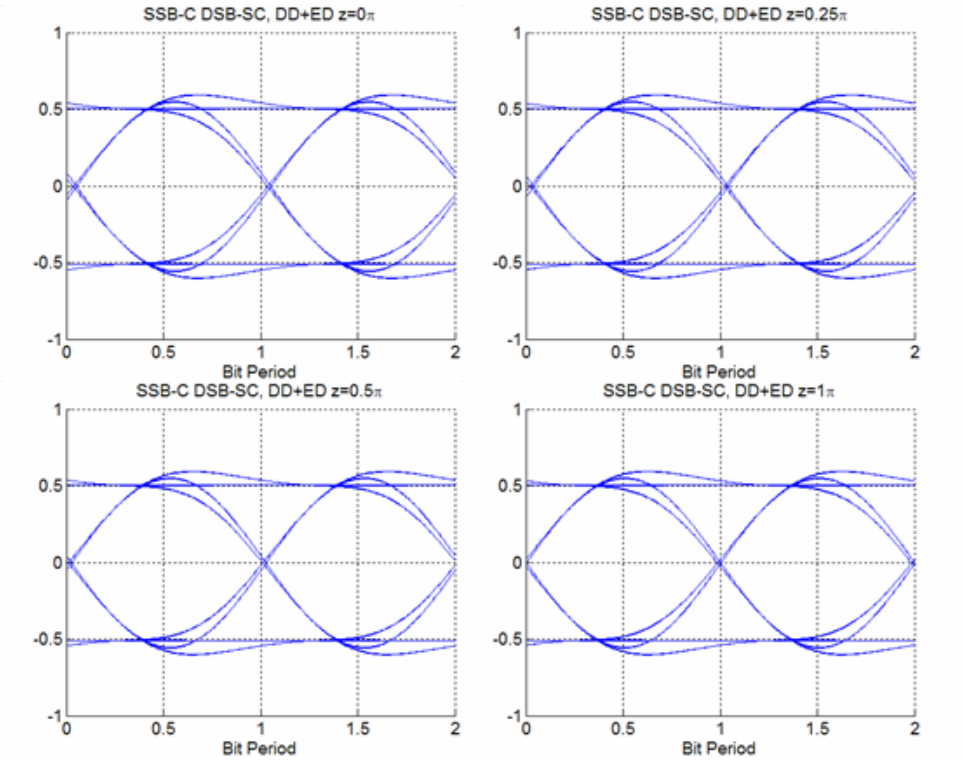

Figure 4.12: SSC carrier with DSB subcarrier using direct detection followed by RF envelope detection. No phase control required.

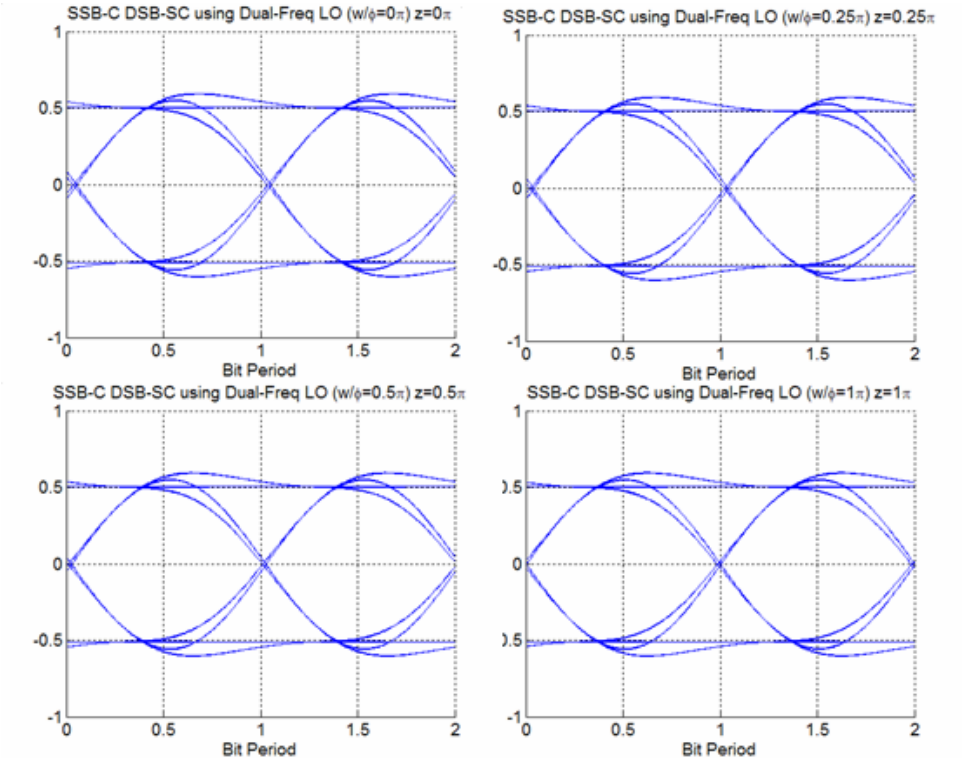

Figure 4.13: SSB carrier with dual-frequency LO homodyne detection.

The third figure above shows the received eye-diagram when the phase correction is applied in the optical domain. If the same technique is used (a dual-frequency LO homodyne detector) with the phase locked to the optical carrier rather than the subcarrier then the power fading is seen.

In Section 3.6 the pulse broadening of the signal was discussed. It was found that for a DSB subcarrier signal on a SSB carrier that pulse broadening starts to become an issue at a distance of 320 times further than the first signal null, or $z = 160\pi$. To verify this, the simulation was run to find the above eye-diagrams for a distance of $z = 160\pi$ to determine the amount of pulse broadening and the result is shown in Figure 4.14.

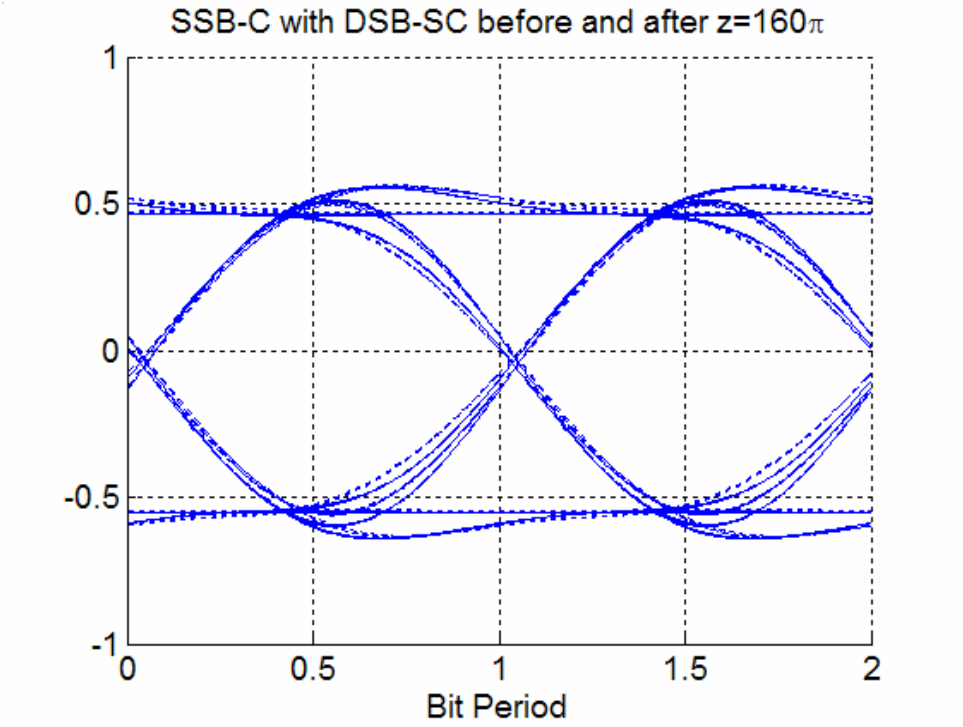

Figure 4.14: Pulse broadening. The dotted line indicates the signal at the end of the fiber.

The rational used in the derivation of the ISI dispersion limit given in equations (3.54) and (3.57) is based on the amount of dispersion accumulated while approximately 95% of the pulse energy remains within its time-slot [8]. By looking at the two traces shown in Figure 4.14 this is observed. This is used to verify that the simulation is accurately predicting the pulse broadening of the signal. Pulse broadening is a well understood phenomenon in optical communications and is therefore not investigated further, but only used as a rationale check for the simulation techniques. The effects of the pulse walk-off, however, will be seen in the figures depicting Q as a function of distance for DSB carrier systems.

Section 4.2.4. SSB Carrier with SSB Subcarrier

According to the analysis shown in Section 3.3 and Section 3.6 an OSCM system with a SSB carrier and a SSB subcarrier has the best resistance to dispersion. This is because power fading is not an issue during detection and pulse broadening is less because of the reduction in signal bandwidth. While fading does not occur, signal distortion does occur due to the relative phase shift between the optical carrier and subcarrier. This phase shift can be compensated either in the RF domain during demodulation or in the optical domain using a either a conventional LO or the dual-frequency LO coherent detection by matching the phase of the LO to the subcarrier rather than the carrier. It should be noted that this last technique can be used only when optically selecting the subcarrier. If the system designer wishes to electrically select the subcarrier the

phase matching needs to be done in the RF domain and the optical LO should be phase locked to the optical carrier.

In this example more demodulation techniques will be considered because some techniques perform better than others. The first figure shows the worst case situation, doing direct detection followed by locking the phase of the RF homodyne detection to the reference. As pointed out in the analysis this would never be done in practice but is used here for comparison to the DSB systems.

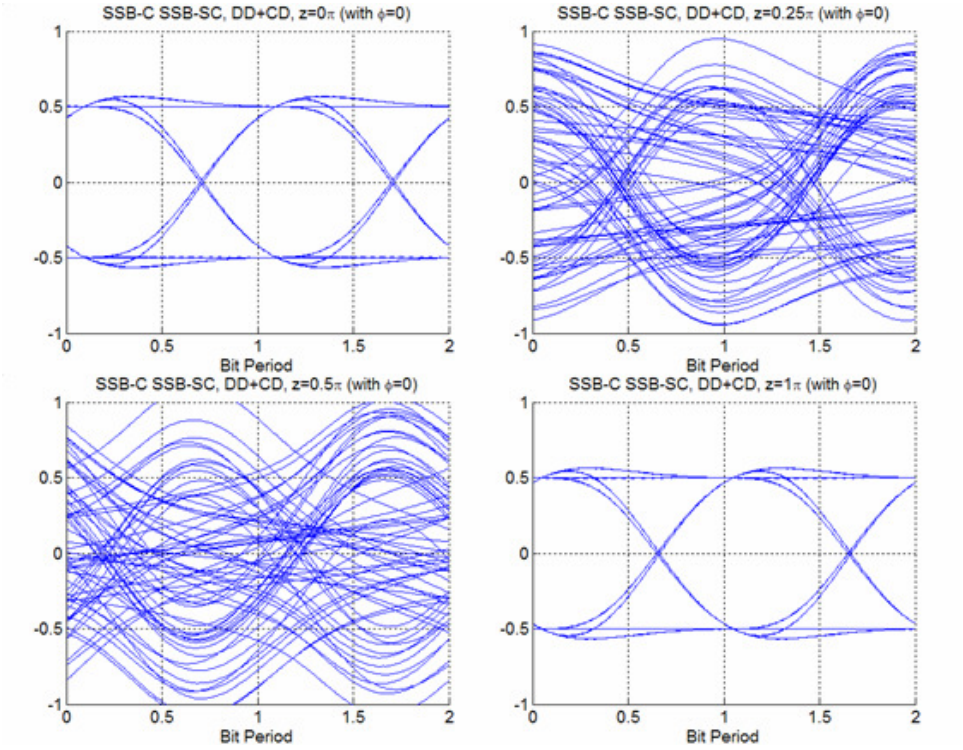

Figure 4.15: SSC carrier with SSB subcarrier using direct detection followed by RF homodyne detection. RF LO phase is locked to the reference phase.

This figure should be compared to Figure 4.11. The same phase shift in the DSB subcarrier system causes a power penalty in that case. Signal distortion is caused by the frequency dependent time delay, as explained in Section 3.3.1, where each frequency component of the received signal experiences a different

time delay. By compensating for the bulk of the phase shift (the phase shift due to the dispersion of the subcarrier frequency) this distortion can be corrected.

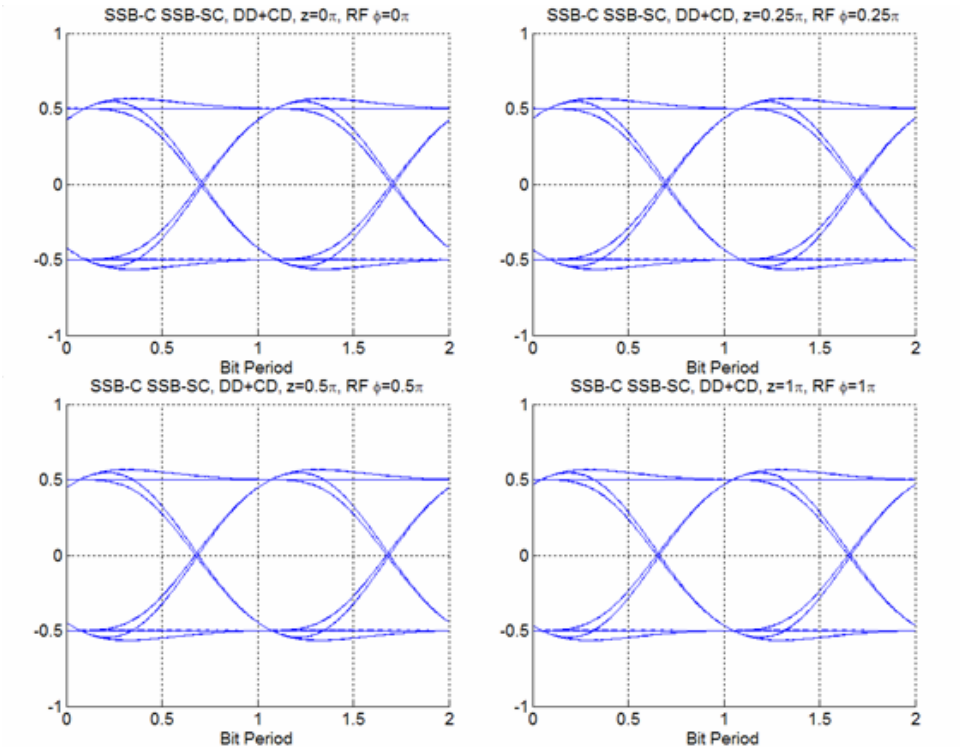

Figure 4.16: SSC carrier with SSB subcarrier using direct detection followed by RF homodyne detection. RF LO phase is locked to the subcarrier phase.

Since this method is the conventional method to correct for the waveform distortion it is the one that would usually be implemented in a SSB-carrier, SSB-subcarrier system. It only requires direct detection of the optical signal followed by electrical homodyne detection with an electrical PLL. However, if the network operator desires a single receiver design that can be used for both SSB and DSB carriers, then one of the dual-frequency LO receiver designs is required.

Use of a dual-frequency LO for the optical-to-electrical conversion still requires that the signal is demodulated in the RF domain. If the dual-frequency

LO is tuned to the desired subcarrier (optical homodyne detection with optical channel selection) then only a baseband filter is required before finding the eye-diagram. This is shown in Figure 4.17.

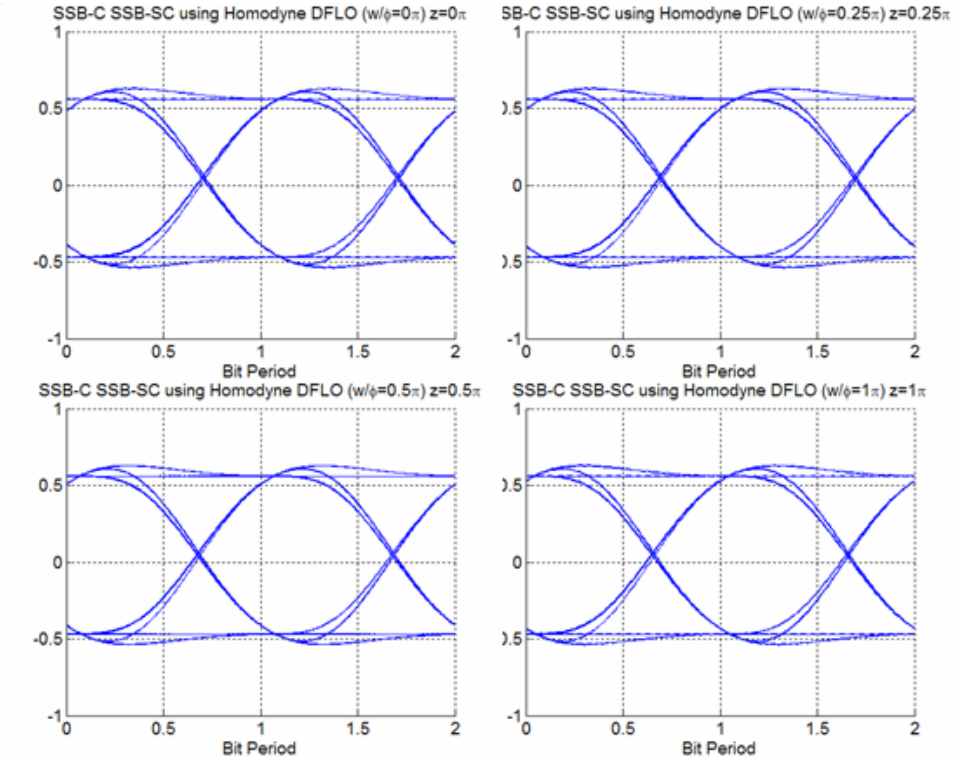

Figure 4.17: SSC carrier with SSB subcarrier using dual-frequency LO with the frequency separation tuned to the desired subcarrier frequency.

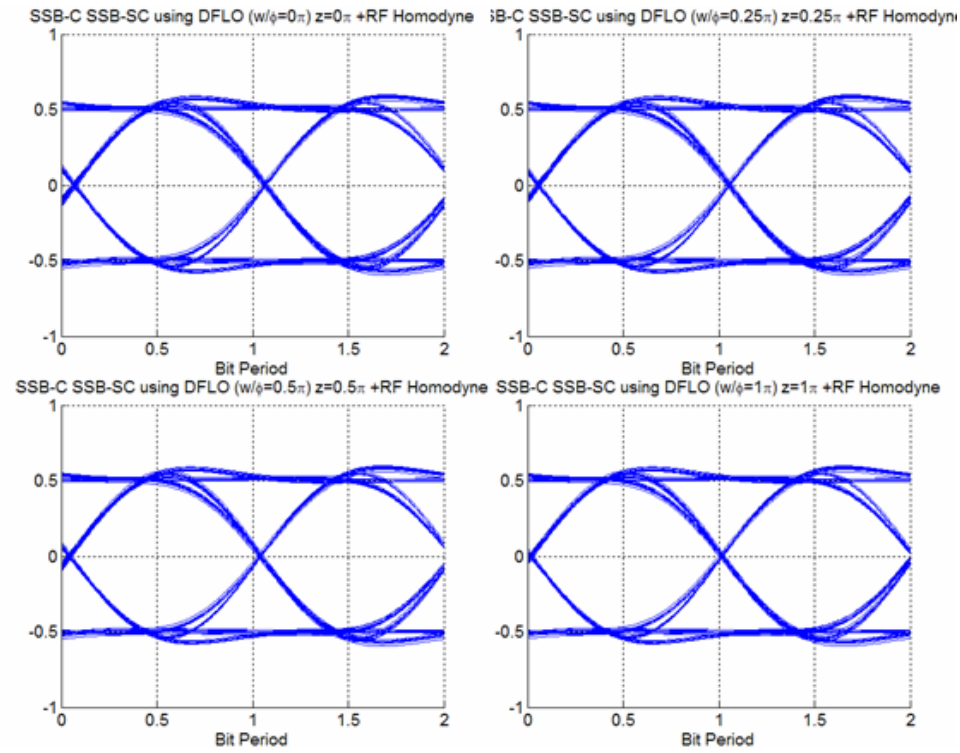

Figure 4.18: SSC carrier with SSB subcarrier using dual-frequency LO and RF homodyne detection.

The three methods above that use some mechanism to correct the phase of the subcarrier have similar performance. However, there are two techniques that can detect a useful signal without any consideration for the relative phase offset between the carrier and subcarrier. These techniques involve using envelope detection of the RF signal. The next two figures will show the results of using envelope detection, the first follows direct detection and the second uses a dual-frequency LO for the optical detection. When using a dual-frequency LO, locking the phase to the subcarrier or carrier produces the same result, since the RF envelope detection is not phase dependent.

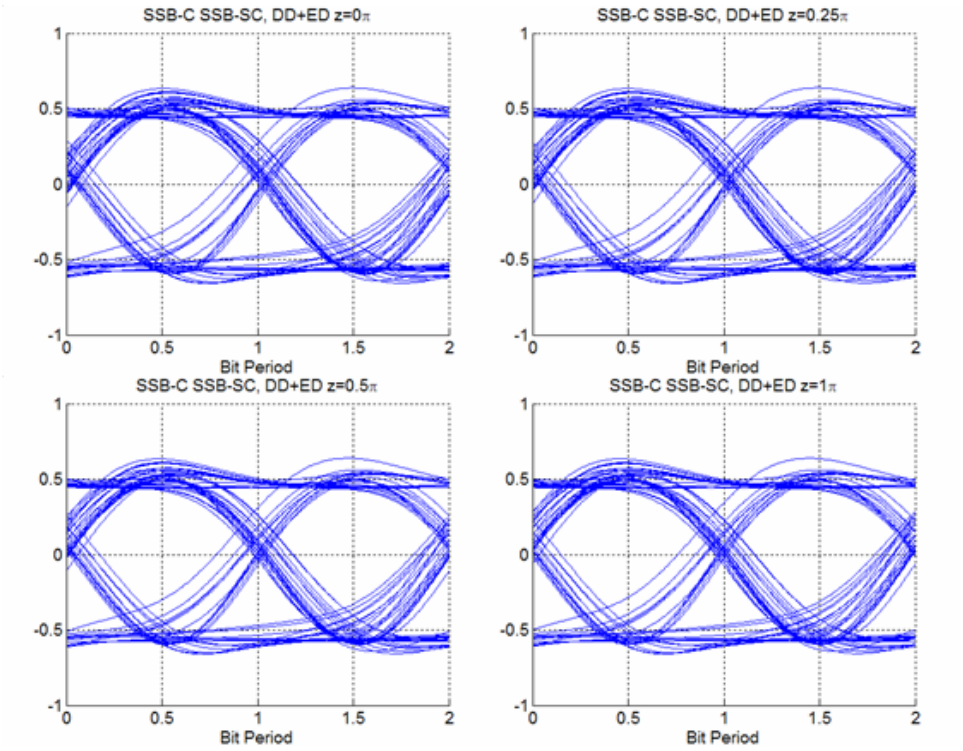

Figure 4.19: SSB carrier and subcarrier using optical direct detection and RF envelope detection.

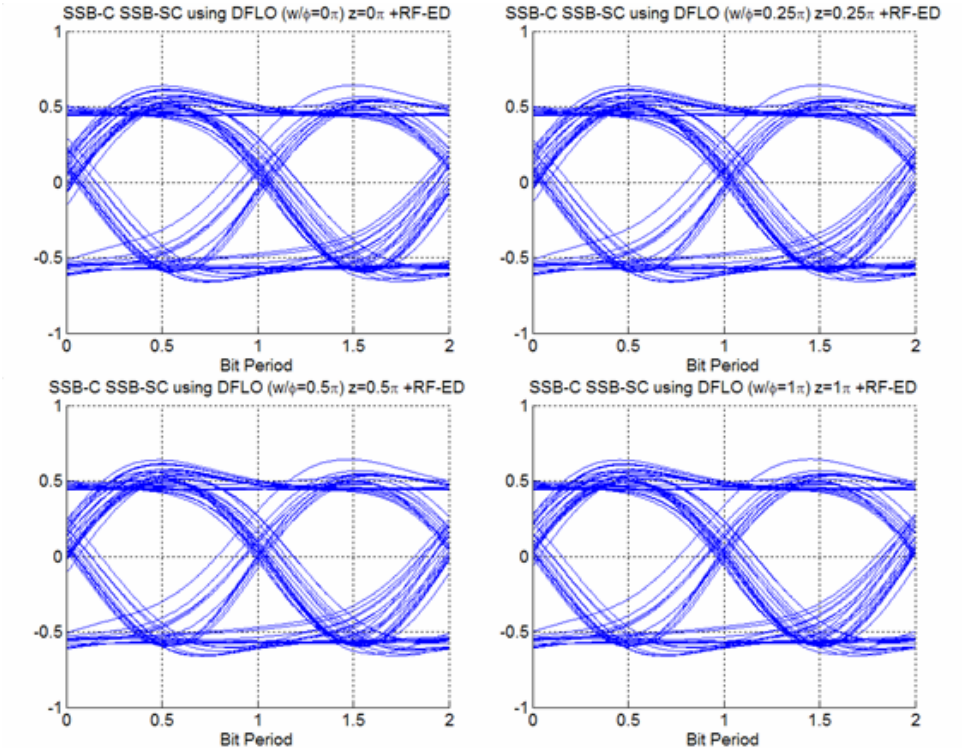

Figure 4.20: SSB carrier and subcarrier using a phase controlled dual-frequency LO and RF envelope detection.

The modulation index of the data onto the subcarrier is the same as that used in Figure 4.15 through Figure 4.18. By using a smaller modulation index the performance of the envelope detection can be improved. The same modulation index for was chosen in all examples for the sake of comparing RF coherent demodulation and envelope detection. It is interesting to note that when RF envelope detection is used with (Figure 4.20) or without (Figure 4.19) phase control the resulting eye-diagrams are equivalent.

For the purpose of comparison to the other detection techniques shown above, the input optical spectrum and the output RF spectrums are shown below. The RF power is normalized during the demodulation to an eye-opening of one.

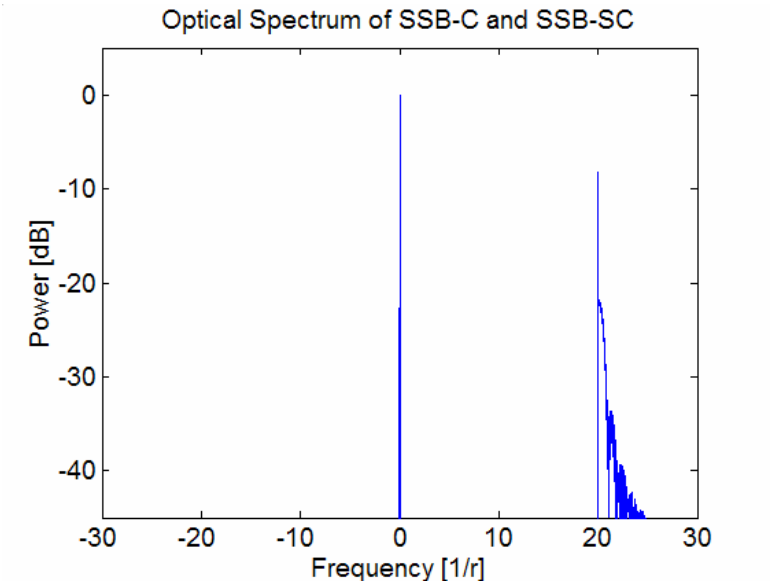

Figure 4.21: SSB carrier with SSB subcarrier at the input of the fiber.

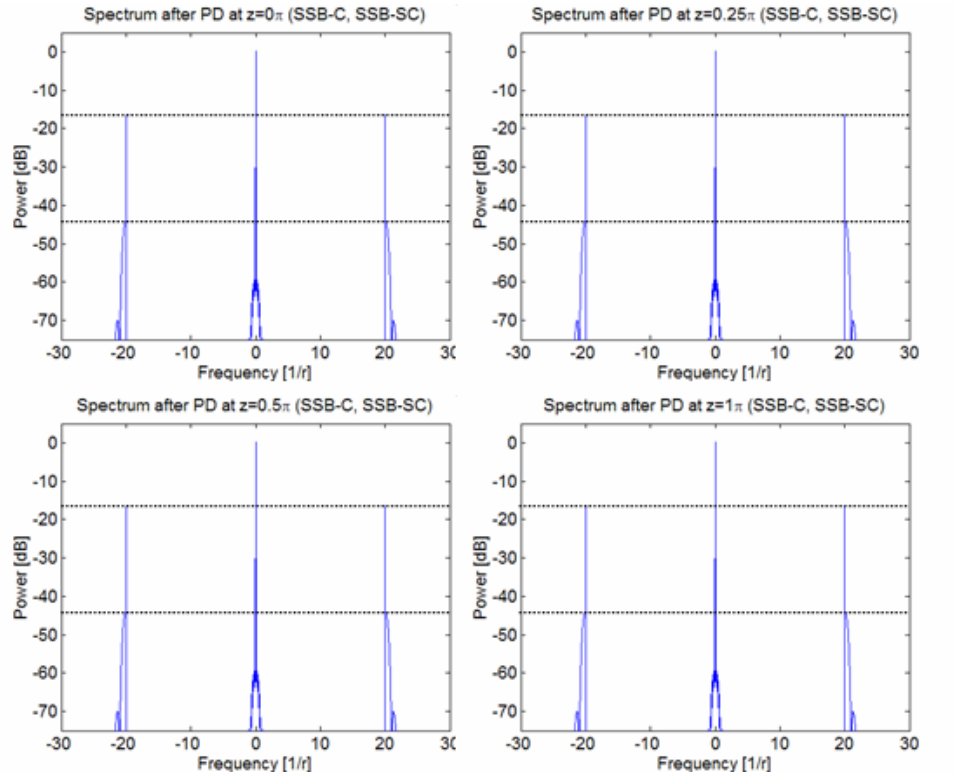

Figure 4.22: SSB carrier with SSB subcarrier spectrum immediately after the photodetector, before any RF demodulation.

The examples above illustrate the signal degradation due to the dispersion induced phase shift and its compensation for signal subcarrier systems. The use of the dual-frequency LO can be used in OSCM systems with multiple channels (subcarriers) as well. The next section will look at a multichannel OSCM system.

Section 4.3. Multichannel OSCM system

The previous section compared the four different OSCM systems depicted in Figure 3.1 for single channel transmission. The results show the effects of dispersion on the subcarrier signal and several detection techniques for each system. This section demonstrates that using a dual-frequency LO with independent phase control also works for multiple subcarrier channels. The

technique can be used to simultaneously correct for dispersion induced power fading and perform channel selection.

To simulate a multichannel system there are two options regarding the simulation parameters. The first option is to use the normalized parameters introduced in Section 2.1 and used in the preceding section. The other option is to choose typical network parameters for the simulation. Normalized parameters have the advantage of giving generalized results that can be applied to any network, but they also introduce some complications. The first complication is that the normalized distance, *z*, is defined for a given subcarrier frequency such that the first power null occurs at a distance of $z = \pi/2$; if multiple subcarriers are present then only the nominal subcarrier has a null at this distance. This means that *z* can only be defined for a single subcarrier at a time. The way to handle this is to either have power nulls at different values of *z* for each subcarrier, or to have different normalized lengths for each subcarrier, even though the physical fiber would be the same length. The second complication arises when defining the data rate to subcarrier frequency ratio (*r*). In the same way each subcarrier requires its own normalized length, each subcarrier would require its own *r* value. Clearly, using normalized parameters in a multichannel OSCM system leads to complicated frequency and length parameters. For instance, if a system had several signals of equal bit rate and traveling a fiber of one length, each signal would have a different associated *r* and *z*. For this reason a numerical example using typical fiber parameters gives a clearer picture of a multichannel OSCM system.

To examine the degradation and compensation of the DSB carrier system, it is useful to simulate four subcarrier signals. By using subcarriers spaced between 15 GHz and 30 GHz the subcarrier frequency to distance relationship of the power fading can be seen. Since the power fading occurs at the same distance for both SSB and DSB subcarriers this simulation focuses on only DSB subcarriers. A 1-Gb/s data signal is on each subcarrier and the dispersion parameter is $17 \frac{ps}{nm\,km}$. The four signals will be shown at a distance of 4 km and 16 km. In each case a dual-frequency LO is used for channel selection, however in the first and third eye-diagrams the phase is locked to the optical carrier as in a conventional coherent detection scheme. The desired subcarrier is selected by tuning the sinusoid of the LO such that the photodetected signal is at a fixed IF.

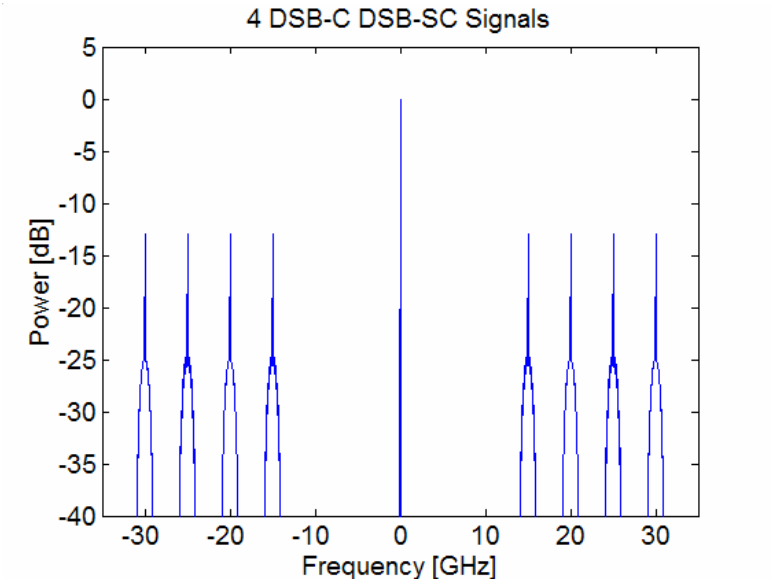

Figure 4.23: Optical Spectrum of DSB carrier with 4 DSB subcarriers

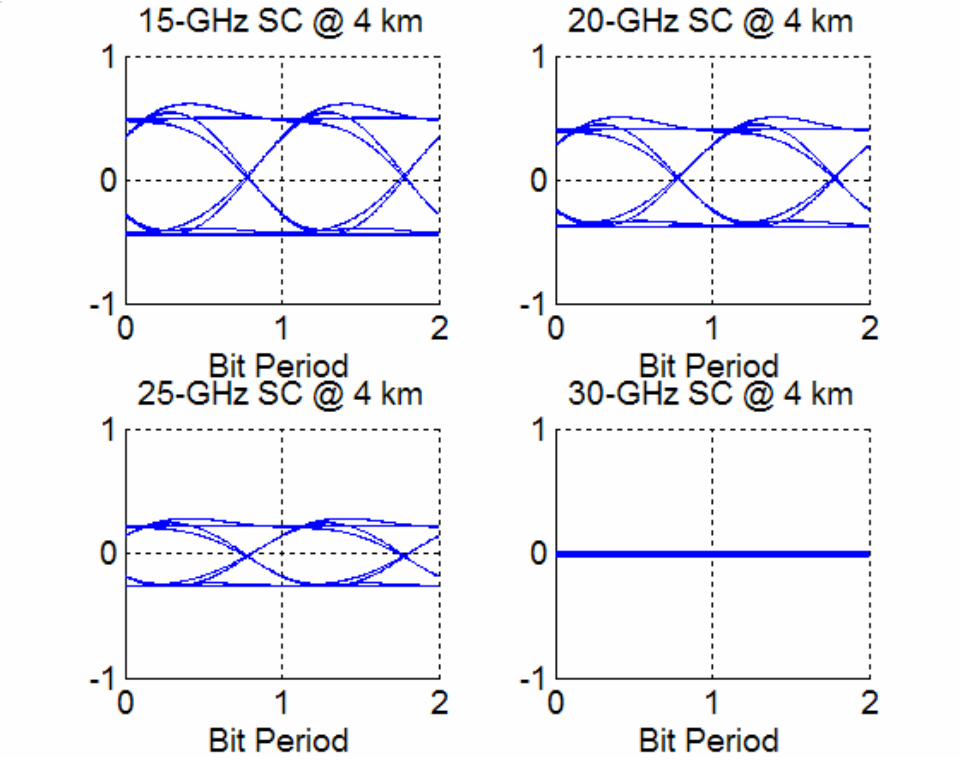

Figure 4.24: All four subcarriers after 4 km without phase compensation.

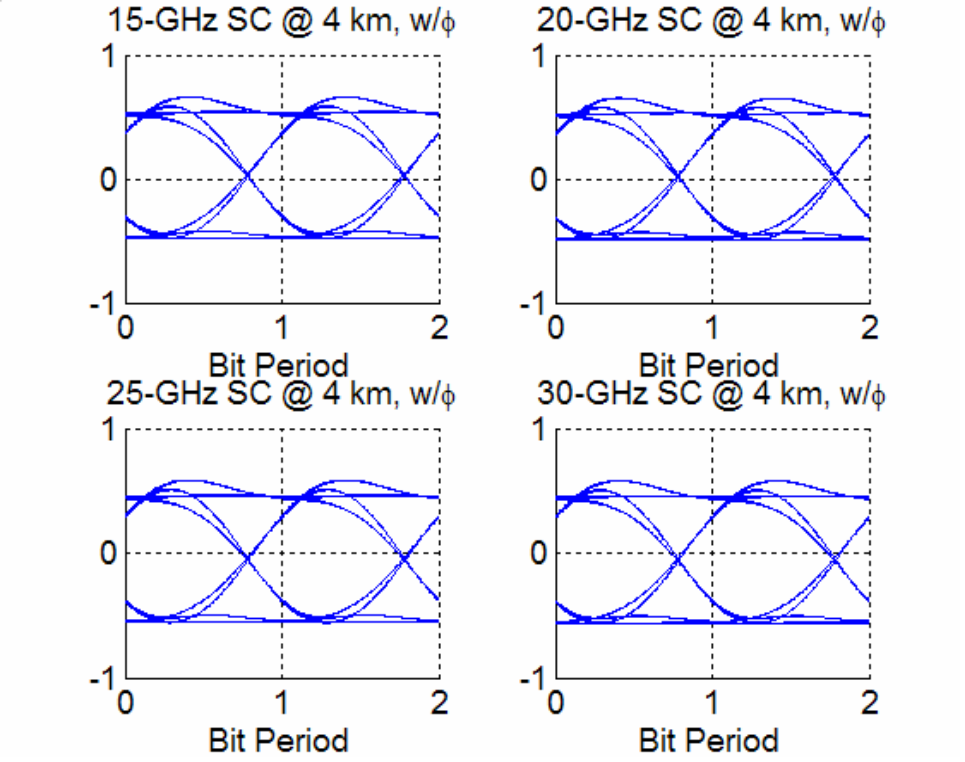

Figure 4.25: All four subcarriers after 4 km with phase compensation.

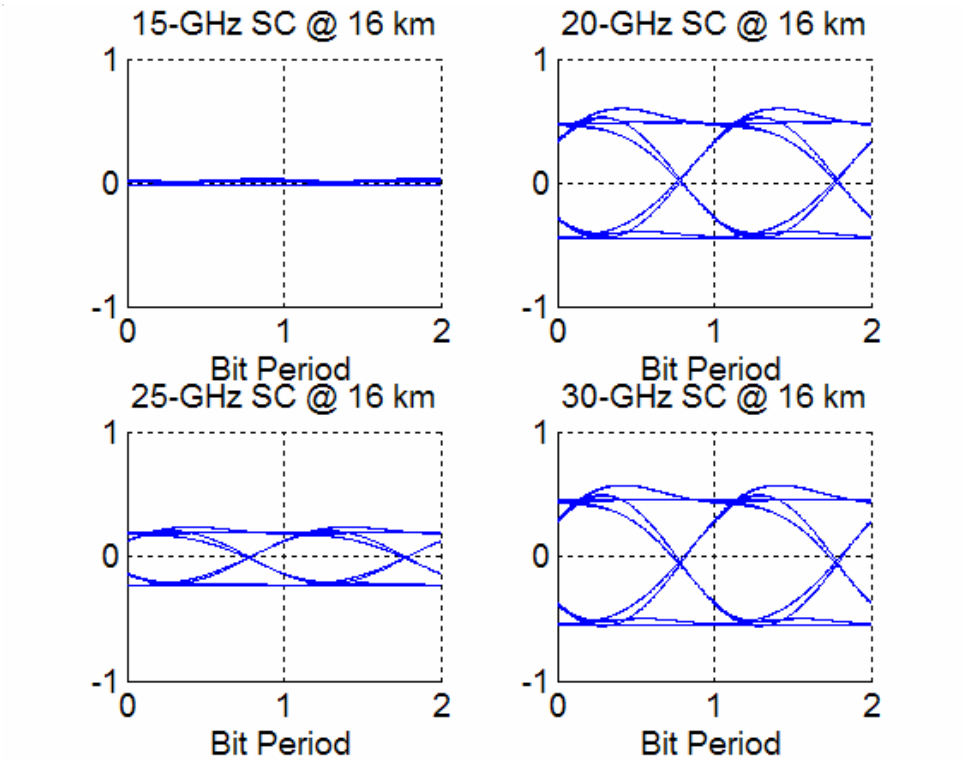

Figure 4.26: All four subcarriers after 16 km without phase compensation.

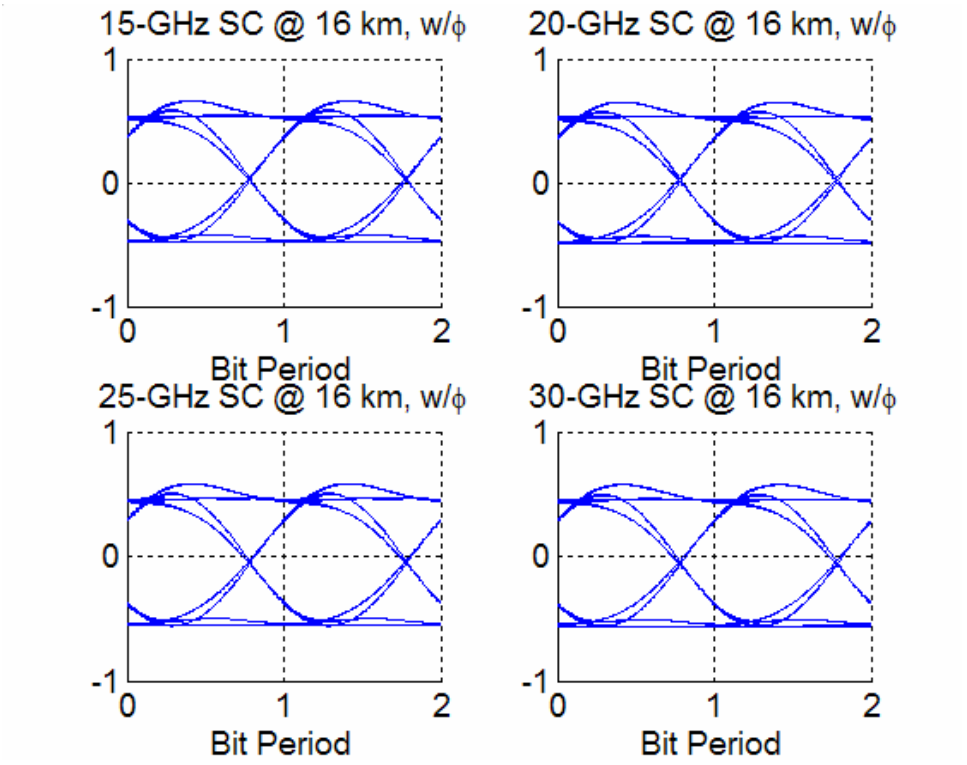

Figure 4.27: All four subcarriers after 16 km with phase compensation.

By comparing the 15 and 30-GHz signals in Figure 4.24 and Figure 4.26 the inverse square relationship between the distance to the first power null and the subcarrier frequency is seen. Figure 4.25 and Figure 4.27 show that the dual-frequency LO can simultaneously select a subcarrier channel and eliminate the phase shift that causes power fading. This section also shows that the technique to compensate for the dispersion in an OSCM system is not limited to the single subcarrier cases shown in the previous section and in much of the analysis.

Section 4.4. Phase Modulated OSCM systems

In Chapter 2 it was stated that much of the analysis was done for arbitrary modulation formats when considering the use of a dual-frequency LO with phase control to correct the dispersion induced phase shift of the subcarriers. So far in the analysis and simulation when a modulation format has been included it has been amplitude modulation. This section will simulate the same set of parameters as Section 4.2.1 using BPSK rather than ASK. The PSK signal uses a π phase shift on the subcarrier frequency and a modulation index of 0.1 between the carrier and subcarrier. The PSK spectrum for one channel at the input of the fiber is shown below.

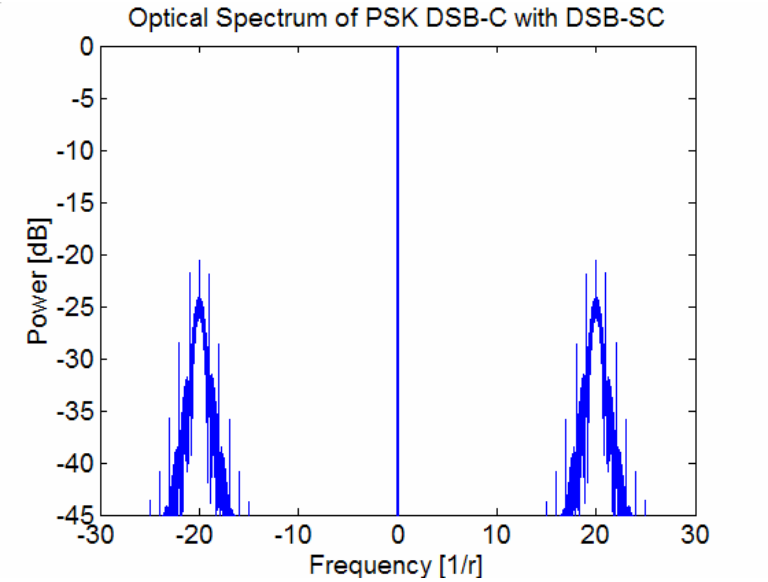

Figure 4.28: Optical spectrum of PSK OSCM signal.

The spectrum along the fiber shows that, just as in the ASK systems, the power loss occurs during the photodetection process of a direct detection receiver. Figure 4.29 shows the spectrum and Figure 4.30 shows the corresponding eye-diagrams. After the direct detection receiver the RF signal is homodyne detected to recover the baseband binary (ASK) waveform.

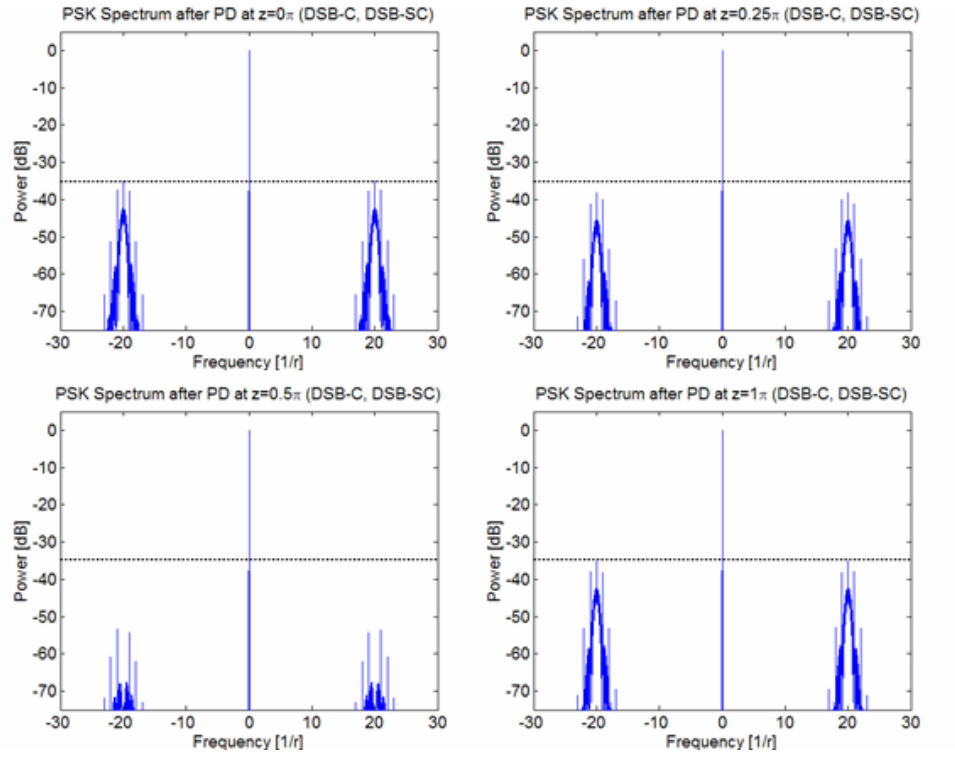

Figure 4.29: PSK spectrum after direction detection.

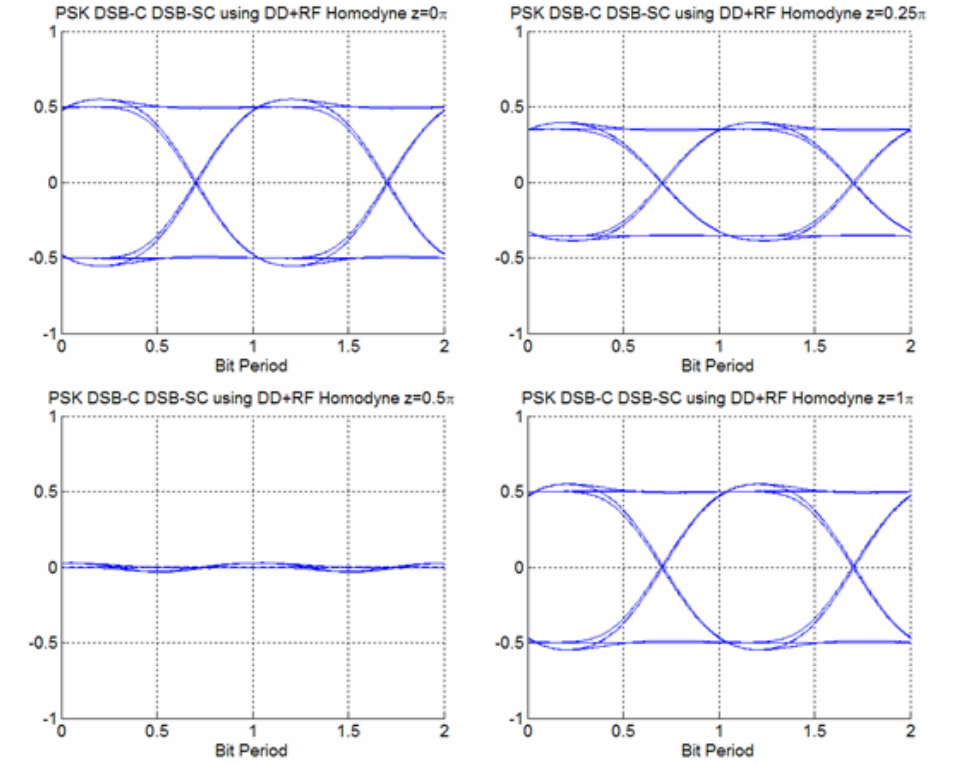

Figure 4.30: Power fading at the same rate as ASK modulation is clearly shown for the PSK signal.

The dual-frequency LO works as expected for the PSK system. The eye-diagrams for the same fiber lengths as above are shown in the following figure. The dual-frequency LO also corrects for the slight skew seen in the $z = \pi/4$ (and any other non-multiple of $\pi/2$) eye-diagram.

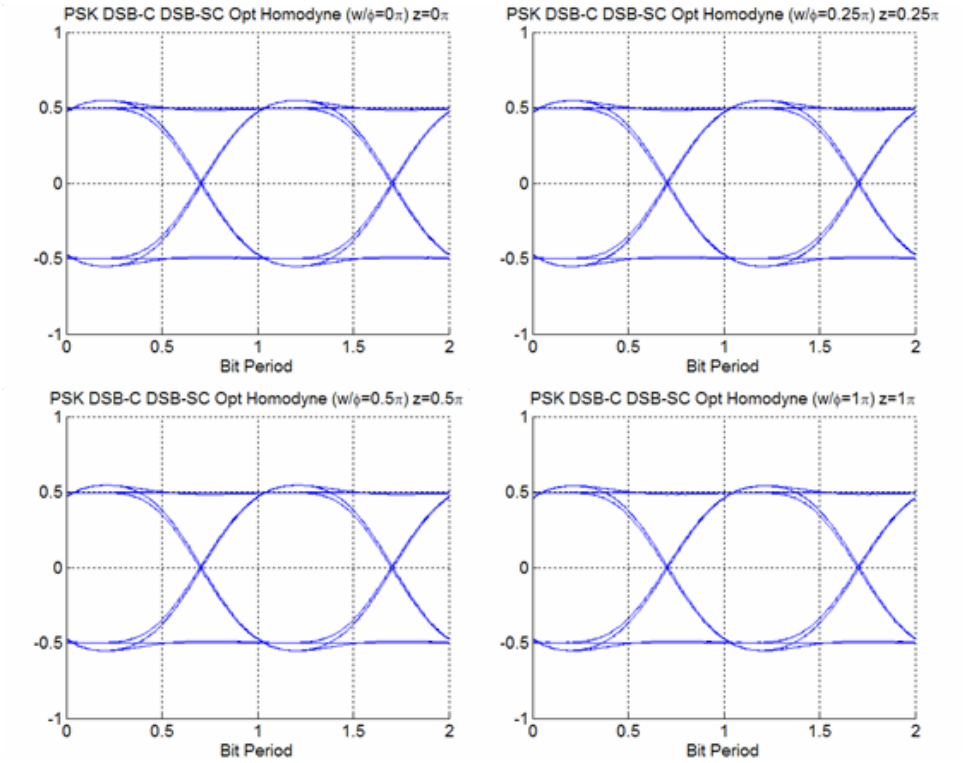

Figure 4.31: PSK signal homodyne detected with a phase-controlled dual-frequency LO.

Section 4.5. Performance of Impaired OSCM Signals

So far the simulation results have shown results for systems without phase noise on either the source or the LO. A linear optical modulator has also been used in the above simulations. Without a source of noise a Q-measurement (or a BER estimated based on the Q) is not appropriate since Q will approach infinity, which is not realistic. The results shown above also have

assumed that the thermal noise of the receiver is zero. In order to examine the dispersion effects of non-ideal signals and receivers, laser phase noise, modulator nonlinearities and receiver noises are included. Receiver noise is included to show that the receiver will be thermal noise dominated at low received powers, but will be phase noise dominated at high power.

By including noise parameters in the simulation, performance can be measured as a series of Q curves. In the curves one source of noise will be varied while holding others constant in order to demonstrate the dependence of each individual parameter on the overall performance. The different aspects modeled below are Q as a function of: (a) phase variance, (b) signal-LO phase offset, (c) number of OSCM channels, and (d) received power.

Section 4.5.1. Performance of systems with phase noise

When examining the performance of an OSCM system with phase noise there are two main areas of interest. First is how the system degrades as the phase variance increases for the source and LO in the absence of dispersion. In this case the direct detection and dual-frequency LO techniques without phase noise have the same performance. The second case is when dispersion effects are included in the signal at the receiver. Here the simulation will indicate the effects of phase noise on the ability of the dual-frequency LO to mediate the power fading.

Lasers are often described in terms of line-width rather than phase variance. The relation between the phase noise and the laser linewidth is given in the following equation [11].

$$\sigma_\phi^2 = 2\pi\Delta f T \quad \textbf{(4.5)}$$

where Δf is the full-width half-maximum (FWHM) laser linewidth and T is the bit period.

The following figure shows two coherent detection techniques compared to the limiting Q predicted by equations (3.87) and (3.88). Both the dual-frequency LO and a conventional optical homodyne (at the carrier frequency) receiver are modeled for varying amount of phase noise on the source and LO. The amount of phase noise is equal on both the LO and source but the random phase is generated independently. The variance of the phase noise is kept less than one so that small angle approximation of the sine function is valid. Since this is the input to the fiber a direct detection receiver would perform considerably better since the carrier and subcarrier phase would be the same even though the laser is noisy.

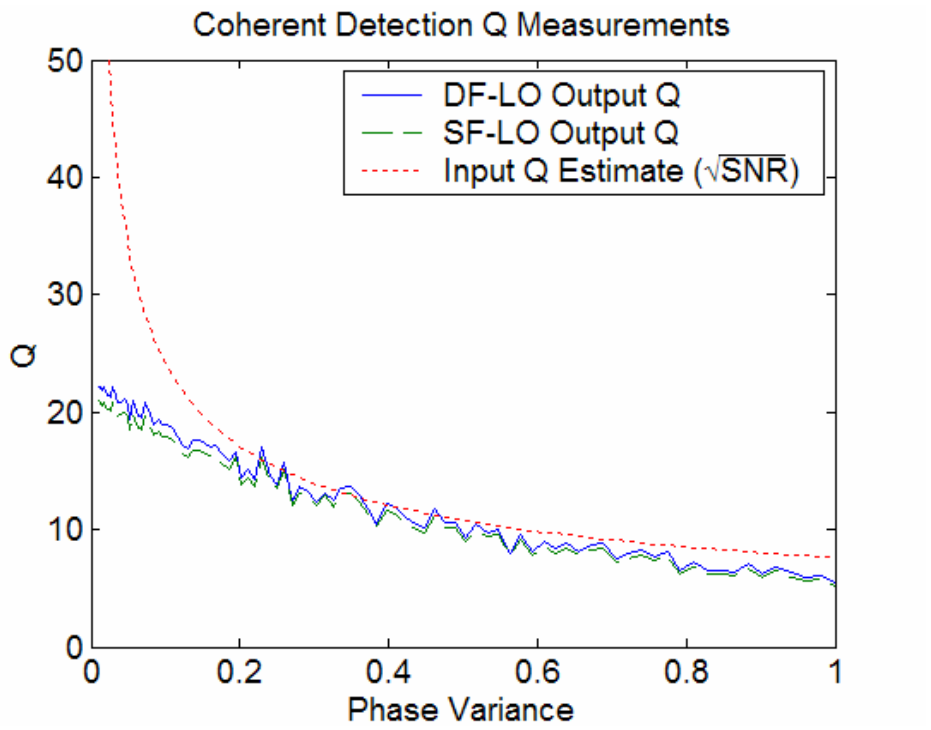

Figure 4.32: Q measured and predicted as a function of the optical phase variance. A dual-frequency LO and single-frequency-LO are compared.

The Q estimate is based on equation (3.87), taking into account the reduction of noise due to the electrical baseband filter. Optical systems are designed to operate between a BER of 10^{-9} and 10^{-15}, which translates to a Q between 6 and 8. The Q estimated by the input parameters (dotted line) matches well with the Q measured from the output signal using the MATLAB® routine in Appendix F.2. The estimated and measured Q values are in good agreement over the majority of the range of the phase variance and the discrepancies at the extremes are easy to explain. With very low phase noise the received signal is dominated by the filtering effects of the transmitter and receiver. The predicted Q is based on an ideal square wave and doesn't take into account the variance in the received ones and zeros due to pulse shape and filtering. This can clearly be seen in the eye-diagrams shown above for signals

with no phase noise. Even in the absence of phase noise the ones have variance as well as the zeros. The predicted Q (dotted line) approaches infinity as the noise approaches zero, yet a realistic system is limited by these other factors. At the other extreme the discrepancy is due to eye closure from the phase noise. The estimate assumes that the mean of Q_s-Q_{LO} is zero and no power loss occurs due to the phase mismatch. However, as the noise increases the mean of Q_s-Q_{LO} does not remain zero across the bit-period and the eye begins to close, thus reducing Q from the ideal value.

Since the figure above shows Q at the input of the fiber, the Q should be higher than the 6-8 needed at the output of the fiber, and in this range the predicted and measured Q are in very good agreement. Also seen in the figure is that the performance of the dual-frequency LO is the same as a conventional coherent detection receiver. The results in Figure 4.32 are for a suppressed optical carrier; however the single-frequency LO at the same frequency as the carrier shows the same performance as a direct-detection system would at a distance great enough for the carrier and subcarrier phases to become uncorrelated [39].

To see the effect of dispersion on a system where both a LO and source include phase noise in the model, the phase variance is held constant as the fiber length increases. A phase variance of 0.5 is picked because it is both in the center of the range where the prediction and calculated Q agree and it results in an input Q above the 6-8 range where the received signal should be for error free performance. The simulation includes the same system design as used for

Figure 4.32 and a total fiber length of 10π, allowing for ten complete fading cycles and the effects of sideband walk-off to become an issue.

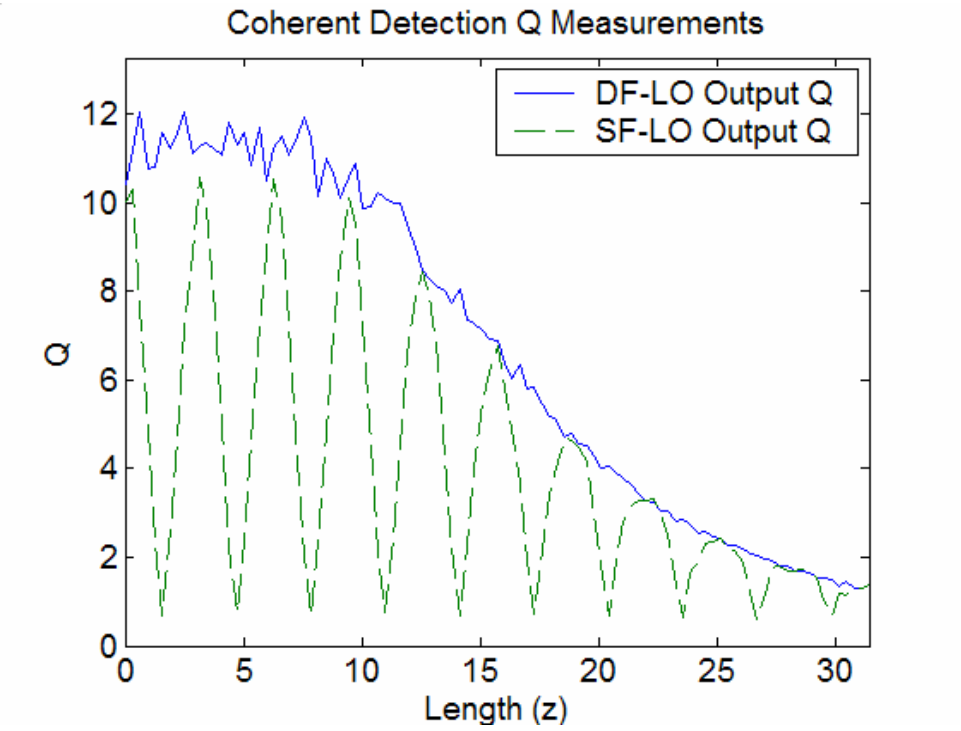

Figure 4.33: DF-LO and SF-LO coherent receivers over a fiber length of 10π. Phase variance is $\sigma_{LO}^2 = \sigma_s^2 = 0.5$.

The figure above clearly shows that the dual-frequency-LO performs at least as well as the conventional coherent detection receiver and avoids the signal nulls that occur at odd multiples of π/2. After $z = 3\pi$ the performance begins to drop off due to the residual phase shift that cannot be corrected by only accounting for the phase shift of the subcarrier. For lower values of *r* this distance increases. Also, as pointed out in the simulations of Section 4.2 and analysis of Section 3.6, the distance is many times farther for SSB optical carriers because the is no walk-off between the upper and lower sidebands. Figure 4.33 shows that the system modeled here has error-free performance

(Q>6, BER<10^{-9}) beyond $z = 5\pi$ when using a dual-frequency LO receiver with independently controlled phases. Also, when the signal is not transmitted with a suppressed optical carrier, either the carrier needs to be removed with an optical notch filter at the receiver or the laser noise needs to be minimized. This is because the noisy carrier mixing with the noisy LO (at the carrier frequency) produces a large noise around DC during photodetection.

Section 4.5.2. Performance of coherent systems with phase offset

The phase difference between the optical carrier and LO leads to a power loss in optical homodyne detection schemes [11]. The dual-frequency LO also requires that the phase of the signal and LO are locked, but with a controlled offset matching the dispersion induced phase shift of the subcarriers. To compare the performance of the dual-frequency LO to a single-frequency LO when a phase offset is included, two plots similar to the ones in the previous section are given. The first will look at the effect of varying the phase offset in the absence dispersion and the second will keep the offset fixed and vary the amount of dispersion. To isolate the effects of the phase offset phase noise is not included.

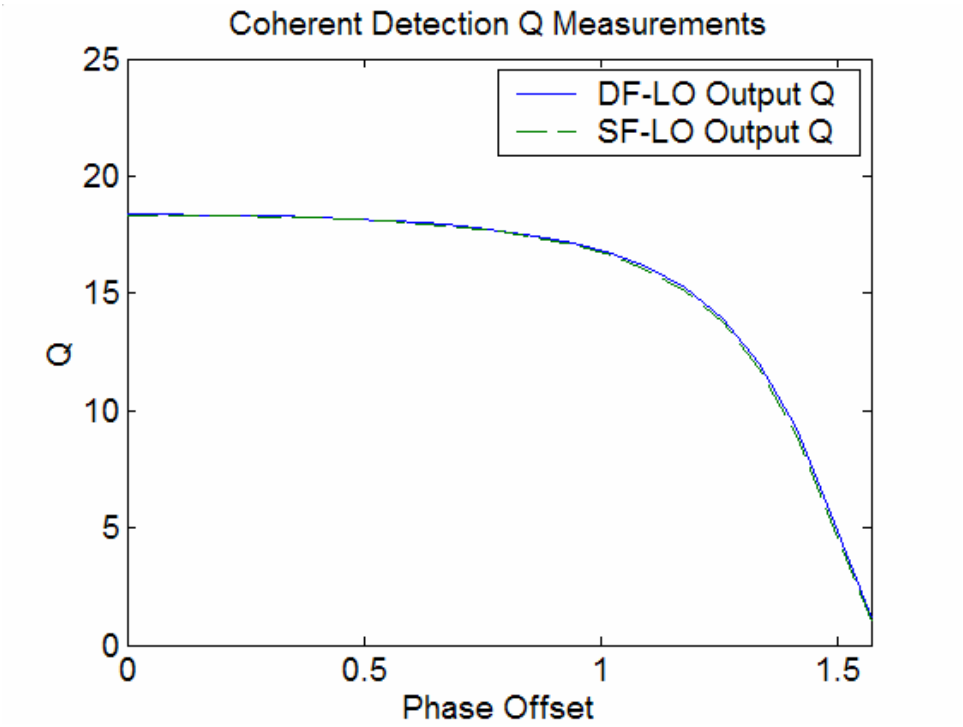

Figure 4.34: Single- and dual-frequency LO with phase offset between LO and carrier.

The system modeled in Figure 4.34 includes a receiver noise variance of 0.01 in order to see a realistic effect of the power loss due solely to the phase error between the LO and carrier. For the sake of comparison the receiver noise and phase error of each design are the same, but in reality the single-frequency LO receiver includes thermal noise from the photodetector that can be amplified by the RF LO. The results shown in Figure 4.34 include the receiver noise just before the final baseband filter. However if the receiver noise is considered to originate in the photodetector (a high bandwidth photodetector, as needed for high subcarrier frequencies, contributes more receiver noise [15]) then the dual-frequency LO performs better than the single-frequency LO. This is specific for homodyne optical detection where the dual-frequency LO selects the subcarrier without the use of an intermediate frequency. When heterodyne

detection is used then both single- and double-frequency LO receivers require a RF LO and the penalty is the same. The following figure plots the same system as above, only the receiver thermal noise is included in the photodetector and not the RF demodulation circuit.

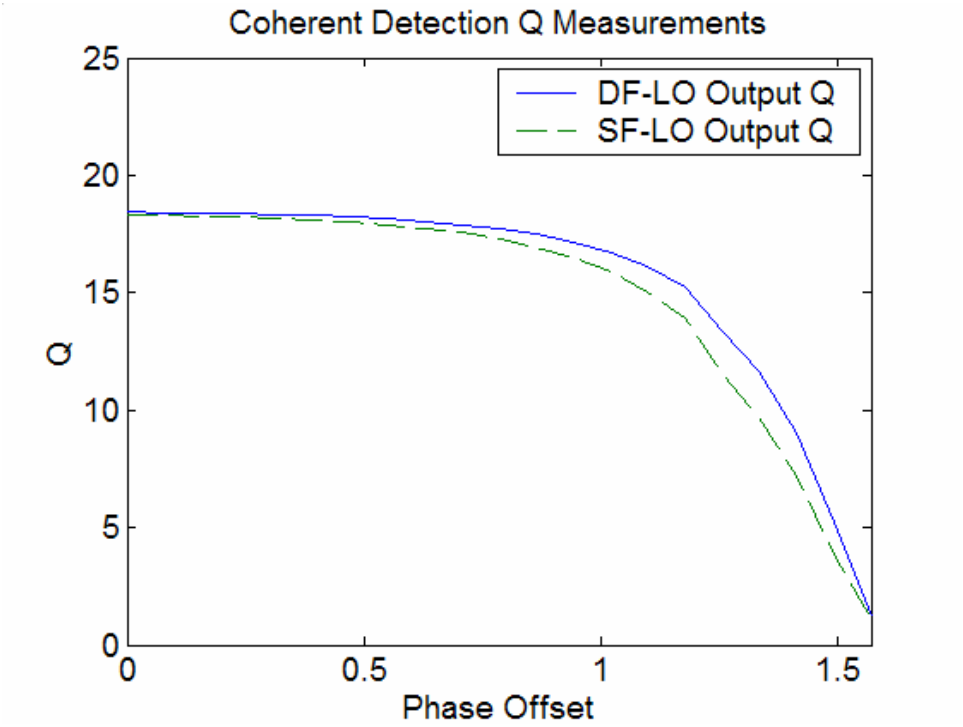

Figure 4.35: Same as Figure 4.34 except the receiver noise is dominated by the photodetector noise.

Both Figure 4.34 and Figure 4.35 show a rapid deterioration after a phase offset of 1 radian. This is where the receiver noise begins to be the dominant noise in the signal. A phase offset of 1.05 is equivalent to a power loss of 3 dB. This plot is useful for seeing the trends and tradeoffs between phase offset, power loss and receiver sensitivity. It should be remembered that the simulation deals with a normalized power of 1 at the fiber input and the receiver sensitivity is related to the bandwidth and therefore one cannot read the figures above as indicating actual performance for a real system, but rather how these aspects

affect the performance. However, the simulations used here could easily be adapted to specific parameters based on photodetectors and receivers available for a specific application.

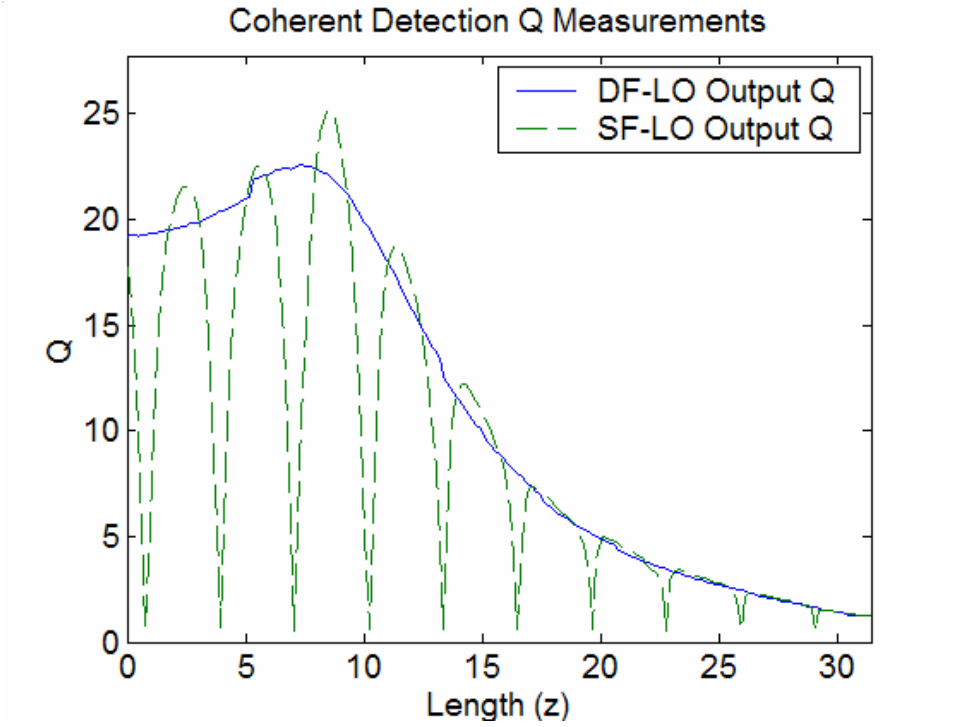

Figure 4.36: Phase offset of $\pi/2$, including dispersion up to $z=10\pi$.

Figure 4.36 is interesting in two aspects that are not immediately clear. The first feature that is different in this figure as compared to the previous figures of this section is that the single-frequency LO receiver has better performance than the dual-frequency LO at certain lengths. This is due to the fact that in the dual-frequency LO the received signal experiences a power penalty due to the phase offset over the entire length of the fiber. In this case the power penalty is $1-\cos(\pi/4)\approx 0.3$. For the single-frequency LO the phase offset shifts the distance to the first null, which is located at $z=z_{null}-\phi_{os}=\pi/4$. This is due to the fact that in the simulation the phase of the carrier is the reference phase,

defined as zero, and therefore a phase offset can maximize the signal at a given distance. It is important to remember that the analysis in Section 3.7 assumes a zero reference phase, so the second phase term of the dual-frequency LO (ϕ_s) is dropped from the equations. In practice this phase term is not dropped, but is locked to the optical carrier. For this reason, a phase shift in a single-frequency LO can shift the distance to the first null, but it cannot eliminate the nulls. A single-frequency LO has a single phase that can either track the phase of the carrier or the subcarrier, but it cannot simultaneously track both as is required eliminate power fading due to both the subcarrier phase mismatch and the carrier phase mismatch.

The second feature seen in Figure 4.36 that is not seen in Figure 4.33 is the system improvement over the first 3π. The reason this is not seen in Figure 4.33 is because in the previous system Q is dominated by phase noise and not pulse shape during the initial propagation. When the phase noise is eliminated (or negligible) then the Q parameter is dominated by the pulse shape. Since a window is used to determine the variance and mean when calculating Q the fact that the pulse is not square increases the variance. As dispersion starts to broaden the pulse the pulse flattens out and the variance in the ones and zeros is reduced and therefore the Q parameter increases. This is partly an artifact of the pulse shape and the method which Q is calculated. However, it is a realistic response since actual Q measurements are subject to timing jitter and if the pulse peaks flatten out then the variance of the ones and of the zeros will be reduced. If the timing jitter is controlled to stricter limits or the system is noise

dominated rather than pulse shape dominated, then the artifact disappears, as seen in Figure 4.33.

Section 4.5.3. Performance of a nonlinear modulator

Another source of noise in an OSCM system is modulator nonlinearity. The modulator nonlinearity adds an intensity noise to each subcarrier signal within the system. The modulator transfer function shown in Section 2.2.3 causes multichannel systems to reduce the signal level of the ones when more ones are present simultaneously. Two examples of the extreme cases illustrate the phenomenon in an easy to understand way. First, if the desired output level for a 'one-bit' is unity, and only a single channel transmits a one while the remaining channels all transmit a zero at a given moment, then the modulator can be biased and driven such that a 'one-bit' is indeed unity. On the other hand, if all of the channels simultaneously transmit a 'one-bit', and the full (or nearly full) dynamic range of the modulator is desired, then each channel will have a 'one-bit' that is less than unity. For this reason, the input RF signal should be limited in amplitude such that the most linear part of Figure 2.2 is used.

Four examples of multichannel systems with nonlinear modulators will be shown and explained in this section. For each example, the system performance, Q, will be found as the number of channels is increased. The ASK systems will be modeled both for when the average optical power is constant (i.e. the modulation index is reduced for each subcarrier added) and when the subcarrier magnitude remains constant, thus increasing the total optical power for the system as the number of subcarriers increases. The total power is

assumed to remain within the modulator's input range. This is modeled both at the fiber input and after a length of fiber. The second four cases repeat the same for phase modulated signals.

In each case a PRBS is generated for each channel in the OSCM system. A PRBS of a given length is the same each time since it is actually a predetermined pattern. In a test of modulator nonlinearly each channel needs an independent bit pattern, yet the same length. Rather than use different PRBS generators for each signal, the PRBS is shifted a random number of samples to insure that each channel is uncorrelated. This is done to ensure that all channels are not a one or all a zero at the same time. The shift is done at the resolution of samples rather than bits in ensure that each channel is not transitioning from a one-to-zero, or zero-to-one, at the same time. This technique is common in producing several uncorrelated signals in optical test beds where the shift is performed with electrical or optical variable delay lines.

The numbers of variations of parameters that can be tested are infinite, but the trends are the same in each case. For this reason, each case will compare the dual- and single-frequency LO receivers with a fixed amount of phase noise ($\sigma_T = 0.1$) at the input to the fiber and after a distance of $z = \pi/4$.

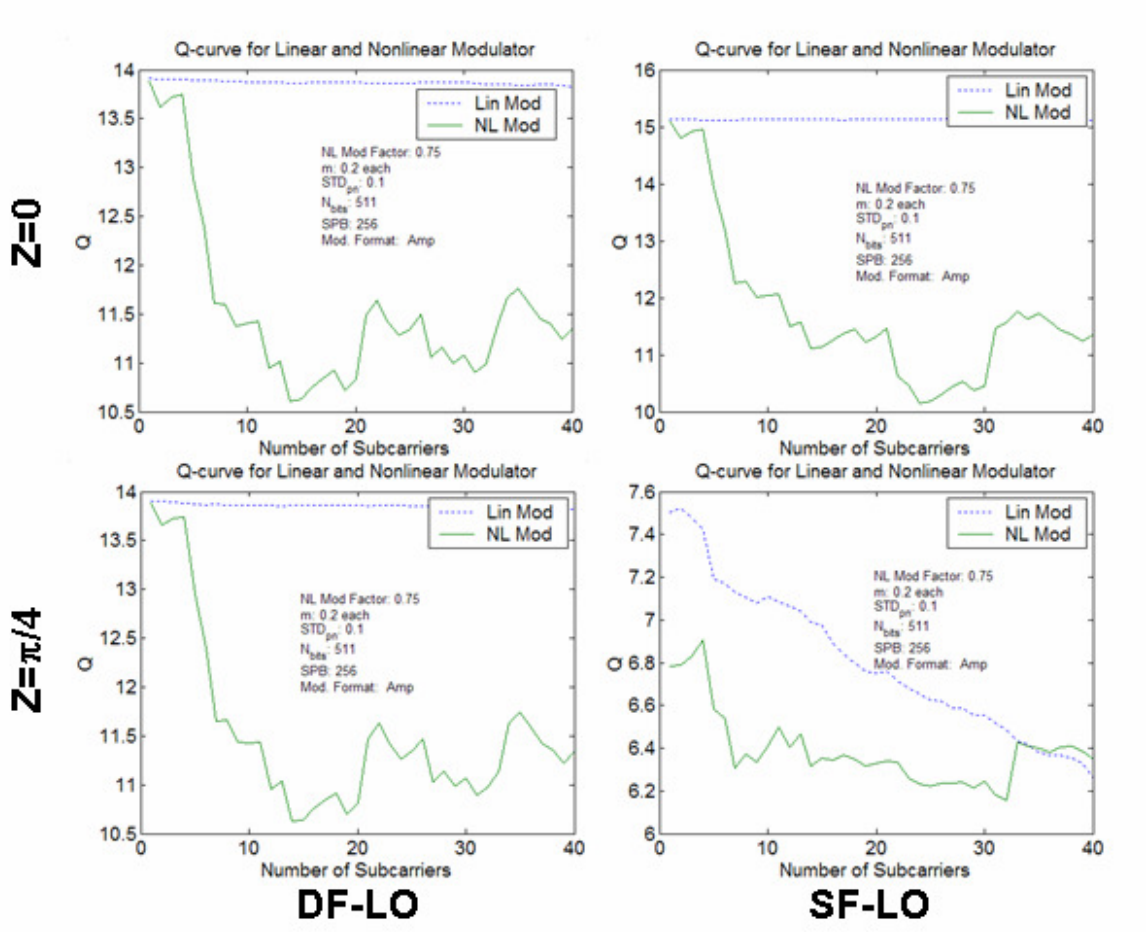

Figure 4.37: Modulator nonlinearity degradation related to number of amplitude modulated optical subcarriers. Each subcarrier power remains constant as the number of subcarriers is changed.

Figure 4.37 shows several aspects of the nonlinear modulator and of multiple subcarrier systems in general. First, by looking at the top row ($z = 0$) a comparison is seen between the dual- and single-frequency LO when no dispersion penalty is present. In this case the linear modulator has slightly better performance for the single-frequency LO; this is a result of the extra filter required during the RF demodulation since the dual-frequency LO homodyne detects the subcarrier of choice. There is an inherent statistical variation of these results because the modulation characteristics are varied according to each input signal. Scaling here keeps the effect of noise on a subcarrier independent of the

number of subcarriers. Therefore the decrease in Q is a result of the nonlinear effect of the modulator. Also, since the simulation was designed to compare the nonlinear and linear modulators the gains of the dual-frequency LO and single frequency LO receivers were not equated. Other than that, both the single- and dual-frequency LO have similar performance for the nonlinear modulator when no dispersion is present. The performance drops off quickly as the number of channels increases and then levels off for 15 or more subcarriers. The leveling off occurs because as the number of channels increases the probability that all of the channels transmit a one bit or a zero bit at the same time decreases. Therefore as the number of channels increases, more of the RF signal imposed on the modulator remains within the region of the modulator that is the most linear. The second row shows the comparison for the two receiver types after a length of fiber ($z = \pi/4$). The dual-frequency LO performs as well at this distance as it did at the fiber input. The performance of the single-frequency LO is much worse, as expected. For a single channel, the Q is half of the Q at the input of the fiber. This is expected since the eye-opening is half of that at the input. What is interesting is how the performance drops as the number of channels increases for both the linear and nonlinear case. This is because each subcarrier experiences power fading at a different rate and therefore the desired channel has a lower power than many of the other channels, causing the interchannel crosstalk to be more detrimental. The channel of interest becomes buried in the noise of the other channels. On the other hand, the dual-frequency LO compensates the desired subcarrier at the expense of the other subcarriers

and therefore its performance is dominated on its own noise (not the noise of the adjacent channels) and performs nearly identical to the signal at the input of the fiber.

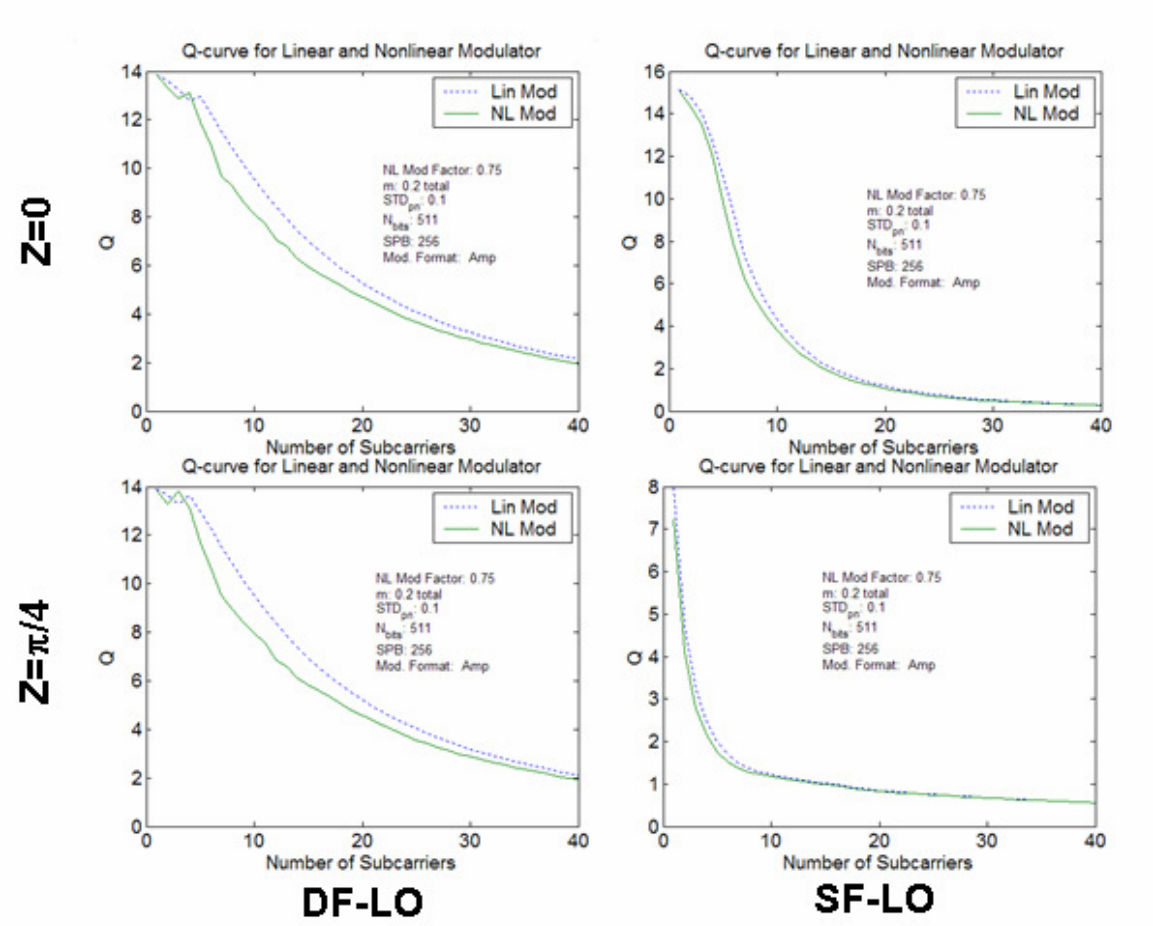

Figure 4.38: Modulator nonlinearity degradation related to number of amplitude modulated optical subcarriers. Total power remains constant as number of subcarriers increases.

In the more realistic situation where the total power is limited and the modulation index per subcarrier decreases as the number of subcarriers increases the performance of both the linear and nonlinear modulator decreases with the number of channels as shown in Figure 4.38. This is because as the modulation index per subcarrier decreases the effect of noise increases. As in the previous figure, the dual-frequency LO has nearly identical results at the fiber

input and after a length of fiber. The nonlinear modulator penalty increases initially as the number of subcarriers increase, but, as before, the penalty becomes less as the number of subcarriers becomes large since the RF signal remains in the mostly linear part of the modulator transfer function. The single-frequency LO drops off more rapidly than the dual-frequency LO because the dual-frequency LO truly homodynes the subcarrier. After a length of fiber and dispersion causes a power fading, the single-frequency LO receiver is penalized both by the decreased modulation index and by the power loss due to dispersion.

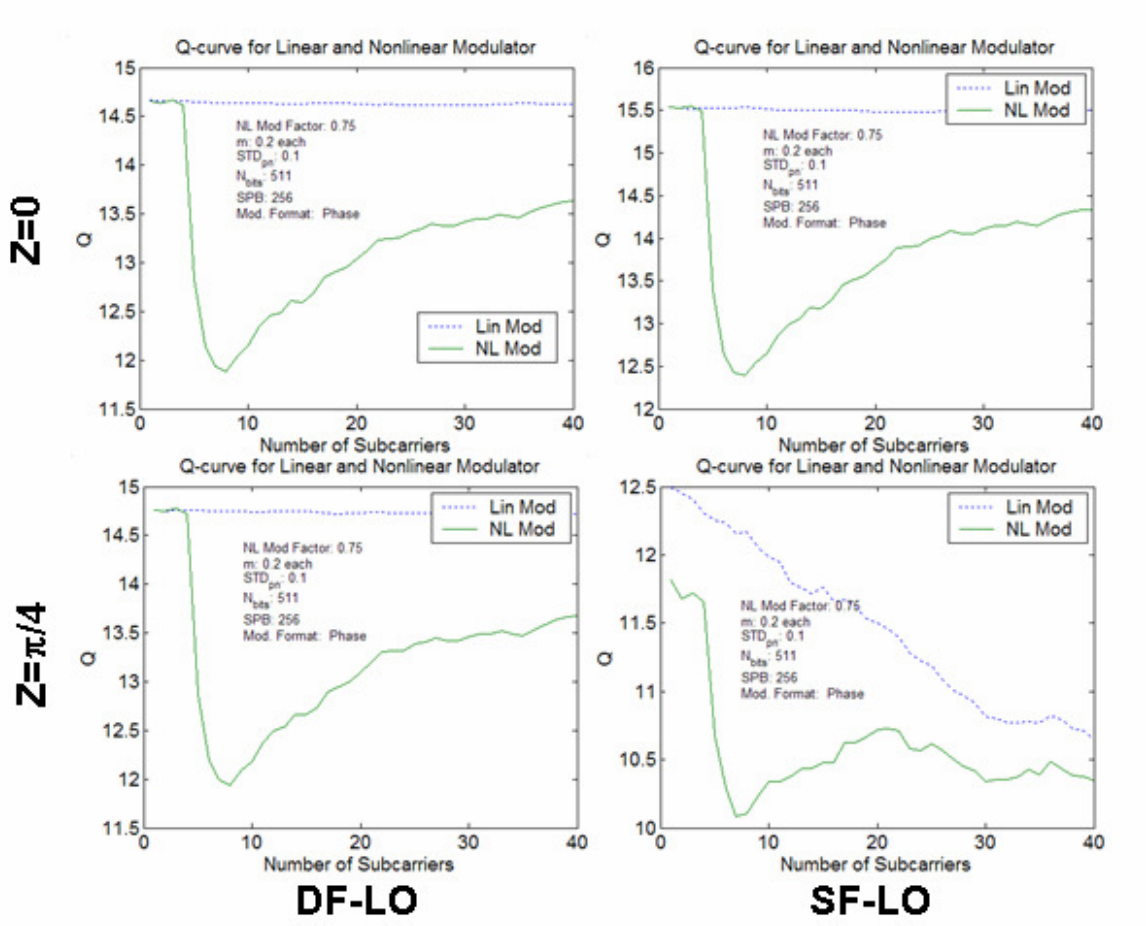

Figure 4.39: Modulator nonlinearity degradation related to number of phase modulated optical subcarriers. Subcarrier power remains constant as the number of subcarriers.

The phase modulation results show that both the single- and dual-frequency LO receivers are more immune to modulator nonlinearities than the amplitude modulated signals. This is expected since the modulator nonlinearity adds amplitude noise to the signal based on the total input RF signal variations. Since the RF amplitude only fluctuates due to the subcarrier sinusoids, not the bit patterns, the modulator nonlinearity does not increase the optical signal noise as much as for the amplitude modulated case. Also, as the number of subcarriers increases the signal remains in the linear portion of the modulator more than for amplitude modulation since the bit sequence does not introduce amplitude variations, so the performance of the nonlinear modulator system actually improves as the number of subcarriers increases. Still, a single channel does not experience the adverse affects of the nonlinear modulator, and has the best performance. The exact profile of the curve depends on the subcarrier frequencies and their spacing, but the trend is consistent for different subcarrier frequency maps. However, for the single-frequency LO receiver after a power loss due to dispersion, the system degrades as the number of channels increases. Again, this is because each channel experiences a different power loss and the desired subcarrier is degraded by the noise of the higher power subcarriers.

The performance of the phase modulated system when the total carrier power is held constant gives similar performance to the corresponding amplitude modulated system. This is because the Q degradation as the number of

subcarriers increases is dictated by the deceased signal amplitude. This can be seen in Figure 4.40 below.

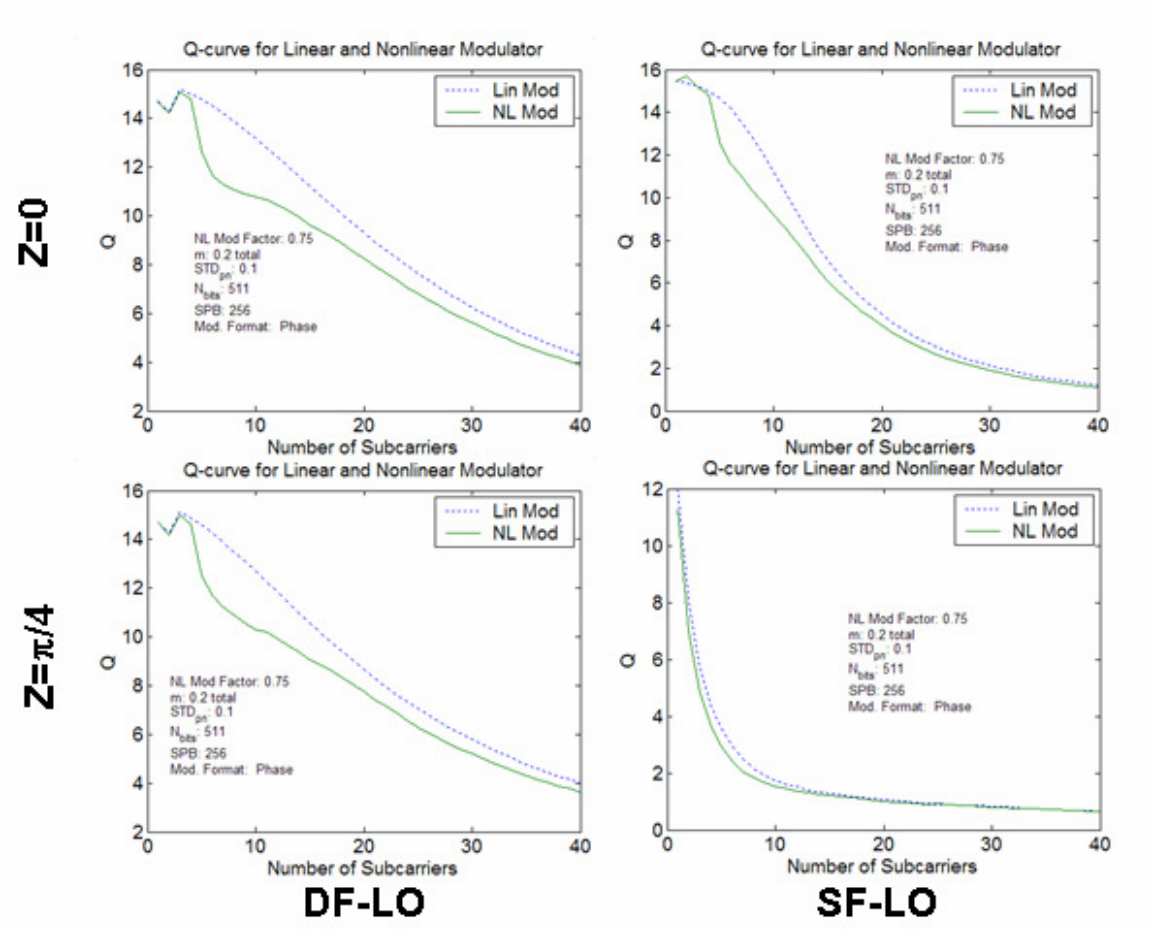

Figure 4.40: Modulator nonlinearity degradation related to number of phase modulated optical subcarriers. Total power remains constant as number of subcarriers increases.

This section shows that when dispersion causes the desired signal to have less power than the undesired subcarriers, the signal quality is greatly reduced. The need for compensating the dispersion induced power fading is greater in the multichannel case because of the increased cross-channel interference. This section also shows that the modulator nonlinearity is not as severe for phase modulated signals and once the number of channels becomes large (more than 10-12 here), the signal degradation levels off or even improves.

This simulation limited the modulator nonlinearity to 75% of the most linear part of the transfer function and changing this limit obviously changes the quantitative results, but the trends are the same.

Section 4.5.4. Implications of received power

The impact of received power on the system performance has already been looked at in the section about phase offset between the LO and carrier and the section on Q as a function of distance when dispersion causes power fading. This section will briefly investigate the effects of loss due to other system aspects besides power fading and how dual-frequency and single-frequency LO receivers compare in such systems. System loss is due both to fiber attenuation and to insertion losses of network components. This section will look at these two loss types separately. First, the received power will be varied independent of the fiber length, and therefore independent of the dispersion induced phase shift. Second, the attenuation will be varied proportional to the fiber length and therefore loss will increase as the dispersion increases. Finally, this section, as in the sections above, uses normalized input powers and receiver sensitivities so trends can be identified but quantitative values for specific systems are not given. This is because receiver sensitivity is dependent on bandwidth and the bit rates and subcarrier frequencies are normalized to the fiber dispersion. Also, since the fiber length is normalized according to the dispersion, the normalized fiber attenuation would be dependent of the particular fiber type. In order to model a realistic dispersion/attenuation pair, standard single-mode fiber is used to find a ratio between attenuation and dispersion (0.2 dB/km and $17 \frac{ps}{nm\,km}$, respectively).

This leads to an attenuation of 1.17 dB per unit z (≈23% per unit z) for a 20-GHz subcarrier.

This section will use the same model as used in Section 4.5.1 and Section 4.5.2, but will use a fixed phase noise ($\sigma_{LO} = \sigma_s = 0.1$) and no phase offset between the source and LO. The receiver noise has a variance of $\sigma_r^2 = 0.01$ as in the previous sections.

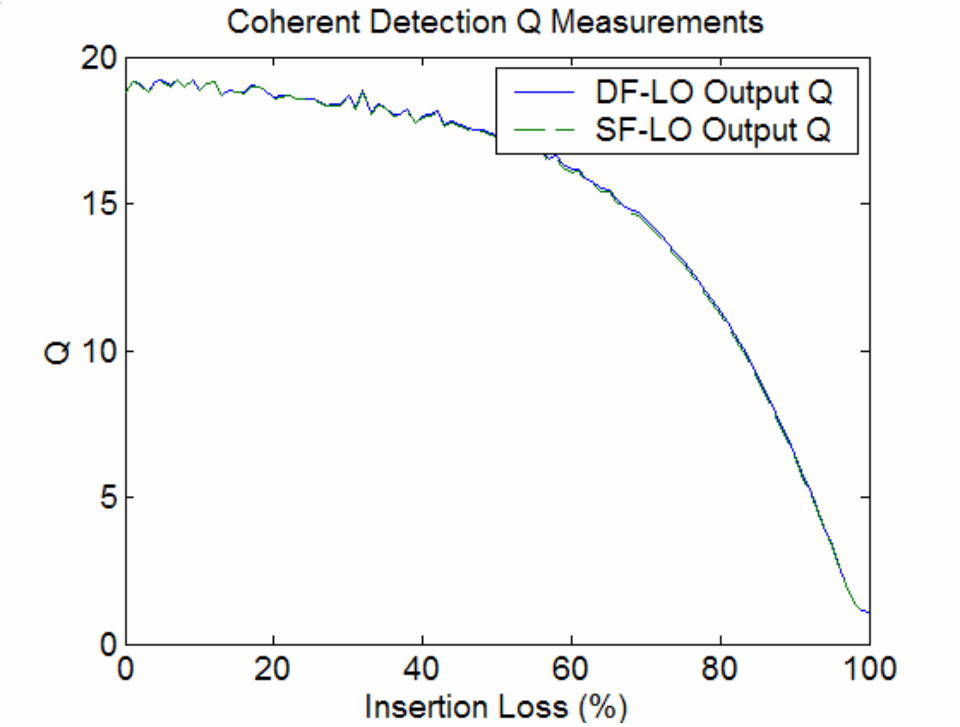

Figure 4.41: Q as a function of system loss, dispersion not considered. Single- and dual-frequency LO are compared.

Figure 4.41 compares the performances of a dual- and a single-frequency LO when dispersion effects are not taken into account and only system loss and noises are considered. As would be expected, the two types of receivers have identical performance since the gains in the receivers are normalized so each receiver design has equal performance at the input of the fiber. When the

thermal noise is included at the front end of the electronics in a single-frequency LO receiver design it has slightly worse performance because the noise is amplified by the RF LO before being filtered by the baseband filter. This effect can be seen in Section 4.5.2 when the loss is due to phase offset and therefore is not repeated here.

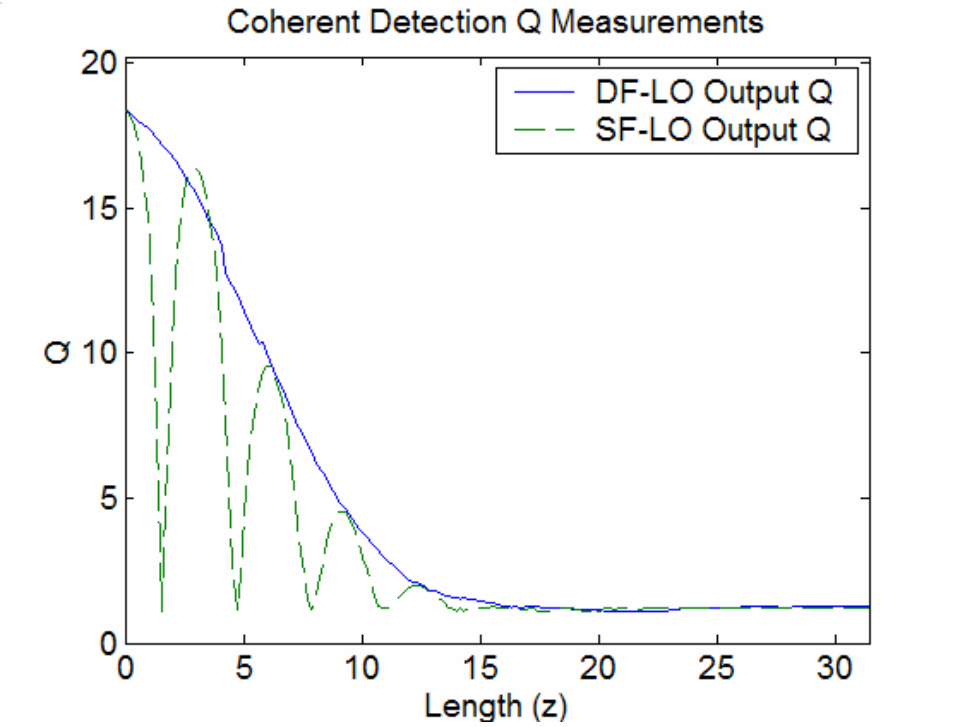

Figure 4.42: Q as a function of fiber length when fiber dispersion and attenuation are considered.

Again, the results here are as one would expect by comparing the results shown in Figure 4.33 and Figure 4.41. The performance of the dual-frequency LO drops due to attenuation and pulse broadening as the fiber length increases. The single-frequency LO receiver has this same degradation in addition to the power fading cycle due to the dispersion induced phase shift between the upper and lower sidebands of the optical carrier.

This brief section on performance of coherent optical systems considering system losses confirms again that the dual-frequency LO performs at least as well as the conventional system even for low received powers. There is nothing in the analysis to indicate otherwise, so the results here are expected.

Section 4.6. Chapter 4 Summary

In this chapter OSCM systems have been simulated for many different possible sources of degradation. It has been assumed, as in the analysis, that power levels are kept low enough that fiber nonlinearities are not an issue and therefore optical powers can be normalized to unity for the input signals. The impairments considered are dispersion, phase noise (or linewidth) of the laser, phase offset between the carrier and LO in homodyne receivers, modulator nonlinearity and system losses. Also included is a small amount of thermal noise in the receiver for the purpose of modeling the Q degradations due to power loss.

For noiseless systems (void of phase noise, amplitude noise, and thermal noise) eye-diagram comparisons are made between DSB and SSB carriers as well as DSB and SSB subcarriers. In both of the DSB carrier system dispersion causes power fading to occur as is shown the analysis of Chapter 3. By plotting the spectrum of the photocurrent this power fading is shown to occur during the photodetection process and therefore must be compensated either before or during the photodetection process. The dual-frequency LO that was proposed in Chapter 3 was shown to completely compensate for power loss when subcarrier frequency is much larger than the data signal bandwidth.

For the SSB carrier cases the dispersion leads to either a power loss or signal distortion if not compensated. However, in the SSB carrier case the phase compensation can occur in either the optical or electrical domain and advantages of each were presented.

Once the simulations illustrated the benefits of the dual-frequency LO, several impairments were introduced that potentially would be detrimental to this technique that relies on control of the phases of the signal and LO. Phase noise is included as a Gaussian random variable and in each case the dual-frequency LO receivers have a Q as high as or higher than the Q of the single-frequency LO receivers. Phase offset between the signal and the LO was also modeled and compared between the two receiver designs. In this case the single-frequency LO receiver performed better than the dual-frequency LO for a few distances, but generally performed worse than the dual-frequency LO because it suffered from dispersion induced power fading.

Modulator nonlinearity was also modeled both for ASK and PSK systems. Once again, when dispersion was included, the dual-frequency LO performed better than conventional optical receivers. In the absence of dispersion, the number of subcarriers influenced the system performance (as estimated by Q). Generally the performance decreases for a nonlinear modulator that modulates up to 10-12 subcarriers, but then levels off or even improves (for PSK) due to the confluence of the RF signal towards the linear portion of the modulator transfer function. Finally, system losses not due to dispersion induced fading or phase offsets were investigated. Nothing surprising was seen in this section since the

technique is not dependent on received signal strength. In the absence of dispersion both dual- and single-frequency LO receivers perform the same. In the presence of dispersion the dual-frequency LO performs the same as it does at the fiber input until the pulse broadening and sideband walk-off causes a Q penalty. The single-frequency LO has this degradation as well as the cyclic power fading.

Chapter 5. Conclusions and Summary

Section 5.1. Summary

Optical subcarrier multiplexed systems have been modeled, analyzed and simulated with respect to many network impairments and receiver designs. OSCM systems have subcarrier frequencies that are higher than the data bandwidth; therefore, the performance of the network is greatly influenced by the subcarrier frequency. Chromatic dispersion of optical fibers causes a phase shift of the subcarrier relative to the optical carrier and this phase shift introduces different adverse effects depending on the modulation techniques of the carrier. The modulation format of the data (onto the subcarrier) is not as important to the system performance as the modulation format of the subcarrier (onto the carrier).

The effects of dispersion and receiver design were presented using both analysis (Chapter 3) and simulation (Chapter 4). Other system impairments are also analyzed and simulated. The effect of laser phase noise (or linewidth) was analyzed for low total phase variance (so a small angle approximation of the sinusoid function can be made). The results of this analysis were then compared to numerical simulations that calculated the variances and didn't require this approximation. The analysis and simulation are in good agreement over the range in which the assumptions hold true. Phase offset between the LO and carrier was also considered in the simulation, while the analysis made the assumption that the phase-locked loop (PLL) could perfectly eliminate any static phase offset. A nonlinear modulator model was introduced in Chapter 2, the

effects of such a modulator are examined using simulation. Finally, fiber and component losses were studied in the simulation. Since the analysis assumed ideal filters and noiseless receivers, signal loss does not affect the Q and therefore was not included in the analysis. The simulation does introduce non-ideal filters and receivers so a signal loss does impair the Q, these results were also shown in Chapter 4.

Of the impairments considered dispersion is of most concern. There are two reasons for this. First, for DSB-carrier systems, dispersion causes the greatest penalty. Second, dispersion is caused by the optical fiber which is the most cost prohibitive component to upgrade, whereas laser and receivers are at the network edges and therefore more easily upgraded to reduce phase and thermal noise. Four types of OSCM systems were compared in the analysis and in the simulations with respect to dispersion. The types included DSB carrier with either DSB or SSB subcarriers and SSB carriers with either DSB or SSB subcarriers. Of these four system types, a DSB carrier with DSB subcarriers has the worst performance. The most detrimental effect of dispersion is the phase mismatch between the upper and lower sidebands of the carrier that cause the photodetector to destructively superimpose the two halves of the signal. At a distance where dispersion causes the subcarrier to have a $\pi/2$ offset relative to the carrier, the received signal is essentially zero. The normalized length for this is

$$z_{null} = \frac{\pi}{2} \qquad \textbf{(5.1)}$$

since the length is in fact normalized to the phase shift of the subcarrier. In terms of the physical parameters, the location of the first power null is

$$L_{null} = \frac{c}{2Df_S^2\lambda^2} \quad \textbf{(5.2)}$$

where c is the speed of light, D is the dispersion parameter (delay difference per unit bandwidth per unit distance), f_s is the subcarrier frequency and λ is the wavelength of the optical carrier.

The other system designs also have penalties related to the phase shift of the subcarrier. The DSB carrier with SSB subcarrier has the same destructive interference problem as above, however the broadening of the pulses is not as severe. The SSB carrier signal can also result in a power fading if the data is DSB modulated on to the subcarrier and the phase offset between the subcarrier and carrier is not corrected for during demodulation. Finally, the SSB carrier with SSB subcarrier is the most robust to dispersion because there is no phase shift induced power fading and the signal bandwidth is the smallest so pulse broadening is smaller than for DSB subcarriers. The signal does, however, experience severe distortion if the phase shift is not mediated.

The dispersion induced power fading and distortion can be compensated in several ways. The literature suggests several methods including using only SSB carriers by removing one sideband by either optical filters or SSB modulation. Other methods include detection schemes that only detect one optical sideband, mid-span phase conjugate techniques, or remote heterodyne detection. These techniques all require special modulation formats, transmitter designs, access to the signal within the network, or discarding half of the optical

signal at the receiver. None of the techniques found in literature offer a method to use the entire optical signal and compensate the signal entirely at the receiver. For installing OSCM systems in an environment where it is desirable to have the expense at the receiver end (such as an uplink from remote location to a central office) a technique where the compensation occurs only in the receiver is required.

A dual-frequency local oscillator is proposed in this dissertation as a means to optically compensate for the phase shift [6,7]. This dual-frequency LO uses a RF sinusoid to modulate an optical carrier and feedback is used to control the phase of both the RF sinusoid and the laser. The following equation shows how such a LO can be constructed.

$$S_{LO} = \cos(2\pi f_\lambda t + \phi_{LO})\cos(2\pi f_s t + \phi_s) \quad \textbf{(5.3)}$$

If the phase of the sinusoid is locked to the optical carrier phase and the LO laser phase is locked to the phase shift of the subcarrier, then the power penalties due to both the carrier/LO phase offset and the USB/LSB phase offset can be simultaneously compensated. The analysis shows that this technique eliminates the power fading of DSB carrier signals, allowing the signal to propagate to a distance where pulse broadening causes inter-symbol interference.

While DSB carrier signals can only be compensated using an optical technique, the power fading or signal distortion of the SSB carrier signal can be compensated either optically or electrically. The electrical technique uses a PLL in the RF domain to eliminate the relative phase shift between the subcarriers and carrier. This technique is common to RF demodulation techniques and is

presented as a comparison to the optical technique introduced. In addition to correcting the phase error, the dual-frequency LO is able to select the desired subcarrier by tuning the sinusoid frequency to the subcarrier frequency (for homodyne detection) or to a fixed offset equal to the intermediate frequency (for heterodyne detection). Both techniques were shown in the simulation.

Once the power penalty due to the dispersion induced phase shift is compensated, the next dispersion penalty is due to pulse broadening. Since the dual-frequency LO can only compensate for the discrete phase shift of the subcarrier, the data signal (which has a non-delta bandwidth) has a differential phase shift across its bandwidth. In the case of SSB carriers, this leads to pulse broadening as defined in many text books and journals. If the system has a DSB carrier, then the differential phase shifts of the USB and LSB have opposite sign, and results in a type of walk-off between the sidebands that causes distortion. This was shown in analysis and simulation for the SSB carrier, and simulated for the DSB carrier.

The work presented here has shown that OSCM systems can use DSB carrier modulation when a dual-frequency LO is used in the receiver design. This technique is not any more sensitive to phase noise, phase offset, or modulator nonlinearity than conventional coherent detection or direct detection of OSCM systems. It also has the added benefit of being able to select the desired OSCM by tuning the optical dual-frequency LO, which can simplify the following RF circuitry. This is especially beneficial for very high subcarrier frequencies where the RF component technology is not as mature.

Section 5.2. Key Contributions

The key contributions of this dissertation are

1. Proposal, analysis, and verification by simulation of a dual frequency local oscillator receiver to remove the power fading in DSB OSCM systems
2. Analysis and simulation of the effects of transmitter and local oscillator phase noise and the effects of modulator nonlinearity to verify that the dual oscillator receiver retains its advantages in the presence of these (and other) impairments.

Section 5.3. Opportunities for Future Work

Areas that would be interesting to study related to this work are the following. First, a complete comparison of the relative advantages and disadvantages between the dual-frequency LO and remote heterodyne techniques may provide unique insight. Also other receiver designs could be found that also eliminate the power fading while preserving the full optical signal. These techniques may be either easier or less expensive to implement and therefore warrant investigation. One could also look at the possibility of controlling the phase of each MLL peak in such a way as to have a multi-frequency (more that dual) LO to compensate the phase shift of several subcarriers simultaneously.

Work that could extend what has been done here to practical systems includes doing system calculations and simulations of practical device and system parameters and limitations to find the maximum link lengths. This could

include modeling other nonlinearities (such as fiber) beyond the modulator nonlinearity. Additionally, similar work could be done to investigate multipath interference in free-space optics where the phase offset also leads to power fading. Finally, analysis of the multiple subcarrier case could be performed using a Gaussian process model, to compliment the multiple subcarrier simulations.

Appendix A. Hilbert Transform RF Homodyne Receiver

Detecting a SSB subcarrier when the subcarrier spacing is less than twice the bit rate takes special consideration. Simple homodyne detection of the signal with a baseband filter causes severe adjacent channel cross-talk. Either a tunable filter or intermediate filter can be used to isolate the desired channel from the adjacent channels before demodulation by either homodyne detection with a baseband filter or envelope detection. When the bandwidth of the subcarrier channel is nearly the same as the subcarrier spacing, the filter requirements are very high. Another approach is to eliminate the adjacent channels during RF demodulation.

The problem arises when the desired channel is shifted to baseband. Both a SSB and DSB optical carrier produced RF signals with positive and negative frequency components after direct detection. Below is a simple illustration of the signal before and after demodulation. (Later in this appendix will be simulation results that illustrate realistic OSCM system.)

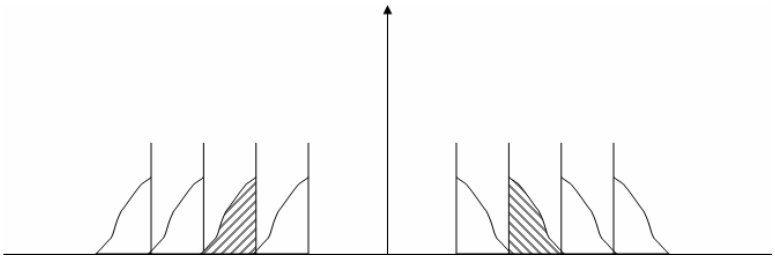

Figure A.1: Sample SSB subcarrier system shown at the subcarrier frequencies. Desired channel is shaded.

After using a LO to shift the desired channel to baseband and before baseband filtering, the signal suffers from adjacent channel cross-talk. This is

seen in the following figure. A baseband filter cannot completely remove the cross-talk.

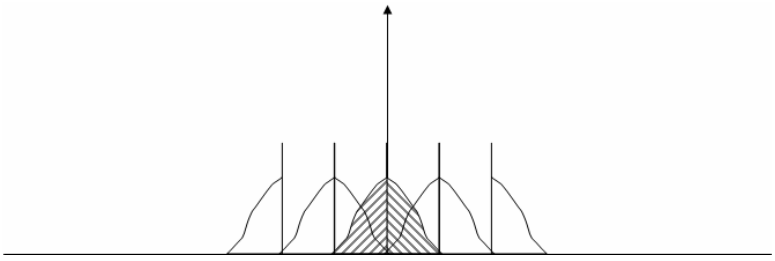

Figure A.2: Sample SSB subcarrier system shown with the desired signal at baseband. Severe adjacent-channel crosstalk is seen.

By incorporating a Hilbert transform into the RF demodulation scheme the adjacent channel crosstalk can be eliminated. The equation required for this is

$$S_{bb} = \frac{1}{2} S\cos(2\pi f_s t) + \frac{1}{2}\mathcal{H}\{S\sin(2\pi f_s t)\} \qquad \textbf{(A.1)}$$

where $\mathcal{H}\{\bullet\}$ is the Hilbert Transform and is described in more detail in Appendix C. S is the signal illustrated in Figure A.1 and f_s is the frequency of the desired subcarrier. By using equation (A.1), the resulting spectrum is illustrated in Figure A.3. The mathematics is very similar to that used to generate a SSB signal shown in Appendix C and is therefore not repeated here.

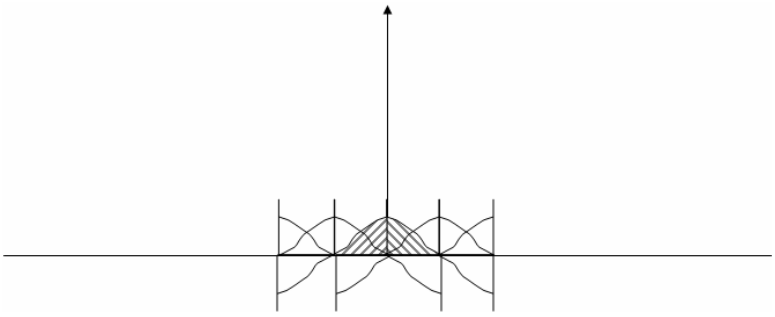

Figure A.3: Simplified spectrum of super imposed signals before summation.

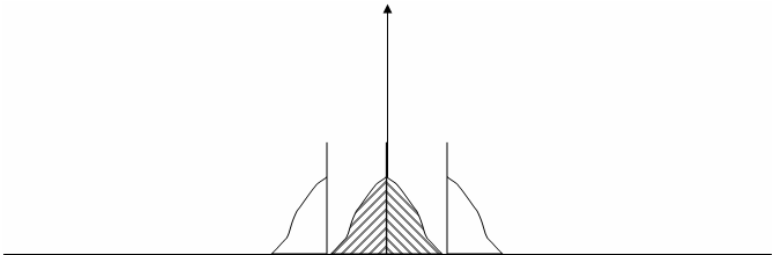

Figure A.4: Spectrum of super imposed signals after summation.

Clearly this figure shows an idealized result, but the adjacent channels are seen to be suppressed by using a Hilbert Transform in the receiver.

The above receiver design (equation (A.1)) is used in a simulation based on the bandwidth and frequency spacing of a cable-television (CATV) signal. The signal bit rate used is 4.5 MHz and the spacing is 6 MHz. In order to produce eye-diagrams for visualization, the signal is a 4.5 Mb/s digital signal, rather than a true analog CATV signal. 4.5 Mb/s was chosen since CATV has a frequency component at 4.5 MHz, and thus gives a spectrum similar to a digital 4.5-Mb/s waveform. The following figures show the spectrum and eye diagrams of four channels that are photodetected then demodulated using either a conventional RF homodyne receiver or the Hilbert homodyne receiver. The homodyne detection is followed by a baseband filter with a 3-dB bandwidth equal to the bit rate. Since no dispersion is included in this simulation the results are the same for SSB and DSB carriers; the following figures depict a SSB optical carrier. (Both SSB and DSB optical carrier signals are 'DSB' after photodetection.)

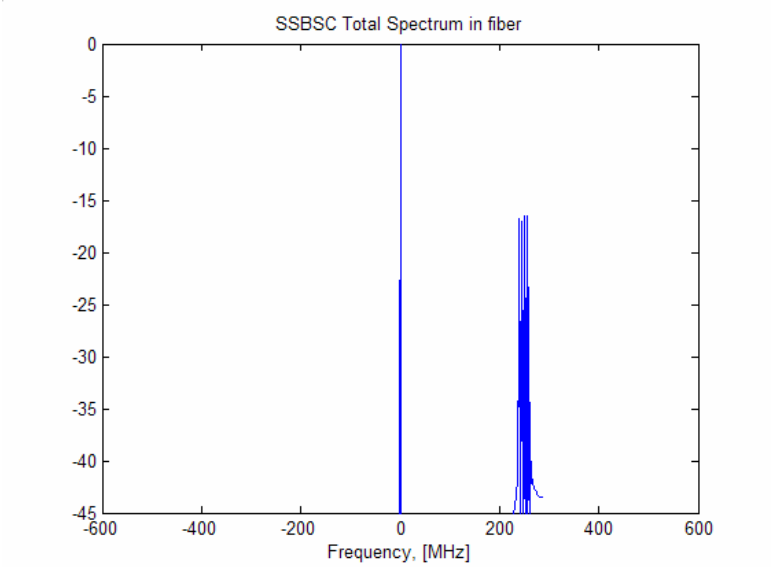

Figure A.5: SSB carrier with SSB subcarrier before photodetection. The subcarriers are spaced less than twice the signal bandwidth.

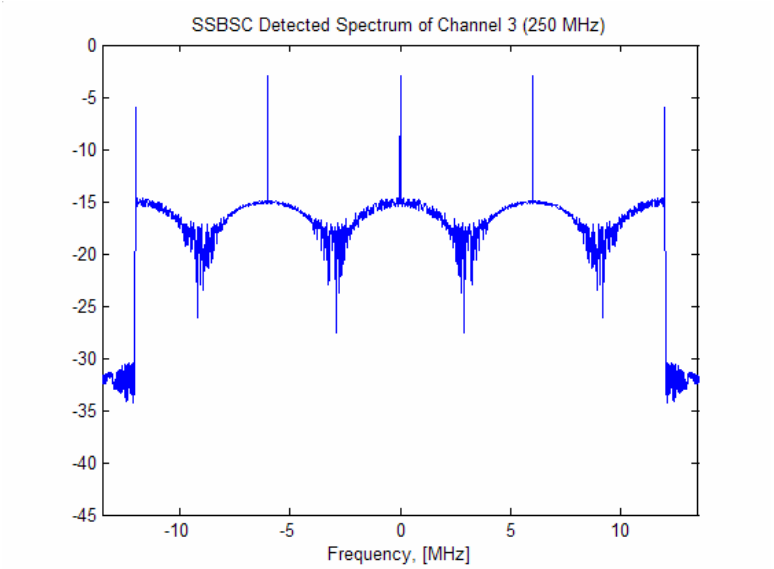

Figure A.6: Spectrum of channel 3 after RF homodyne detection, before the baseband filter. The adjacent-channel crosstalk is seen.

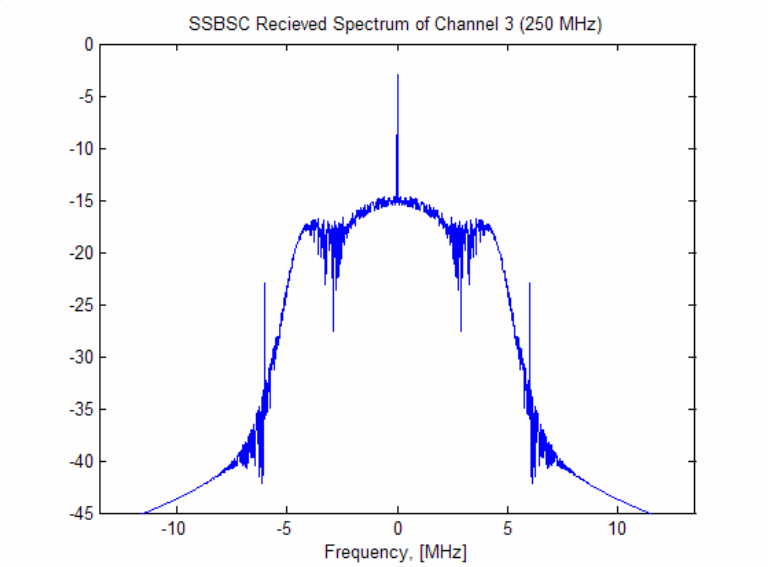

Figure A.7: Spectrum of channel 3 after RF homodyne detection, after the baseband filter. The adjacent-channel crosstalk is still seen.

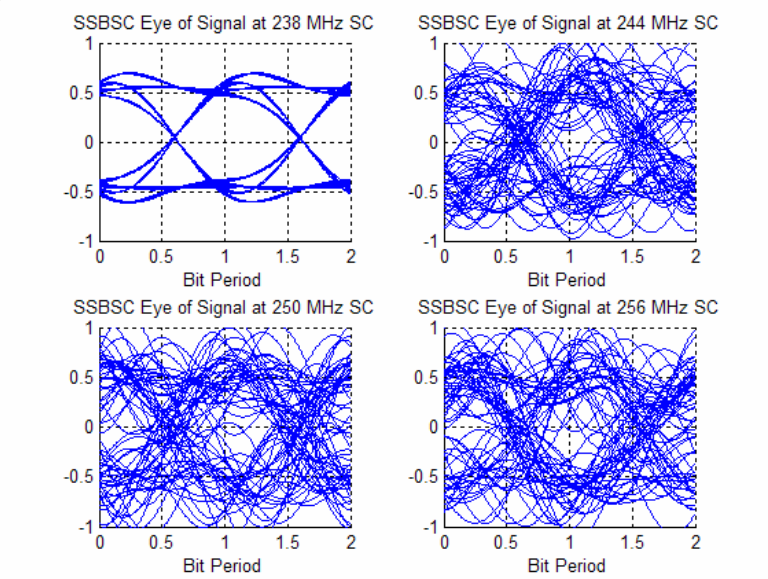

Figure A.8: Eye diagram for each channel using conventional RF homodyne detection.

The final picture above shows that three of the channels are severely impacted by the crosstalk. Since the first channel (238-MHz subcarrier) does not have a lower frequency subcarrier adjacent to it, it is not degraded. Clearly a method to remove the adjacent channel is required, specifically the channel adjacent, and lower in frequency, to the desired channel. This requirement

would be reversed if the subcarrier retained the LSB instead of the USB. The following three figures repeat the previous three figures using the Hilbert homodyne receiver described above.

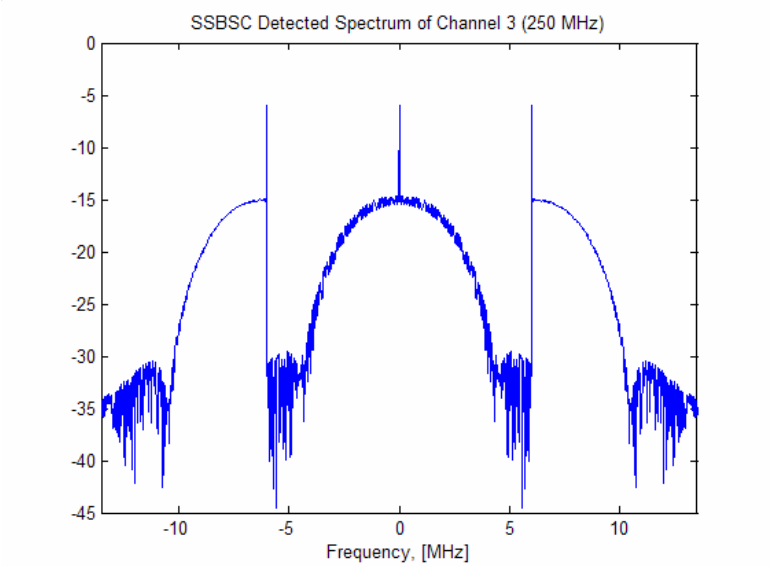

Figure A.9: Spectrum of channel 3 after Hilbert homodyne detection, before the baseband filter. The adjacent-channel crosstalk is reduced.

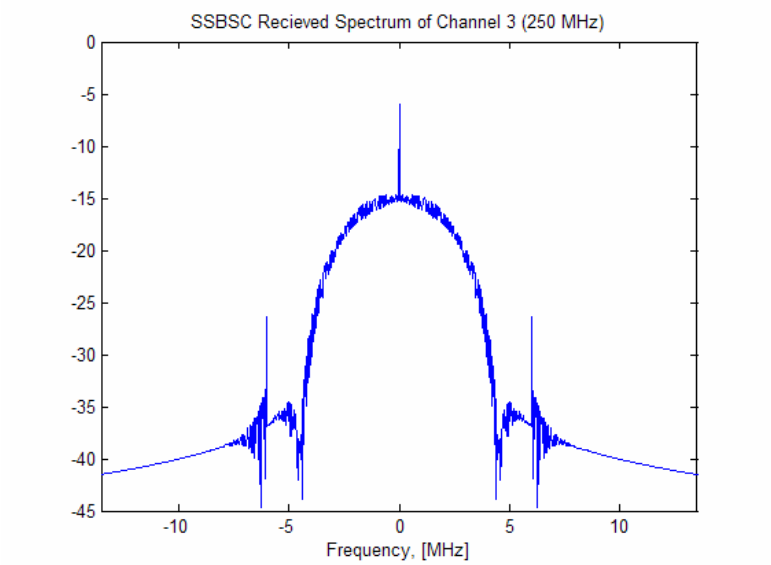

Figure A.10: Spectrum of channel 3 after Hilbert homodyne detection, after the baseband filter. The adjacent channel-crosstalk is further reduced.

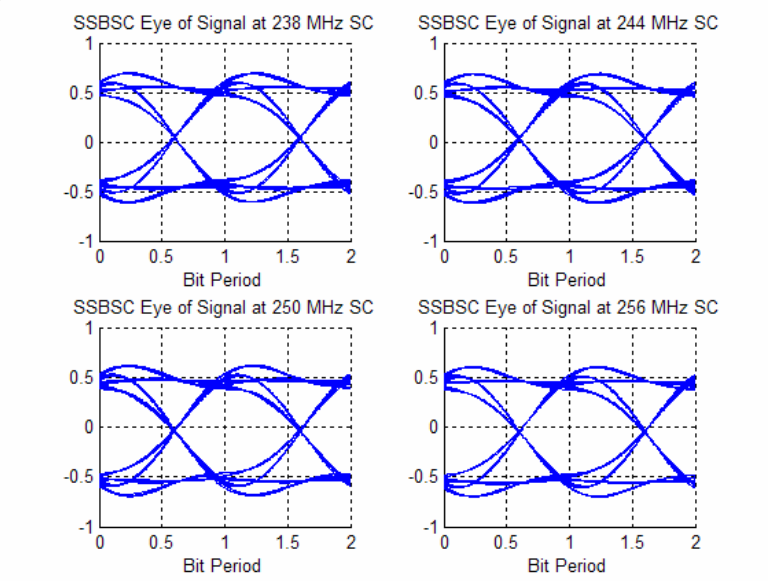

Figure A.11: Eye diagram for each channel using RF homodyne detection that incorporates a Hilbert transform.

The use of the Hilbert transform in the RF receiver greatly improves the eye-diagrams of the received signals. This is the technique used in the simulations conducted while investigating OSCM system whenever the subcarrier spacing was too small to detect a quality signal using conventional methods. The results presented in the main part of this dissertation, however, used subcarrier spacing that was more than twice the signal bandwidth in order to avoid these complications.

Appendix B. Mode-Lock Laser Local Oscillator

In Section 2.2.7 the idea of using a Mode-Locked Laser (MLL) as the optical LO is introduced. By using a MLL an entire OSCM or wavelength division multiplexed (WDM) system can be detected and the resulting RF FDM system will have frequency spacing different than that of the OSCM or WDM signal.

Appendix B.1. Using a MLL to Coherently Detect an OSCM

In order to look at using a MLL to heterodyne an OSCM or WDM set of channels an equation needs to be identified to represent the OSCM channels and the MLL spectrum. Since the same technique can be applied to either an OSCM system or WDM system the analysis below will only refer to OSCM systems, and specifically the OSCM systems will be USB, suppressed carrier. The essential difference between the two systems is the frequency spacing of the channels.

The energy of a single channel can be simply represented as in equation (2.7), repeated here in cosine notation for convenience.

$$S_1 = A_1 \cos(2\pi f_1 t) \qquad \textbf{(B.1)}$$

where A_1 is the magnitude power of the signal and f_1 is the optical carrier frequency; which in the OSCM system is the optical carrier plus the subcarrier frequency. Strictly speaking, A is $A(t)$ and represents the data of an on-off-keyed (OOK) signal. Also, if other modulation types were involved time dependence could be present in the frequency and/or the phase terms of the subcarrier. To investigate whether a MLL can be used to detect a OSCM, the simplification of ignoring the modulation is sufficient here since it is assumed that if the subcarrier can be detected then the signal carried by the subcarrier is also detected. Data modulation can always be incorporated in the final equations by replacing A with $A(t)$. However, as will be seen later, the modulation bandwidth will need to be considered when making some assumptions.

To represent N channels that are wavelength multiplexed together,

$$S = \sum_{i=1}^{N} A_i \cos(2\pi f_i t) = \sum_{i=1}^{N} A_i \cos(\omega_i t) \quad \textbf{(B.2)}$$

where A_i is the amplitude in the i^{th} channel. This is the baseband form of equation (2.11) with the carrier suppressed. The same equation can be used to represent the MLL LO by replacing ω_i with $\omega_{LO,i}$

The energy of a single wavelength local oscillator (LO) is

$$S_{LO} = A_{LO} \cos(\omega_{LO} t + \phi) \quad \textbf{(B.3)}$$

ϕ is the phase offset between the LO and the signal. Since this discussion is for heterodyne detection the relative phase term can be dropped. Also, as in the discussion of coherent detection in Section 2.2.7 the polarizations of the LO and signal are assumed to be aligned. Using equation (2.27) for photodetection and before removing the DC terms, a single heterodyne detected signal is

$$I_P = A_1^2 + A_{LO}^2 + 2A_1 A_{LO} \cos\left((\omega_1 \pm \omega_{LO})t\right) \quad \textbf{(B.4)}$$

In order to apply this to a MLL spectral comb and OSCM set of channels, one needs to expand the frequency and power terms to include a sum of frequencies.

By using the N-channel OSCM system as defined in (B.2) the photocurrent for the resulting FDM system is found to be

$$I_P = N A_{sig}{}^2 + N A_{LO}^2 + 2A_{sig} A_{LO} \left(\sum_{i=1}^{N} \cos(\omega_{os,i} t) \right) \quad \textbf{(B.5)}$$

It is assumed here that each channel has the same signal power, and that each spike of the LO comb has the same LO power. Also, as above, it is assumed that the polarizations are perfectly aligned. $\omega_{os,i}$ is the offset frequency of the i^{th} channel such that $\omega_{os,i} = \omega_i - \omega_{LO,i}$.

To generalize equation (B.5) for signals and LO or differing powers, NA_{xx} needs to be a summation of $A_{xx,i}$ over N, and the $2A_{sig}A_{LO}$ terms needs to be moved inside the final summation.

In order to further simplify equation (B.5) for the case of equally spaced OSCM channels and equally spaced LO comb spikes, the following relationship can be found.

$$\omega_{LO,i} = \omega_0 + \omega_{os} + i(\omega_\Delta + \omega_{os}) = \omega_0 + i\omega_\Delta + (i+1)\omega_{os} \qquad \textbf{(B.6)}$$

ω_Δ is the OSCM channel spacing in radians, and ω_{os} is the offset between the LO spacing and the OSCM spacing, and is the frequency spacing of the signal after detection.

For everything above to work, a few more assumptions need to be pointed out. First, the total number of channels detected must be such that two spikes of the LO do not place two detected channels at the same ω_{os}. To insure this, the last channel, $i=N$, must ensure that $\omega_{OS,i} \le \omega_\Delta$. This leads to equation (B.7). The 2 in the denominator is due to the fact that both $\omega_1 + \omega_{LO}$ and $\omega_1 - \omega_{LO}$ can be tuned to the intermediate frequency.

$$N < \frac{\omega_\Delta}{2\omega_{os}} \qquad \textbf{(B.7)}$$

Modulation has also been ignored in the above situation, and must be considered when choosing an ω_{os}. ω_{os} must be larger than the modulation bandwidth, to whatever extinction ratio is considered appropriate in terms of interchannel cross-talk.

As an example we can choose a WDM spacing and bit rate, then determine an appropriate offset frequency. With this information the maximum number of channels (*N*) can be determined. Let us assume some common numbers.

ω_{Δ} = 10 GHz

B = 10 Mb/s

With a bit rate, *B*, equal to 10 Mb/s, we need to insure that ω_{os} is large enough so the cross-channel interference is not significant. We can assume that at 10 Mb/s, we can filter the signal with a high finesse filter so we do not need large guard bands. Let us assume for now that we can use 10% guard bands so ω_{os} = 2 * 11 MHz = 22 MHz. From equation (B.7) we find that *N* < 10 GHz/(2*22 MHz) = 227.27. So the maximum *N* in this case is 227. This number appears very large and in practical situations 10 Mb/s signals probably would not be spaced 10 GHz apart because that is very spectrally inefficient.

It is evident that for low bit rate applications, like 10 or 100 Mb/s Ethernet, that this approach can potentially simultaneously shift many optical channels to a compact RF domain frequency division multiplexed system. For low bit rate systems the number of channels is limited by fiber and MLL performance. As the bit rate increases, RF filters are not as sharp and larger guard bands will be required. This will reduce the number of channels. So for large bit rates, the number of channels becomes limited by the performance of the RF electronics.

Appendix B.2. Tuning Range of MLL Detection Techniques

One way to select a desired OSCM channel to be located at a fixed IF is to tune the wavelength of the MLL. In order to look at the tuning range and number of channels possible using a MLL to detect a WDM or OSCM a number of terms need to first be defined. These terms are related to the frequency (or wavelength) of the MLL and OSCM.

The first frequencies that need to be defined are those related to the OSCM system of channels. As above, consider the simple case of equally spaced (in frequency, not wavelength) channels. In this case one can define a first, or lowest, frequency and frequency spacing. Let the first frequency be ω_0 and the frequency spacing be ω_Δ.

Similarly, the MLL frequencies can be defined by ω_{L0} for the initial frequency and $\omega_{\Delta L}$ for the frequency spacing. Here the subscript '*L*' is used to identify the frequencies as relating to the *L*ocal oscillator (LO), which is the MLL. ω_{L0} is defined as the first frequency in the range of interest, or more specifically as the smallest frequency of a MLL spike ≥ ω_0.

In the case where there are an equal number of MLL spikes and WDM channels an offset frequency, ω_{os}, can be defined. This is the offset in the spacing, and will become the spacing of the electrical section after detection. This is the same value used in equation *(B.6*).

$$\omega_{os} = \omega_{\Delta L} - \omega_{\Delta} \qquad \textbf{(B.8)}$$

When the number of MLL spikes is not equal to the number of WDM channels, that is when there is not a one-to-one correlation, then ω_{os} has no relevant meaning.

Before talking about the signal after detection one final term needs to be defined. There will be some difference in the initial frequency of the MLL and OSCM signals. Since ω_{L0} is defined above as the first spike with a greater frequency than ω_0, this difference can be defined as below, and will be positive. In practice it is not necessary to be positive, but it greatly simplifies the math in this summary to define it that way. Let ω_δ be this difference.

$$\omega_\delta = \omega_{L0} - \omega_0 \qquad \textbf{(B.9)}$$

In a system with N channels, let $n<N$ such that the frequency of the n^{th} channel of the OSCM system can be represented by (B.10).

$$\omega_n = \omega_0 + n\omega_\Delta \qquad \textbf{(B.10)}$$

Similarly the m^{th} spike of the MLL spectrum can be represented by (B.11). M is the total number of spikes in the frequency range of interest.

$$\omega_{Lm} = \omega_{L0} + m\omega_{\Delta L} \qquad \textbf{(B.11)}$$

In the case where there is a one-to-one correlation between the OSCM channels and LO spikes, $M=N$ and $m=n$.

With all of the frequency terms related to the OSCM and MLL, one can look at the terms generated after detection using a photodetector. The intermediate frequency, ω_{IF}, is defined for the n^{th} channel to be the frequency of the signal after heterodyne detection. By adjusting either ω_{L0} or $\omega_{\Delta L}$ any channel

can be detected at ω_{IF}. In this appendix we will only consider tuning ω_{L0}. Also, ω_{IF} is considered to be a constant here; however, it may in fact prove to be better to tune the electronics to a new IF than to tune the optics to a new LO frequency. In the case where *M=N*, the intermediate frequency is given by

$$\omega_{IF} = \left|\omega_{Ln} - \omega_n\right| = \left|\omega_{L0} + n\omega_{\Delta L} - \omega_n\right| \quad \textbf{(B.12)}$$

Using the definitions of ω_δ and ω_{os} from above the intermediate frequency is expressed in following equations. Each equation can be useful in different situations.

$$\omega_{IF} = \left|\omega_0 + \omega_\delta + n\omega_{\Delta L} - \left(\omega_0 + n\omega_\Delta\right)\right| \quad \textbf{(B.13)}$$

$$\omega_{IF} = \left|\omega_0 + \omega_\delta + n\omega_{\Delta L} - \omega_0 - n\omega_\Delta\right| \quad \textbf{(B.14)}$$

$$\omega_{IF} = \left|n\omega_{\Delta L} - n\omega_\Delta + \omega_\delta\right| \quad \textbf{(B.15)}$$

$$\omega_{IF} = \left|n(\omega_{\Delta L} - \omega_\Delta) + \omega_\delta\right| \quad \textbf{(B.16)}$$

$$\omega_{IF} = \left|n\omega_{os} + \omega_\delta\right| \quad \textbf{(B.17)}$$

When determining how far ω_{L0} has to be turned to detect all channels of the OSCM or WDM system at a given ω_{IF} there are three schemes to considered based on the ratio of the number MLL peaks to the number of channels. First is using one LO peak, which is the normal heterodyne scheme. Second is the case used through most of the summary above, that is *M=N*. The third case considered now is for *M=N*/2.

To tune the LO through all *N* of the OSCM channels using a single frequency LO, one has to tune the LO through a frequency range of ω_R.

$$\omega_R = N\omega_\Delta - 2\omega_{IF} \quad \textbf{(B.18)}$$

The $2\omega_{IF}$ term is included because the LO needs to turn from $\omega_0 + \omega_{IF}$ to $\omega_N - \omega_{IF}$ in order to detect all channels at ω_{IF}. In this case *N* is not limited by the relation between the OSCM (or WDM) and LO, but on the physical capabilities of the fiber and optical components.

In the case where *M*=*N*, the tuning range is given by

$$\omega_R = \frac{\omega_\Delta}{2} \quad \textbf{(B.19)}$$

Here *N* is limited by the relation between the MLL and WDM systems. The relation was found in the previous section to be $N < \omega_\Delta/(2\omega_{os})$. *N* can be found by finding frequency of the first and last possible channel in the RF domain, and the channel spacing. One can set any channel to be at the IF, so let us set channel one to be at the IF.

1st channel $$\omega_{IF} = \omega_{L0} - \omega_0 \quad \textbf{(B.20)}$$

***n*th channel** $$\omega_{IF} + n\omega_{os} = \omega_{L0} + n\omega_{\Delta L} - (\omega_0 + n\omega_\Delta) \quad \textbf{(B.21)}$$

When $n\omega_{os} = \omega_\Delta/2$ then the n^{th} channel is

$$\omega_{IF} + n\omega_{os} = \omega_0 + n\omega_\Delta - (\omega_{L0} + n\omega_{\Delta L}) \quad \textbf{(B.22)}$$

It is at this point were the channels will start to overlap in the RF domain due to the fact that the IF is determined by both $\omega_{signal} - \omega_{LocalOscillator}$ and $\omega_{LocalOscillator} - \omega_{signal}$. In other words, at this point two different channels simultaneously are located at the IF.

In the final case, where there is one MLL peak for every other OSCM channel the following condition is true.

$$\omega_{\Delta L} > 2\omega_{\Delta} \quad \textbf{(B.23)}$$

With this in mind, it is found that the above restriction does not apply. The channels will not start to overlap in the RF domain since the overlapping term no longer exists. Therefore the tuning range is found to be

$$\omega_R = \omega_{\Delta} \quad \textbf{(B.24)}$$

Since the MLL needs to tune trough the entire ω_{Δ}, the maximum number of channels is $N < \omega_{\Delta} / \omega_{os}$.

Appendix B.3. Simplifying the Expression for MLL-LO Detection

So far the analysis in Appendix B has used simplified expressions for the MLL and OSCM signals. This section will detail and verify the simplification used. Plots generated in MATLAB® will compare the full equations to the abbreviated ones. A mode-locked laser (MLL) can be used to simultaneously coherently detect several channels in a WDM or OSCM. This has been shown above for the case where one channel is selected by either tuning the initial (or central) MLL wavelength. A similar result can be obtained by tuning the MLL spacing. Here it will be shown that an electrical comb can be generated at a new RF spacing (ω_{os}) during the photodetection. The result of this simplification was used in the previous section. Both the WDM and MLL local oscillator (LO) can

be expressed as sum of cosines, with each entry in the summation representing a single WDM channel or MLL peak. The representation of each is shown below.

$$S_{sig} = \sum_{n=0}^{N-1} A_{sig,n} \cos\left(\left(\omega_0 + n\omega_\Delta\right) t\right) \quad \textbf{(B.25)}$$

$$S_{LO} = \sum_{m=0}^{M-1} A_{LO,n} \cos\left(\left(\omega_{L0} + m\omega_{\Delta L}\right) t\right) \quad \textbf{(B.26)}$$

The detected current is proportional to the square of the sum of equations (B.25) and (B.26). The detected signal will be represented by I_P, which is defined in equation (2.32). The photocurrent in terms of the OSCM and MLL-LO is

$$I_P = \left| \sum_{n=0}^{N-1} A_{sig,n} \cos\left(\left(\omega_0 + n\omega_\Delta\right) t\right) + \sum_{m=0}^{M-1} A_{LO,n} \cos\left(\left(\omega_{L0} + m\omega_{\Delta L}\right) t\right) \right|^2 \quad \textbf{(B.27)}$$

Expanding I_P for just a few terms produces results that are unmanageable. For instance, if N=M=3, then I_P has 36 terms before simplification. The 36 terms are even before expanding the cos(a)cos(b) terms, which will double the number of terms to track. In order to simplify the math involved one only needs to consider the terms that will produce RF terms that are detectable and useful. For this purpose it is useful to only consider terms less than $\omega_\Delta / 2 + \omega_\delta$, where ω_Δ and ω_δ are defined below.

$$\omega_{\Delta L} = \omega_\Delta + \omega_{os} \quad \textbf{(B.28)}$$

$$\omega_{LO} = \omega_0 + \omega_\delta \quad \textbf{(B.29)}$$

ω_Δ is the WDM spacing, $\omega_{\Delta L}$ is the MLL spacing, ω_0 is the initial WDM frequency and ω_{L0} is the initial LO frequency of interest. Since we are only interested in

producing one comb to represent the FDM system in the RF domain, only the lowest frequency terms need to be collected. It has been shown earlier that the RF comb must fit within $\omega_\Delta / 2$ to avoid superposition of the terms during the squaring that occurs in the photodetector. When the higher order harmonics are ignored (or filtered out in a real system), I_P can be simplified to

$$I_P = \frac{N}{2} A_{sig}^2 + \frac{M}{2} A_{LO}^2 + 2 A_{sig} A_{LO} \sum_{n=0}^{N-1} \sum_{m=0}^{M-1} \cos\left((\omega_0 + n\omega_\Delta) t \right) \cos\left((\omega_{L0} + m\omega_{\Delta L}) t \right) \quad \textbf{(B.30)}$$

Equation (B.30) assumes that all WDM powers are equal and all LO powers are equal. This assumption is easily undone at the end if desired. However, only when *n=m* does the double summation produce a frequency in the desired range. Using that knowledge and equations (B.28) and (B.29), I_P can further be simplified to the equation below.

$$I_P = \frac{N}{2} A_{sig}^2 + \frac{M}{2} A_{LO}^2 + 2 A_{sig} A_{LO} \sum_{n=0}^{N-1} \cos\left((\omega_\delta + n\omega_{os}) t \right) \quad \textbf{(B.31)}$$

This approximation is exact for all the desired terms, as long as the conditions pointed out earlier are meet to avoid any aliasing or superposition of the OSCM signals in the RF domain.

The following figures show some examples plotted with MATLAB® that illustrate the equivalence of equations (B.27) and (B.31) of terms with frequency less than $\omega_\Delta / 2 + \omega_\delta$. From this it can be seen that using equation (B.31) is more efficient both when doing calculations by hand or in simulation.

For this example a WDM system with five channels and a MLL also with five peaks is used. The following table shows all of the frequencies used in the example.

$\omega_0 = 1000$ $\omega_\delta = 5$ $\omega_\Delta = 100$ $\omega_{os} = 15$

Using equations (B.25), (B.26), (B.28) and (B.29), the full spectrum of the WDM and MLL are shown in Figure B.1. All WDM and LO amplitudes are set to 2 [a.u.]. The variance seen in the powers in Figure B.1 is due to the fact that the peak of each channel is not necessarily sampled in the frequency domain. In the simulation care was taken to make sure that the peaks are sampled for the low RF detected signals.

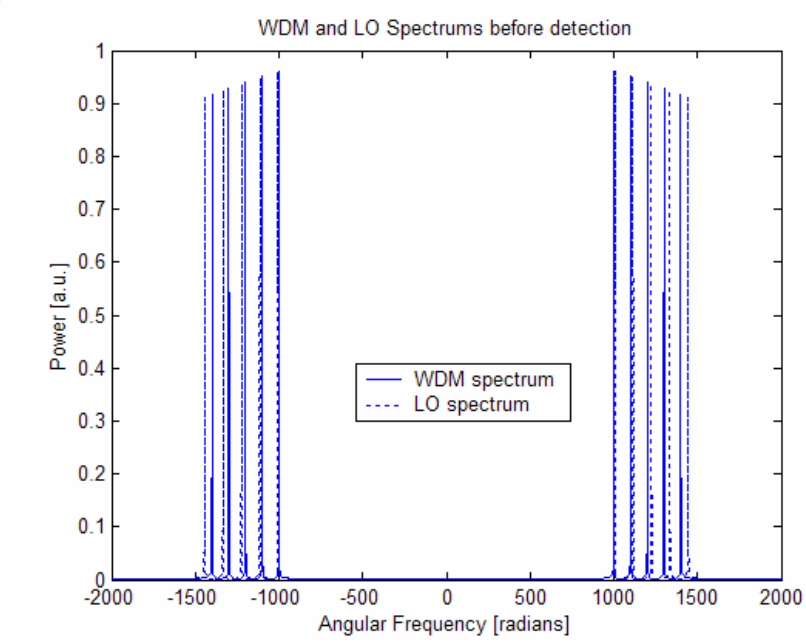

Figure B.1: WDM and LO spectrum before detection

After detection using equation (B.27) the following spectrum is generated. As is seen the number of terms is immense, and the frequency domain needs to be represented to several times the initial frequency. This adds to complexity in

the results and also computation time in the simulation. It is obvious that a simplification of equation (B.27) is required for any serious computations.

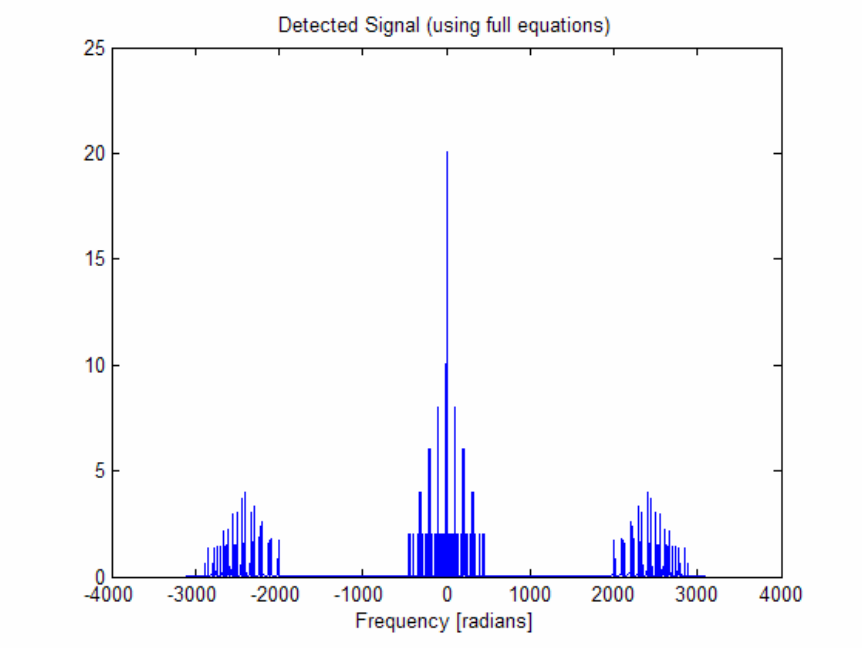

Figure B.2: Detected signal using full equations

The next three figures illustrate the equivalence of equations (B.27) and (B.31). The first figure is simply zoomed in on the area of interest of Figure B.2.

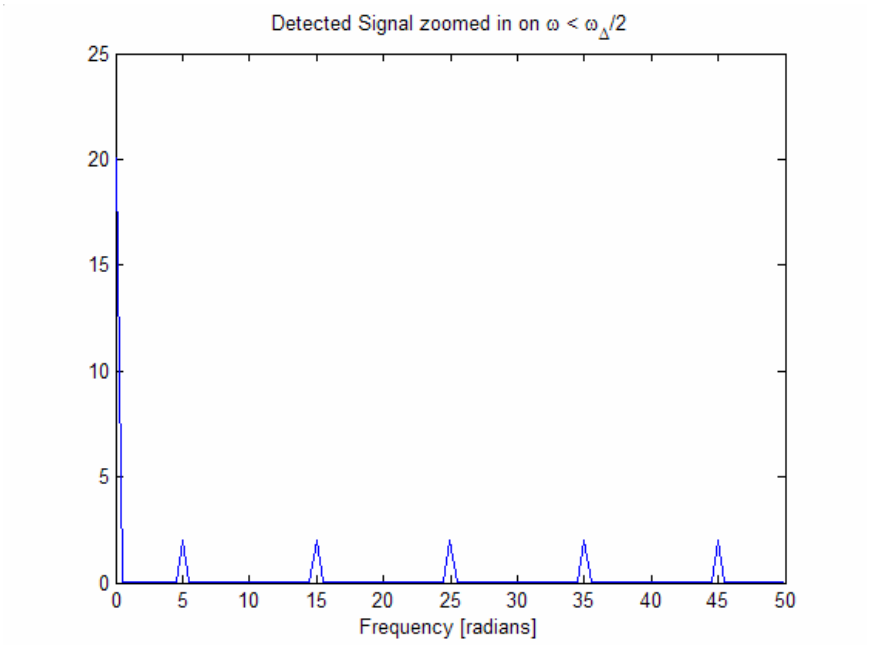

Figure B.3: Detected signal zoomed in (using the full photodetection signal, with no approximation)

In Figure B.4 the frequency scale has been extended to $1.5\omega_\Delta$ to emphasize that only the frequencies below $\omega_\Delta / 2 + \omega_\delta$ are included.

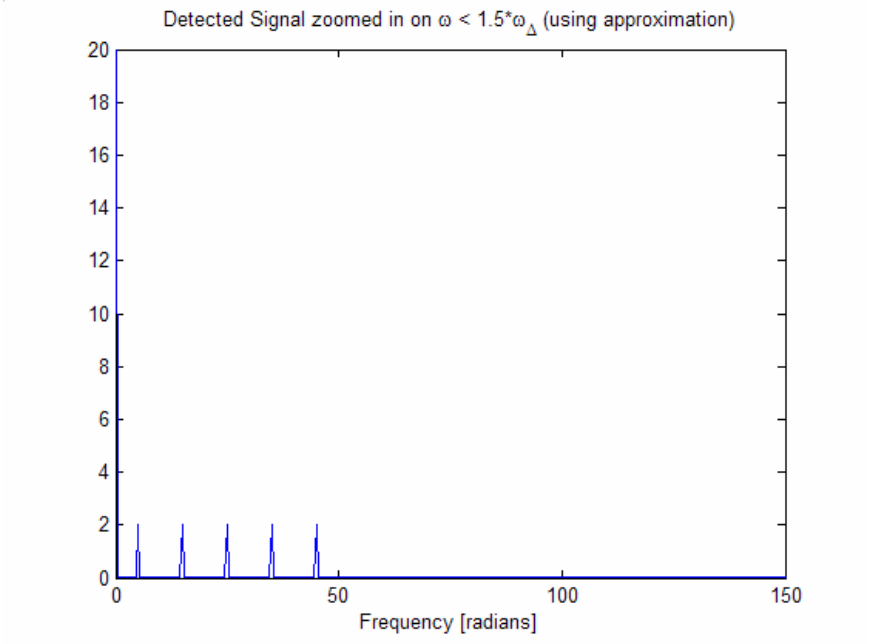

Figure B.4: Detected signal using approximation

By plotting both the full expression for the detected signal along with the approximation of the detected signal it is seen that for the terms we are interested in the equations are equivalent.

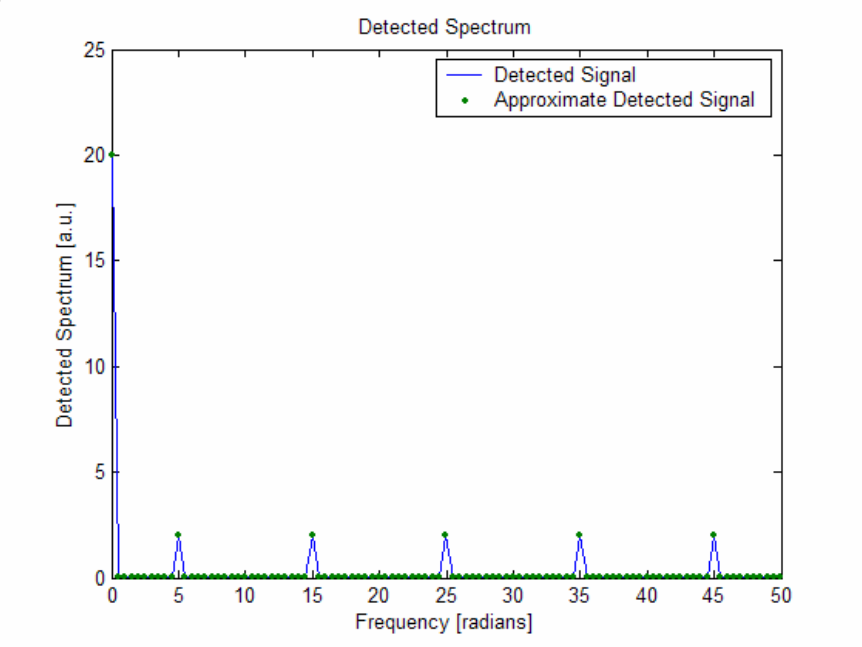

Figure B.5: Detected spectrum, analytical and approximation.

It is important to point out that equation (B.31) only uses the initial offset between the MLL and WDM channels and the difference in spacing between the WDM and MLL spacing. Since these terms are in the gigahertz or megahertz range one avoids the need to simulate signals in the terahertz (optical frequency) range. Having a simplified equation to investigate the RF comb generated by the detection of a WDM signal with a MLL enables using simulation and hand calculations of more complex problems of this type.

An area of interest to which this technique can be applied to is in the area of performance monitoring. Since all of the information contained in the WDM system is present in the RF comb one can monitor the optical and digital

properties using established RF techniques. This may produce a cost effective way to monitor several WDM channels simultaneously while obtaining all of the required performance statistics.

Appendix C. SSB Derivation

This appendix details the derivation of equation (3.5).

First, by substituting (2.9) into equation (3.4), one finds

$$S_{USB} = 1 + \mu \frac{1}{2}\left(2\cos(2\pi f_s t + \phi_s) + j\mathcal{H}\left\{2\cos(2\pi f_s t + \phi_s)\right\}\right) \quad \textbf{(C.1)}$$

where $\mathcal{H}\{\bullet\}$ is the Hilbert transformation. The Hilbert transform imposes a -π/2 phase shift to positive frequencies and a π/2 phase shift to negative frequency. The Hilbert transform is sometimes defined as the inverse of this [13], however the definition used here is consistent with MATLAB® so as to be consistent with the simulation [42]. f_s is a positive frequency shift here, so

$$\mathcal{H}\left\{2\cos(2\pi f_s t + \phi_s)\right\} = 2\sin(2\pi f_s t + \phi_s) \quad \textbf{(C.2)}$$

and

$$2\cos(2\pi f_s t + \phi_s) = e^{j(2\pi f_s t + \phi_s)} + e^{-j(2\pi f_s t + \phi_s)} \quad \textbf{(C.3)}$$

$$2\sin(2\pi f_s t + \phi_s) = -je^{j(2\pi f_s t + \phi_s)} + je^{-j(2\pi f_s t + \phi_s)} \quad \textbf{(C.4)}$$

By substituting equations (C.3), (C.4) and (C.2) back into (C.1), S_{USB} becomes

$$S_{USB} = 1 + \mu \frac{1}{2}\left(e^{j(2\pi f_s t + \phi_s)} + e^{-j(2\pi f_s t + \phi_s)} + e^{j(2\pi f_s t + \phi_s)} - e^{-j(2\pi f_s t + \phi_s)}\right) \quad \textbf{(C.5)}$$

and after simplifying,

$$S_{USB} = 1 + \mu e^{j(2\pi f_s t + \phi_s)} \quad \textbf{(C.6)}$$

This equation is used for the baseband representation of a single SSB subcarrier without data. SSB data is included in a similar fashion. For multiple subcarriers, the exponential term of (C.6) is simply summed over the set of subcarrier frequencies (f_s).

Appendix D. Non-suppressed Carrier Dispersion Penalties

In Chapter 3 of the body of the dissertation, the analysis shows the power fading and distortion of signals with suppressed carrier and subcarriers. This was done to greatly simplify the equations and make the derivation easier to follow. In that derivation, wherever a strong carrier was required it was assumed to be present. This assumption was made during photodetection to make the signal linear, and when envelope detection was used for RF demodulation.

This appendix carries out the same analyses for a DSB carrier with a DSB subcarrier signal as in Section 3.5, but does not assume suppressed carriers. Since the analysis follows the same steps for DSB and SSB carriers and subcarriers, only one case will be repeated for non-suppressed carrier signals. The modulation index of the subcarrier onto the carrier is μ, and the modulation index of the data onto the subcarrier is η. Using μ and η the signal at the input to the fiber is

$$S_{0,DD} = \left(1+\mu\left[1+\eta 2\cos\left(2\pi f_r t\right)\right]2\cos\left(2\pi f_s t\right)\right)2\cos\left(2\pi f_\lambda t\right) \qquad \textbf{(D.1)}$$

As in Chapter 3 each cosine function has a multiplier of 2 so that the ½ multiple can be removed when written in exponential form. Also, to eliminate the repetition of many 2π terms, the relation $2\pi f_x = \omega_x$ is used.

$$\begin{aligned} S_{0,DD} = {} & 2\cos(\omega_\lambda t) + 2\mu\cos\left((\omega_\lambda + \omega_s)t\right) + 2\mu\cos\left((\omega_\lambda - \omega_s)t\right) + \\ & 2\eta\mu\cos\left((\omega_\lambda + \omega_s + \omega_r)t\right) + 2\eta\mu\cos\left((\omega_\lambda + \omega_s - \omega_r)t\right) + \\ & 2\eta\mu\cos\left((\omega_\lambda - \omega_s + \omega_r)t\right) + 2\eta\mu\cos\left((\omega_\lambda - \omega_s - \omega_r)t\right) \end{aligned} \quad \textbf{(D.2)}$$

Rewriting equation (D.2) in exponential form, the baseband representation is

$$S_{0,DD} = 1 + \mu e^{j\omega_s t} + \mu e^{-j\omega_s t} + \eta\mu e^{j(\omega_s+\omega_r)t} + \eta\mu e^{j(\omega_s-\omega_r)t} + \eta\mu e^{-j(\omega_s+\omega_r)t} + \eta\mu e^{-j(\omega_s-\omega_r)t} \quad \textbf{(D.3)}$$

By comparing equation (D.3) to (3.42), it is seen that (3.42) is composed of the $\eta\mu$ terms from (D.3). The terms with only μ are the subcarrier terms, which are now not suppressed, and the '1' represents the unsuppressed optical carrier. At the end of the fiber, dispersion adds a phase shift to each subcarrier and information bearing signal (ω_r) according to Section 3.3.1. The phase shift at the subcarrier frequency is ϕ_D, and is $\phi_{DU} = \phi_{DL}$ for the USB and LSB of the subcarrier, respectively.

$$\begin{aligned} S_{F,DD} = {} & 1 + \mu e^{j(\omega_s t + \phi_D)} + \mu e^{-j(\omega_s t - \phi_D)} + \eta\mu e^{j(\omega_s+\omega_r+\phi_{DU})t} + \\ & \eta\mu e^{j(\omega_s-\omega_r+\phi_{DL})t} + \eta\mu e^{-j(\omega_s+\omega_r-\phi_{DU})t} + \eta\mu e^{-j(\omega_s-\omega_r-\phi_{DL})t} \end{aligned} \quad \textbf{(D.4)}$$

After photodetection with a square law detector, and removing any double frequency terms, the resulting photocurrent is given by (D.5). The double frequency terms are proportional to either μ^2 or $\eta^2\mu^2$, for the subcarrier and data terms, respectively, and therefore negligible for large optical carriers (i.e. $\mu \ll 1$).

$$
\begin{aligned}
I_P = 1 + \mu e^{j(\omega_s t + \phi_D)} + \mu e^{-j(\omega_s t - \phi_D)} + \eta\mu e^{j(\omega_s + \omega_r + \phi_{DU})t} + \\
\eta\mu e^{j(\omega_s - \omega_r + \phi_{DL})t} + \eta\mu e^{-j(\omega_s + \omega_r - \phi_{DU})t} + \eta\mu e^{-j(\omega_s - \omega_r - \phi_{DL})t} + \\
\mu e^{-j(\omega_s t + \phi_D)} + \mu e^{j(\omega_s t - \phi_D)} + \eta\mu e^{-j(\omega_s + \omega_r + \phi_{DU})t} + \\
\eta\mu e^{-j(\omega_s - \omega_r + \phi_{DL})t} + \eta\mu e^{j(\omega_s + \omega_r - \phi_{DU})t} + \eta\mu e^{j(\omega_s - \omega_r - \phi_{DL})t}
\end{aligned}
\qquad \textbf{(D.5)}
$$

After rearranging and writing in cosine form, using $\phi_{DU} = \phi_{DL}$, as in Section 3.5, the resulting signal is

$$
I_p = 1 + 2\mu\cos(\omega_s t)\cos(\phi_D) + 8\eta\mu\cos\left((\omega_s + \omega_r)t\right)\cos(\phi_{DU}) \qquad \textbf{(D.6)}
$$

At this point, the signal is demodulated and the DC term removed with a DC block, the final current for the data waveform is

$$
I_p = 8\eta\mu\cos(2\pi f_r t)\cos(\phi_{DU}) \qquad \textbf{(D.7)}
$$

In Section 3.5 it was indicated that gain is used in the RF demodulation circuit to eliminate the modulation index and the responsivity of the photodetector. Here, the responsivity was assumed to be unity, so the appropriate gain is $1/(\eta\mu)$, and the final received photocurrent is the same as given in (3.51).

Appendix E. Analysis of Dual-Frequency LO at the Optical Frequency

In Section 3.7 the analysis of using a dual-frequency LO started with the signal and LO represented at the optical frequency, but once the phase terms were established the rest of the analysis was done using the complex envelope. That was done to simplify the long equations in order to make the procedure more readable. Here the analysis will be repeated for dual-frequency LO homodyne detection using equations that include the optical frequency. The signal and LO are repeated here for convenience. A SSB subcarrier is used to

reduce the number of terms in the equations. Also, the approximation that $D_s(f_s)+\Delta D_r \approx D_s(f_s)=\phi_D$ is used.

$$S_{LO} = e^{j(2\pi(f_\lambda+f_s)t+\phi_{LO}+\phi_s)} + e^{j(2\pi(f_\lambda-f_s)t+\phi_{LO}-\phi_s)} + e^{-j(2\pi(f_\lambda+f_s)t+\phi_{LO}+\phi_s)} + e^{-j(2\pi(f_\lambda-f_s)t+\phi_{LO}-\phi_s)} \quad \textbf{(E.1)}$$

$$S_{F,DS} = e^{j(2\pi(f_\lambda+f_s+f_r)t+\phi_D)} + e^{j(2\pi(f_\lambda-f_s-f_r)t+\phi_D)} + e^{-j(2\pi(f_\lambda+f_s+f_r)t+\phi_D)} + e^{-j(2\pi(f_\lambda-f_s-f_r)t+\phi_D)} \quad \textbf{(E.2)}$$

Both (E.1) and (E.2) are suppressed carrier and suppressed subcarrier for the purpose of reducing the number of non contributing terms that are carried along, but as seen in Appendix D and Chapter 4 non-suppressed carrier systems have the same penalties due to the dispersion induced phase shift.

Next photodetection is performed by multiplying the sum of (E.1) and (E.2) by the complex conjugate of the sum. After dropping any terms that are beyond the bandwidth of the baseband filter ($2f_\lambda$, $2f_s$, $f_\lambda+f_s$, etc.) the resulting photocurrent has eight terms at $\pm f_r$. It should be clarified that this is homodyne detection of the optical subcarrier, not of the optical carrier.

$$\begin{aligned} I_P = {} & e^{j(-2\pi f_r t-\phi_D+\phi_{LO}+\phi_s)} + e^{j(2\pi f_r t+\phi_D-\phi_{LO}-\phi_s)} + e^{j(2\pi f_r t-\phi_D+\phi_{LO}-\phi_s)} + e^{j(-2\pi f_r t+\phi_D-\phi_{LO}+\phi_s)} + \\ & e^{j(2\pi f_r t-\phi_D-\phi_{LO}-\phi_s)} + e^{j(-2\pi f_r t-\phi_D+\phi_{LO}+\phi_s)} + e^{j(-2\pi f_r t+\phi_D-\phi_{LO}+\phi_s)} + e^{j(2\pi f_r t-\phi_D+\phi_{LO}-\phi_s)} \end{aligned} \quad \textbf{(E.3)}$$

The remaining simplification steps are the same as that presented in Section 3.7, so they will be stepped through quickly.

$$\begin{aligned} I_P = {} & e^{-j(2\pi f_r t-\phi_s)}e^{-j(\phi_D-\phi_{LO})} + e^{+j(2\pi f_r t-\phi_s)}e^{+j(\phi_D-\phi_{LO})} + \\ & e^{-j(2\pi f_r t-\phi_s)}e^{-j(-\phi_D+\phi_{LO})} + e^{+j(2\pi f_r t-\phi_s)}e^{+j(-\phi_D+\phi_{LO})} + \\ & e^{-j(2\pi f_r t-\phi_s)}e^{-j(\phi_D-\phi_{LO})} + e^{+j(2\pi f_r t-\phi_s)}e^{+j(\phi_D-\phi_{LO})} + \\ & e^{-j(2\pi f_r t-\phi_s)}e^{-j(-\phi_D+\phi_{LO})} + e^{+j(2\pi f_r t-\phi_s)}e^{+j(-\phi_D+\phi_{LO})} \end{aligned} \quad \textbf{(E.4)}$$

$$\begin{aligned} I_P = {} & 2e^{-j(2\pi f_r t-\phi_s)}e^{-j(\phi_D-\phi_{LO})} + 2e^{+j(2\pi f_r t-\phi_s)}e^{+j(\phi_D-\phi_{LO})} + \\ & 2e^{-j(2\pi f_r t-\phi_s)}e^{-j(-\phi_D+\phi_{LO})} + 2e^{+j(2\pi f_r t-\phi_s)}e^{+j(-\phi_D+\phi_{LO})} \end{aligned} \quad \textbf{(E.5)}$$

$$I_P = 2\left(e^{-j(2\pi f_r t-\phi_s)}\left(e^{j(\phi_{LO}-\phi_D)} + e^{-j(\phi_{LO}-\phi_D)}\right) + e^{j(2\pi f_r t-\phi_S)}\left(e^{j(\phi_{LO}-\phi_D)} + e^{-j(\phi_{LO}-\phi_D)}\right)\right) \quad \textbf{(E.6)}$$

$$I_P = 2\left(e^{-j(2\pi f_r t-\phi_s)} + e^{j(2\pi f_r t-\phi_s)}\right)\left(e^{j(\phi_{LO}-\phi_D)} + e^{-j(\phi_{LO}-\phi_D)}\right) \quad \textbf{(E.7)}$$

$$I_P = 8\cos\left(2\pi f_r t - \phi_s\right)\cos\left(\phi_{LO} - \phi_D\right) \quad \textbf{(E.8)}$$

The only difference between this result and the result in Section 3.7 is a factor of two. The factor of two is a result of the decision to normalize each exponential term in the equation to unity, and here the optical frequency is considered, so there are twice as many terms in the photocurrent after baseband filtering. This shows that the analyses shown in Chapter 3 and the simulations in Chapter 4 sufficiently represents the dual-frequency LO homodyne detection using the baseband representation of optical signal. A similar analysis shows that the same is true for dual-frequency LO heterodyne detection, as well as for DSB subcarriers and SSB optical carriers.

Appendix F. Common MATLAB® Routines

The following section of this appendix record some of the MATLAB® routines that are used in many of the simulations presented in this dissertation. They are chosen because of their abundant use in the results of Chapter 4, and because they may be the more useful routines to others doing similar work in the future.

Appendix F.1. Eye Diagram Generation

```
1: function plot_eye(bitstr,SPB,varargin)
2: %this fuction will plot an eye-diagram of a waveform
3: %the waveform should be a bitstream
4: %this function needs two inputs to plot an eyediagram
5: %bitstr is the waveform to plot
6: %SPB is the number of samples per bit
```

```
%the eye diagram is two bits wide

%normalize the height to 1 prior to calling this routine;

if length(varargin)==0
os=0;
else
os=varargin{1};
end

%only keep the middle half of the bits
Nc=length(bitstr)/SPB;
if length(bitstr)>250*SPB;
bitstr=bitstr([floor(Nc/4)*SPB:end-(floor(Nc/4)*SPB)]);
%get rid or atleast the first and last 10 bits if above not case
%now get rid of first and last bit if >10 bits;
elseif length(bitstr)>10*SPB;
bitstr=bitstr([SPB:end-SPB]);
end

%this is to normalize the eye to remove any DC component
bitstr=bitstr-mean(bitstr);

w=SPB*2; %width of the eyediagram window
tw=1:w; %one time pass;
%tw=shift(tw,length(tw)/2);
eye_t=[];
N=length(bitstr)/SPB;
bitstr=shift(bitstr,os);
for k=1:N/2+1;
eye_t=[eye_t tw];
end
eye_t=eye_t([1:length(bitstr)])./SPB;
%call the figure or subplot before calling this routine
hold on
for trace=0:2:N-2
plot(eye_t([trace*SPB+1:(trace+2)*SPB]),bitstr([trace*SPB+1:(trace+2) ↵
    *SPB]))
end
plot(eye_t([(trace+2)*SPB+1:end]), bitstr([(trace+2)*SPB+1:end]))
grid on
title('Eye Diagram')
xlabel('Bit Period')
axis([0 2 -1 1]);
hold off
```

Appendix F.2. Q measurement and BER estimate

```
function [Q,BER]=findber(wf,spb,pf);
%this function will take as an input the waveform (wf) and the Samples-Per-Bit (spb)
%and a plotflag (pf)
%if the plotflag is set to 1, then it will plot a histogram of the data
%if the plotflag is set to 0, then it will just return the BER
%the BER is determined from the Q and is assumed to have Gaussian noise

```

```
8: %as in the plot_eye, the leading and trailing bits need to be dropped
9: wf_in=wf;
10: Nc=length(wf)/spb;
11: drop=1;
12: if length(wf)>250*spb;
13: wf=wf([floor(Nc/8)*spb:end-(floor(Nc/8)*spb)]);
14: %get rid or atleast the first and last 10 bits if above not case
15: %now get rid of first and last bit if >10 bits;
16: drop=floor(Nc/8);
17: elseif length(wf)>10*spb;
18: wf=wf([spb:end-spb]);
19: drop=1;
20: end
21:
22: %find histogram of all points in wf
23: [num,bc]=hist(wf-mean(wf),50);
24:
25: %actually, don't use the offset but find the average '1' and '0'
26: %first serperate each bit into a seperate row of the matrix
27: wf_bits=reshape(wf_in,spb,Nc)';
28: size(wf_bits);
29: wf_bits=wf_bits([drop:end-drop],:);
30: [nb,np]=size(wf_bits);
31:
32: %now seperate each bit into a one or zero matrix,
33: one_bits=[];
34: zero_bits=[];
35: for m=1:nb
36: if mean(wf_bits(m,:))>mean(wf)
37: one_bits=[one_bits;wf_bits(m,:)];
38: elseif mean(wf_bits(m,:))<mean(wf)
39: zero_bits=[zero_bits;wf_bits(m,:)];
40: end
41: end
42:
43: avg1=mean(one_bits,1); %find the average '1'
44: avg0=mean(zero_bits,1); %find the average '0'
45:
46: %find the widest part of the eye
47: max1=find(avg1==max(avg1));
48: min0=find(avg0==min(avg0));
49: wideeye=(max1+min0)/2;
50:
51: %shift the whole thing so that the eye opens in the center
52: sh=round(wideeye-spb/2);
53: wf_sf=shift(wf_in,sh);
54: % figure
55: % plot_eye(wf_sf,spb);
56: % title('centered eye');
57:
58: %now that the eye is centered, seperate the ones and zeros like above
59: %first serperate each bit into a seperate row of the matrix
60: wf_bits_c=reshape(wf_sf,spb,Nc)';
61: size(wf_bits_c);
62: %drop the first and last 1/8 of bits;
63: wf_bits_c=wf_bits_c([drop:end-drop],:);
```

```
64: [nb,np]=size(wf_bits_c);
65:
66: %now seperate each bit into a one or zero matrix,
67: one_bits_c=[];
68: zero_bits_c=[];
69: for m=1:nb
70: if mean(wf_bits_c(m,:))>mean(wf)
71: one_bits_c=[one_bits_c;wf_bits_c(m,:)];
72: elseif mean(wf_bits_c(m,:))<mean(wf)
73: zero_bits_c=[zero_bits_c;wf_bits_c(m,:)];
74: end
75: end
76:
77: avg1_c=mean(one_bits_c,1); %find the average '1'
78: avg0_c=mean(zero_bits_c,1); %find the average '0'
79:
80: sam_beg=round(0.37*spb);
81: sam_end=round(0.53*spb);
82: keep1=one_bits_c(:,[sam_beg:sam_end]);
83: keep0=zero_bits_c(:,[sam_beg:sam_end]);
84:
85:
86: %now finally find the std, mean and Q;
87: len0=prod(size(keep0));
88: len1=prod(size(keep1));
89: array0=reshape(keep0',1,len0);
90: array1=reshape(keep1',1,len1);
91: mu1=mean(array1);
92: mu0=mean(array0);
93: sigma1=std(array1);
94: sigma0=std(array0);
95: Q=(mu1-mu0)/(sigma1+sigma0);
96:
97: %find the BER from Q;
98: BER_Q=(0.5*erfc(Q/sqrt(2)));
99:
100: if pf==1; %put all plots here
101: figure; plot_eye(wf_in,spb);
102: hold on; plot(num/max(num),bc,'r');
103: title('Eye Diagram with Histograms')
104: hold off;
105: figure
106: plot([1:spb],one_bits_c,'m',[1:spb],zero_bits_c,'c',[sam_beg:sam_end],keep1,'r.',...
107:      [sam_beg:sam_end],keep0,'g.');
108: legend('Kept 1s','Kept 0s','All 1s','All 0s')
109: title('Just the samples included in Q')
110: end
111:
112: BER=BER_Q;
```

References

1 H. Al-Raweshidy, S. Komaki, ed., *Radio over fiber technologies for mobile communications networks*, Artech House, Boston, 2002.

2 A. Loayssa, D. Benito, "Dispersion-Tolerant All-Optical Subcarrier Modulator for Broad-Band BPSK Transmissions", *IEEE Photonics Technology Letters*, Vol. 16, No 4, April 2004.

3 T. Kuri, K. Kitayama, "Optical heterodyne detection of Millimeter-Wave-Band Radio-on-Fiber Signals With a Remote Dual-Mode Local Light Source, *IEEE Transactions on Microwave Theory and Techniques*, Vol. 49, No. 10, October 2001.

4 R. Hui, B. Zhu, C. T. Allen, K. R. Demarest, D. Richards, "Subcarrier Multiplexing for High-Speed Optical Transmission", *Journal of Lightwave Technology*, Vol. 20, No. 3, March 2002.

5 M. Sieben, J. Conradi, D.E. Dodds, "Optical Single Sideband Transmission at 10 Gb/s Using Only Electrical Dispersion Compensation", *Journal of Lightwave Technology*, pp. 1742-1749, Vol. 17, No. 10, 1999.

6 D. Tebben, I. Jacobs, "Coherent Detection Techniques to Eliminate Power Fading in Optical Subcarrier Systems", *Proceedings SPIE*, Vol. 6012*,* Optical Transmission Systems and Equipment for WDM Networks, pp. 159-166, 2005.

7 D. Tebben, I. Jacobs, "Coherent Detection Techniques to Eliminate Phase Error and Power Fading in Optical Subcarrier Systems", Optics East, Optical Transmission Systems and Equipment for WDM Networking IV (IT102), 23-26 October 2005, Boston, MA.

8 G.P. Agrawal, *Nonlinear Fiber Optics, Second Edition,* Academic Press, San Diego, 1995.

9 B. B. Dingel, R. Madabhushi, N. Madamopoulos, "Super-linear optical modulator technologies for optical broadband access network: development and potential", *SPIE 6012*, 60120R, 2005.

10 M. M-K. Liu, *Principles and Applications of Optical Communications,* Irwin, Chicago, 1996.

11 P. E. Green Jr., *Fiber Optic Networks,* Prentice-Hall, Inc., New Jersey, 1993.

12 W. H. Tranter, K. S. Shanmugan, T. S. Rappaport, and K. L.Kosbar, *Principles of Communication Systems Simulation with Wireless Applications*, Prentice Hall, 2004. (Taken from ECE 5604 course handout)

13 D. Zwillinger, *CRC Standard Mathematical Tables and Formulae, 30th Edition*, CRC Press, Boca Raton, 1996.

14 J.G. Proakis, D.G. Manolakis, *Digital Signal Processing, Third Edition,* Prentice Hall, New Jersey, 1996.

15 G.P. Agrawal, *Fiber-Optic Communication Systems, Third Edition,* John Wiley & Sons, Inc., New York, 2002.

16 S. Camatel, V. Ferrero, R. Gaudino, P. Poggiolini, "Optical phase-locked loop for coherent detection optical receiver", *Electronics Letters*, Vol. 40, No. 6, March 18, 2004.

17 S. Shimada, *Coherent Lightwave Communications Technology*, Chapman & Hall, London, 1995.

18 J. R. Barry and E.A. Lee., "Performance of Coherent Optical Receivers", *Proceedings of IEEE*, vol. 78, no. 8, pp. 1369-1394, Aug. 1990.

19 T. Okoshi and K. Kikuchi, *Coherent Optical Fiber Communications*, KTK Scientific Publishers, Tokyo, 1988.

20 D. Tebben, *Optical Link Quality Monitoring in WDM Networks*, Master's Thesis at the University of Kansas, 1998.

21 Mario A. Santoro and Craig D. Poole, "Polarization Scrambling Using a Short Piece of High-Birefringence Optical Fiber and a Multifrequency Laser Diode", *Journal of Lightwave Technology*, vol. 12, no. 2, pp. 288-293, February 1994.

22 T. G. Hodgkinson, R. A. Harmon, and D. W. Smith, "Polarization-Insensitive Heterodyne Detection Using Polarization Scrambling", *Electronics Letters*, vol. 23, no. 10, pp. 513-514, May 7, 1987.

23 T. Ohno, K. Sato, S. Fukushima, Y. Doi, Y. Matsuoka, "Application of DBR Mode-Locked Lasers in Millimeter-Wave Fiber-Radio System", *Journal of Lightwave Technology*, pp. 44-49, Vol. 18, No. 1, January 2000.

24 P.W. Milonni, J.H Eberly, *Lasers*, Johns Wiley and Sons, New York, 1988.

25 R. Ramaswami, K.N. Sivarajan, *Optical Networks, A Practical Perspective,* Morgan Kaufmann, San Francisco, 1998.

26 V. Annovazzi-Lodi, A. Sciré, M. Sorel, S. Donati, "Dynamic Behavior and Locking of a Semiconductor laser Subjected to External Injection". *IEEE Journal of Quantum Electronics*, pp. 2350-2357, Vol. 34, No. 12, December 1998.

27 L.R. Chen, N. Bélanger, "Wavelength tunable, modelocked semiconductor fibre ring laser incorporating a high-birefingence Sagnac loop", *Electronics Letters*, Vol. 41, No. 4., February 17, 2005.

28 S.Y. Set, H. Yaguchi, Y. Tanaka, M. Jablonski, "Laser Mode Locking Uning a Saturable Absorber Incorporating Carbon Nanotubes", *Journal of Lightwave Technology*, pp. 51-56, Vol. 22, No. 1, January 2004.

29 D. Derickson,ed., *Fiber Optics Test and Measurement*, Prentice Hall PTR, New Jersey, 1998.

30 N.S. Bergano, F.W. Kerfoot, and C.R. Davidson, "Margin measurements in Optical Amplifier Systems", *IEEE Photonics Technology Letters*, pp. 304-306, Vol. 5, No. 3. March 1993.

31 MAXIM High-Frequency/Fiber Communications Group, "Optical Signal-to-Noise Ratio and the Q-Factor in Fiber-Optic Communication Systems", *MAXIM*, Application Note: HFAN-9.0.2, Feb. 27, 2002.

32 J.D. Downie, D.J. Tebben, "Performance monitoring of optical networks with synchronous and asynchronous sampling", *Optical Fiber Communications Conference 2001*, paper WDD50, Vol. 3.

33 J.D. Downie, "Relationship of Q Penalty to Eye-Closure Penalty for NRZ and RZ Signals With Signal-Dependent Noise", *Journal of Lightwave Technology*, pp. 2031-2038, Vol. 23, No. 6, June 2005.

34 A. Loayssa, C. Lim, A. Nirmalthasas, D. Benito, "Optical Single-Sideband Modulator for Broad-Band Subcarrier Multiplexing Systems", IEEE Photonic Technology Letters, pp. 311-313, Vol. 15, No. 2, February 2003.

35 P.N. Freeman, N.K. Dutta, "Intermodulation Distortion for a Hybrid AM-VSB/Digital System Using a 1.55-μm Laser and an Optical Amplifier",

IEEE Photonics Technologies Letters, pp. 1558-1560, Vol. 8, No. 11, November 1996.

36 Z. Zhu, V.J. Hernandez, M.Y. Jeon, J. Cao, Z. Pan, S.J. Ben Yoo, “RF Photonics Signal Processing in Subcarrier Multiplexed Optical-Label Switching Communication Systems”, Journal of Lightwave technology, pp. 3155-3166, Vol. 21, No. 12, December 2003.

37 T. Kuri, K. Kitayama, “Optical Heterodyne Detection Technique for Densely Multiplexed Millimeter-Wave-Band Radio-on-Fiber Systems”, Journal of Lightwave Technology, pp. 3167-3179, Vol. 21, No. 12, December 2003.

38 H. Sotobayashi, K. Kitayama, “Cancellation of the Signal Fading for 60 GHz Subcarrier Multiplexed Optical DSB Signal Transmission in Nondispersion Shifted Fiber Using Midway Optical Phase Conjugation”, Journal of Lightwave Technology, pp. 2488-2497, Vol. 17, No. 12, December 1999.

39 U. Gliese, S. Norskov, T.N. Nielsen, “Chromatic Dispersion in Fiber-Optic Microwave and Millimeter-Wave Links”, IEEE Transaction on Microwave Theory and Techniques, pp. 1716-1724, Vol. 44. No. 10, October 1996.

40 U. Gliese, S.N. Nielsen, T.N. Nelsen, “Limitations in Distance and Frequency due to Chromatic Dispersion in Fibre-Optic Microwave and Millimeter-Wave Links”, Microwave Symposium Digests, IEEE MTT-S Digest, Vol. 3. TH3D-1, June 1996.

41 D. Wake, C.R. Lima, P.A. Davies, “Optical Generation of Millimeter Wave Signals for Fiber-Radio Systems Using a Dual-Mode DFB Semiconductor Laser”, IEEE Transactions on Microwave Theory and Techniques, pp. 2270-2276, Vol. 43, No. 9, September 1995.

42 Mathworks demo “Single Sideband Modulation via the Hilbert Transform”, http://www.mathworks.com/products/signal/demos.html?file=/products/demos/shipping/signal/hilberttransformdemo.html, as of March 4, 2006.